Fast and energy-efficient hybrid mold drive

A design, simulation, and technical feasibility analysis of drive concepts

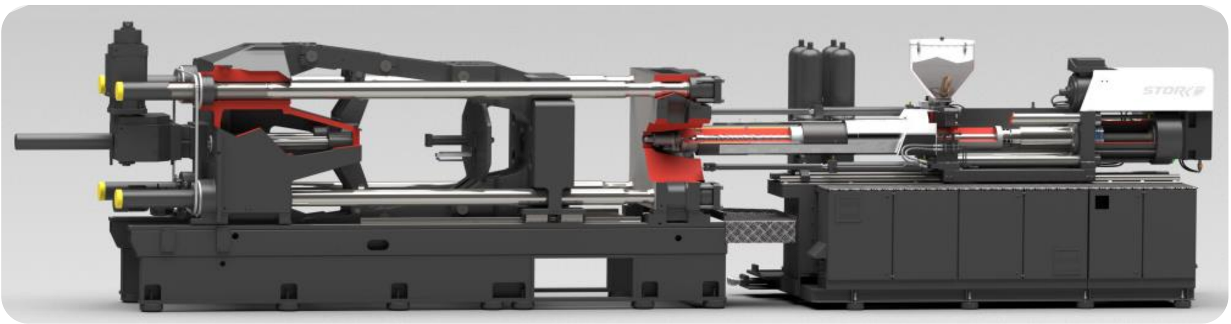

C. Lunshof

Bachelor's thesis
Hanzehogeschool Groningen
Mechanical Engineering

Stork IMM
May 31, 2021

Student:	Corné Lunshof
Student number:	372089
Contact:	*c.lunshof@st.hanze.nl*
Company:	Stork IMM
Location:	Hengelo, The Netherlands
Supervisor:	Hans van Vlierberghe
Contact:	*hans.vanvlierberghe@storkimm.com*
School:	Hanzehogeschool Groningen
First examinator:	Geert Mollema
Contact:	*g.mollema@pl.hanze.nl*
Second examinator:	Hans van de Meent
Contact:	*j.n.van.de.meent@pl.hanze.nl*

Date:	May 31, 2021, Hengelo
Version:	2

Preface

Before you lies the thesis ‘Fast and energy-efficient hybrid mold drive’, wherein the drive behavior of the Stork IMM injection molding machines is thoroughly researched. It was written as a final report of the bachelor mechanical engineering at Hanzehogeschool (University of Applied Sciences) Groningen.

First of all, I would like to thank Stork IMM for the opportunity to graduate by carrying out this challenging assignment. During the time that I worked on the assignment at Stork IMM, I was assisted by enthusiastic colleagues with help and knowledge where necessary.

I would especially like to thank my supervisor H. van Vlierberghe for the technically good, motivating, and pleasant guidance during my graduation project, I have learned a lot from your experience. Also J. Spenkelink for thinking along to solutions and asking critical questions. To all my other colleagues at Stork IMM: I would like to thank you for the assistance where I needed the help and knowledge.

At the Hanzehogeschool Groningen, I would like to thank G. Mollema for the supervision and critical feedback during my graduation project.

I hope you enjoy your reading.

Corné Lunshof

Hengelo, May 31, 2021

Statement regarding originality / anti-plagiarism statement

I hereby declare that I have written this thesis independently, without outside help, and that it is entirely the result of my own work.

I have only used the sources which have been faithfully and accurately quoted in the reference list, including books, magazines, handouts, internet sites and significant personal communication, and I have marked the pages taken either directly or as regards content from those sources.

The thesis was in this or similar style never shown to another board of examiners nor was it published.

I am aware that not complying with these requirements will result in the marking of the thesis to be declared invalid and that, if plagiarism is detected, disciplinary measures will be taken.

Name: Corné Lunshof

Signature: 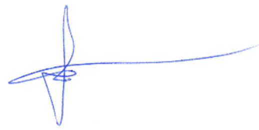

Place/date/year: Hengelo, May 31, 2021

Abstract

Energy usage is a fundamental property of injection molding machines. The development of these machines is accompanied by two contradictory objectives. On the one hand, a producer wants to produce as quickly as possible, cycle times must be as short as possible, and the number of products produced simultaneously must be as high as possible. On the other hand, the importance of energy-efficient production is increasing, but it is contrary to the previous desire. Energy usage in the industry is a hot topic, wherein energy consumption and grid load are crucial characteristics. The current hydraulic injection molding machine from Stork IMM has a lot of energy loss and thus consumption in comparison to a full electric molding machine. The electric drive can recover large amounts of energy by using the motor as a generator during braking phases. However, the electric drive components are very large to provide required peak powers, resulting in more rotational inertia and costs. This report examines whether a hybrid drive is technically feasible, wherein the electric drive is constructed smaller and a separate hydraulic drive assits to provide peak powers.

The research starts with a thorough examination of the current injection molding machines. The current energy consumption and operating speeds are benchmarks for a new concept. Hereafter, concepts for a hybrid drive are designed. Considerations concerning the release, recovery, and storage of energy are assiduously examined and weighed. A calculation model is constructed to properly graph the behavior of the machines with changing masses, accelerations, and cycle times. In the extensive calculation model, many iterations are done in the aforementioned changing parameters. Interesting conclusions about energy and power users emerge from the calculation. The energy efficiency, technical integration, and costs are conclusively the parameters by which the new concept is compared with the current drive.

In the concept, an electric motor together with a hydraulic motor are mounted in parallel on the gearbox, in which the rotating movement is linearized with a gear rack. The opening and closing of the mold can be performed hybrid (fast) or fully electric (energy efficient). Both drives are required during the mold pressing phase to ensure enough closing power. The recovery of kinetic and rotational energy is carried out purely electrical. The recovered energy is passed between the electric and hydraulic drive frequency converters, hereafter the energy is stored in hydraulic accumulators. The new concept in electric mode is just as fast as the current drive, while half the size of the motor has been used. This reduces the rotational energy demand. In hybrid mode, the cycle time can be reduced. Energy consumption decreases by 7.7% and the concept has major consequences for the grid load. The peak return of energy on the grid and the peak usage of the hydraulic system cancel each other out and the energy is used directly within the limits of the machine. The lowering of the grid load and energy consumption makes the concept very interesting. Moreover, the concept is roughly equal in costs and even allows faster operation. In addition, it appeared that the current electrical cycle time can be reduced by 11 percent. This is just as fast as the hybrid concept in hybrid mode, but much more energy efficient.

Table of contents

List of symbols and abbreviations

Symbol	Description	General used unit	Unit
A	Area	m^2	Meter squared
d	Diameter	m	Meters
E	Energy	J	Joule
F	Force	N	Newton
f	Direction	-	-
I	Rotational inertia	$kg\ m^2$	Kilogram-meter squared
i	Transmission ratio	$mm\ rotation^{-1}$	Millimeters per rotation
l	Length	m	Meters
m	Mass	kg	Kilogram
n	Rotation speed	rpm	Rounds per minute
N	Samples	-	-
p	Pressure	Pa	Pascal
P	Power	W	Watt
Q	Volume flow	$m^3\ hr^{-1}$	Cubic meter per hour
SF	Safety factor	-	-
T	Torque	Nm	Newton-meter
t	Time	s	Second
v	Velocity	$m\ s^{-1}$	Meters per second
vd	Volume displacement	$cc\ rot^{-1}$	Centiliter per rotation
w	Moving average range	-	-
X	Horizontal position	m	Meters
Y	Young's modulus	Pa	Pascal
ε	Strain	-	-
σ	Stress	Pa	Pascal
ω	Angular velocity	$rad\ s^{-1}$	Radians per second

Abbreviation	Desciption
CH	Crosshead
CPR	Common pressure rail
E / Elec.	Electric
EH	Electric hybrid
H / Hydr.	Hydraulic
HH	Hydraulic hybrid
HST	Hydrostatic transmission
HT	Hydraulic transmission
IPM	Ideal Physical Model
KERS	Kinetic energy recovery system
kin	Kinetic
LSP	Mobile clamping plate
MA	Moving average
PH (E/H)	Parallel hybrid (electric/hydraulic)
rot	Rotational
SH (E/H)	Series hybrid (electric/hydraulic)
Stork IMM	Stork Injection Moulding Machines
tot	Total
VSP	Fixed clamping plate

1. Introduction

Time and global interests change. Today, energy consumption is a hot topic, also in industry. The reliable, fast, low mass, and relatively cheap hydraulic injection molding machine has a major disadvantage: a lot more energy consumption in comparison to the Stork IMM electric injection molding machine. However, the electric machine also has its disadvantages. A high closing force has to be achieved, so the electric components are big and robust. This makes the system very expensive and results in parts having high rotational inertias. The challenge is to design a new energy-efficient drive that is faster and consumes less energy.

The research investigates whether a hybrid drive for the back and forth translation of the mold is technically feasible. The hybridization must combine the powerful hydraulic advantages with the energy-efficient electric properties. A hybrid drive results in a lower demand of the electric drive, thus less mass, and a decrease in rotational inertias. The additional problem is the lack of knowledge on the technical feasibility of a hybrid-driven concept in this type of machine. So, research must be conducted on hybrid system concept possibilities and the additional technical feasibility in terms of component costs, energy efficiency, and cycle time. A potential new concept must perform equally well or better compared to the existing drive. The practical relevance is evident from the changing demand in the production industry. In addition to the desire of plastic product manufacturers to produce as quickly as possible, energy consumption and grid load are increasingly important. The research is conducted based on the following research questions:

1. What are the current hydraulic and electric drive performances?
2. What is a suitable hybrid drive concept?
3. How does a change in motor power affect the system behavior in speed, time, and energy?
4. What is the technical feasibility of the concept in terms of technical integration in the machine, energy efficiency, and component costs?

The report starts with an analysis of the current hydraulic and electric driven closing units in chapter 2. In this phase, current systems are examined by researching system components, control, and performance. subsequently, chapter 3 investigates the possibilities for a hybrid system by examining the system drive options and thoroughly looking into potential system solutions. Once a concept has been designed, Chapter 4 elaborates the dynamic behavior of the machine using a calculation model. Finally, the technical feasibility is examined in Chapter 5.

2. Analysis of current closing units

To design a new drive concept that meets the performances of the existing machines, firstly the current machines must be analyzed. This chapter looks into the working principles, the drive performances, and determines the requirements of the new drive. In particular, research is conducted on running speeds and energy consumption. The research is done based on measurements and tested data. The report zooms in chronologically from the machine, to the closing unit, and the crosshead, as displayed in Figure 2.1.

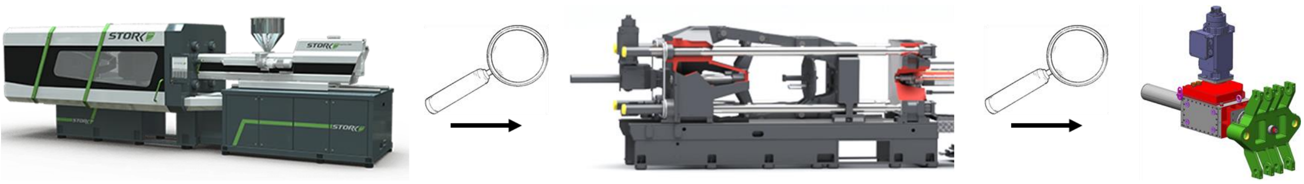

Figure 2.1, chronological schematization of the subject introduction

2.1 General machine description

All Stork IMM injection molding machines contain two subparts: an injection unit and a closing unit. This paragraph first takes a brief look at the components of the injection unit. Hereafter, the operation of the locking unit is discussed. The purpose of the injection unit is to plasticize the plastic granules and inject the liquid, homogeneous plastic into the mold (Stork IMM, 2021). The injection unit contains an injection nozzle to inject the fluid, a plasticizing screw driven by an electric motor and gearbox to plasticize the granules, and the control elements. The control elements refer to the electrical and hydraulic systems.

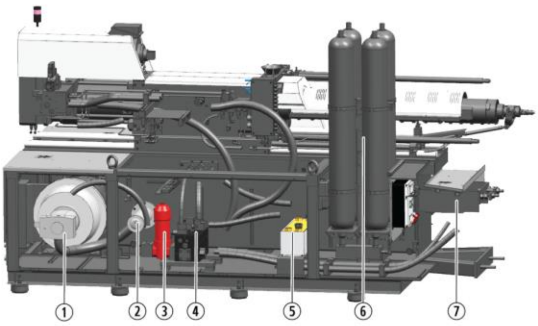

Figure 2.2, Hydraulic system components

The hydraulic control elements can be seen in Figure 2.2. The numbered system components are described in the following summary:

1. Main motor and pump
2. Suction filter
3. Press filter
4. Pump manifold
5. Oil cooler
6. Hydraulic accumulator
7. Reservoir for hydraulic oil

The parts of the closing unit are shown in Figure 2.3. The VSP (fixed clamping plate) (3) is the only fixed part on the frame, and it merges the injection unit (4) to the closing unit. The rear clamping plate (1) is fixed by four tie-bars (7) to the VSP, but linearly slides on the frame while working. The sliding movement is caused by high tensile stresses, resulting in stretching tie-bars. The electric drive (8)(9) drives the crosshead (5). The crosshead can also be driven by a hydraulic cylinder.

1. Rear clamping plate
2. Mobile clamping plate (LSP)
3. Fixed clamping plate (VSP)
4. Injection nozzle
5. Crosshead
6. Toggles
7. Tie-bars
8. Electric motor
9. Gearbox

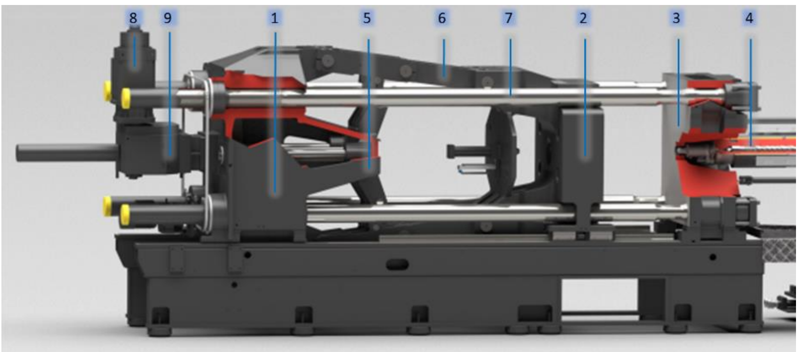

Figure 2.3, the closing unit

The toggles (6) are designed to press the molds forcefully and lock the LSP (moving clamping plate) (2) on the final reach. This latter described process can be seen in Figure 2.4, which gives a schematic representation of the force transmitting mechanism.

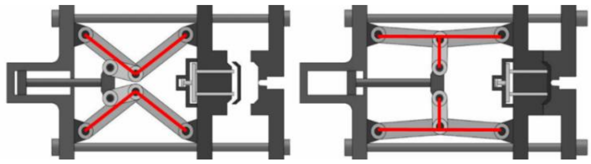

Figure 2.4, schematic view of the press movement

2.2 Hydraulic closing unit

To thoroughly examine the existing machines, several tests are performed on the machine. The test data is added in Appendix A. The hydraulic operation data is examined in this paragraph. The goal of the investigation is to understand the behavior, controls, and power characteristic of the hydraulic machine.

2.2.1 The closing process

The crosshead is driven by, in this case, a hydraulic cylinder. The changeover times are not in the interest of the research and thus ignored. The crosshead position and velocity during closing and opening can be seen in Figure 2.5 and Figure 2.6 respectively. The dry cycle time (net moving time) is 1.86 seconds.

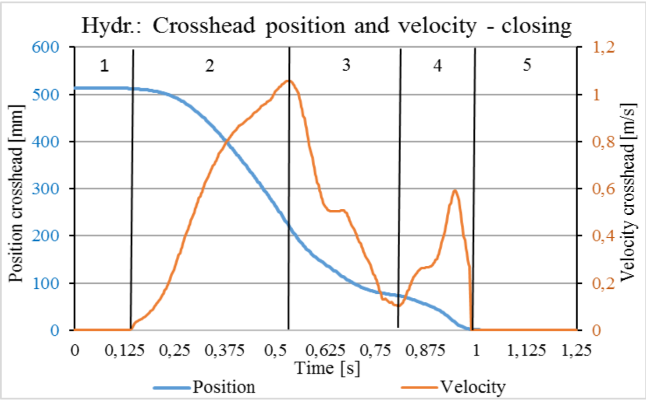

Figure 2.5, position and velocity during closing the crosshead

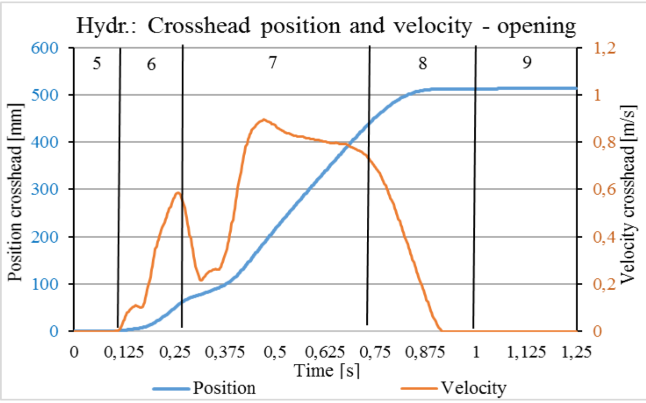

Figure 2.6, crosshead position and velocity during opening

The indicated processes are described in the following summary:

1. Mold fully opened, starting position.
2. Accelerating to close the mold.
3. Decelerating, slow-closing approach to protect mold and prevent harsh joining.
4. Mold is already closed, crosshead translates further to lock the mechanical mechanism.
5. Injection process (injecting, cooling, plasticizing, and decompression).
6. The crosshead is starting to translate and unlock the mechanical mechanism.
7. The mold opens, accelerates, and holds speed rearward.
8. Decelerating to starting position.
9. The mechanism is fully opened, ejecting the product.

2.2.2 Controls

The hydraulic cylinder is controlled by a proportional hydraulic valve, whose control voltage fluctuates between -10 V and 10 V. Also, the system contains a differential switched valve. An activated differential valve is causing the fluid to directly flow from one side to the other side of the piston, resulting in a fast operation. If the differential valve is closed, the fluid is rejected to the tank and the system delivers the maximum force. The latter described processes and the operating pressures during the closing and opening movements can be seen in Figure 2.7 and Figure 2.8, respectively. The control behavior is indicated by the control valve voltage. The hydraulic control scheme can be seen in Appendix A.

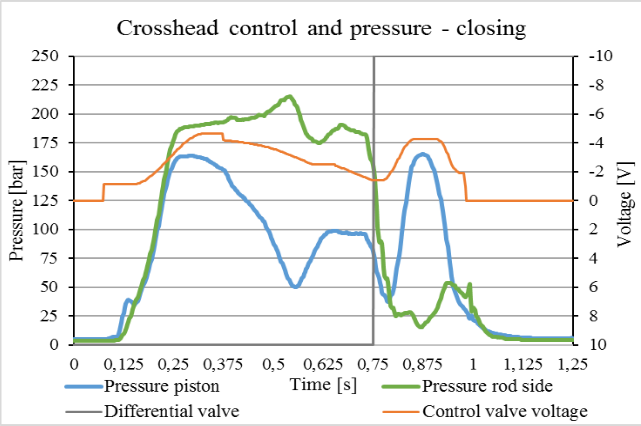

Figure 2.7, Crosshead control and pressure during closing

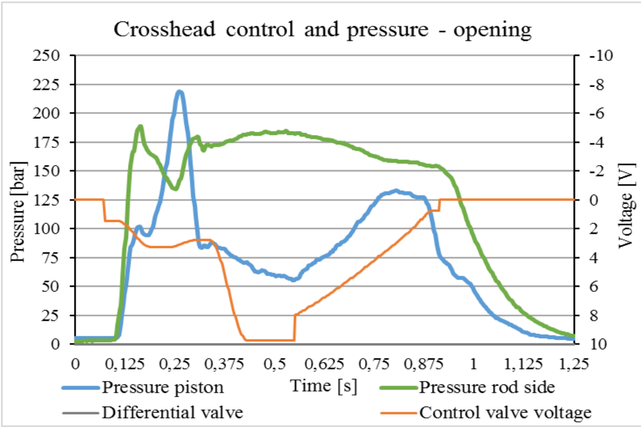

Figure 2.8, Crosshead control and pressure during opening

2.2.3 Hydraulic efficiency loss

The hydraulic pump is continuously supplying the hydraulic accumulators, which can deliver a lot of power in a short period of time. However, not all pressure is required to regulate the system accurately and in a controlled manner, so the first loss is throttling. Lowering the hydraulic pressure in the batteries to prevent throttling loss is not an option, the maximum pressure is required at peak loads. Figure 2.7 shows the use of only 40% during the closing process, losing a significant part of the energy. The throttled energy must also be cooled, this takes a lot of power too. In addition, the kinetic and spring energy cannot be absorbed with the hydraulic drive. In truth, energy is needed to absorb these forces. All these factors are causing a low hydraulic efficiency.

2.2.4 Hydraulic drive performances

The pressure and the force are nonlinearly related to the piston diameter. The piston bore of this particular hydraulic cylinder is 115 mm, the rod diameter is 80 mm. The relation between the force F_c and the surface diameter $d_{p,r}$ is described by equation 1. The power P_c can be determined using equation 2.

$$F_c = \frac{\pi}{4} * p * (d_p^2 - d_r^2) \qquad (1)$$

$$P_c = F_c * v_c \qquad (2)$$

The latter determined system properties are graphed in Figure 2.9 and Figure 2.10, respectively. The required clamping force is 160 kN and the maximum required power is approximately 90 kW.

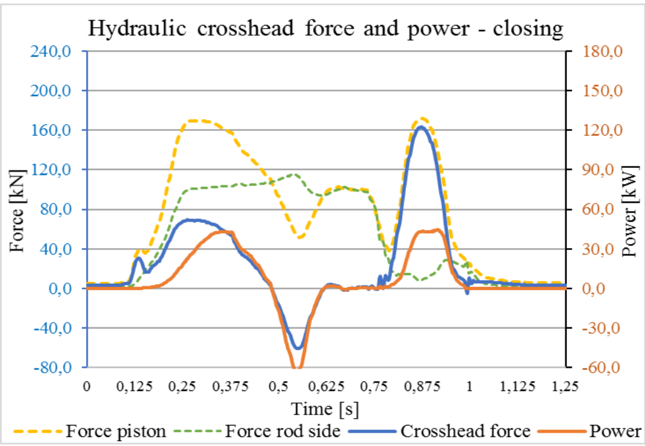

Figure 2.9, force and power during closing the crosshead

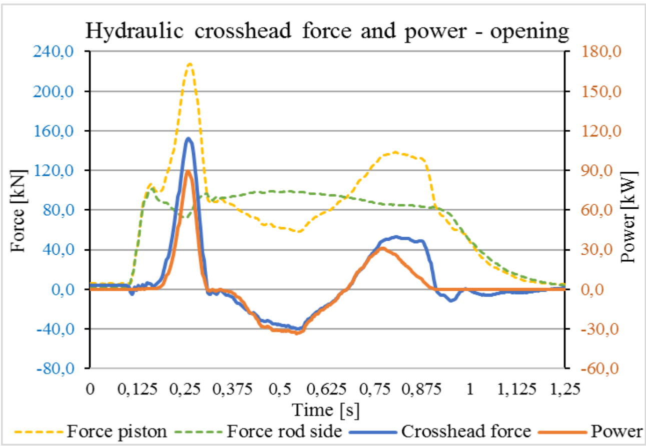

Figure 2.10, Crosshead force and power during opening

2.3 Electric system and control

A well understanding of the electric drive plays a critical role in the design phase, wherein this electric drive is redesigned. This paragraph looks into the working principles, is analyzing test data of the electric machine, performs calculations, and concludes drive requirements.

2.3.1 Electric system working principles

The electrical system consists of, listed starting from the energy grid, a regeneration unit, a frequency inverter, and an electric motor. Between the steps, the current is filtered and transferred multiple times (KEB Automation KG, 2016, 2017a). Figure 2.11 shows a schematic overview of the electric system.

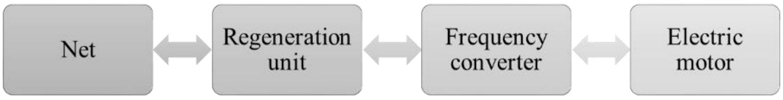

Figure 2.11, Schematic overview of the electric system

Excess kinetic energy is normally dissipated through friction (braking), but this unused energy has a valuable potential. Using a regenerative unit, the regenerated energy can be fed back into the main power supply line (KEB Automation KG, 2017b). The position and the speed of the crosshead during closing and opening the mold, can be seen in Figure 2.12 and Figure 2.13 respectively.

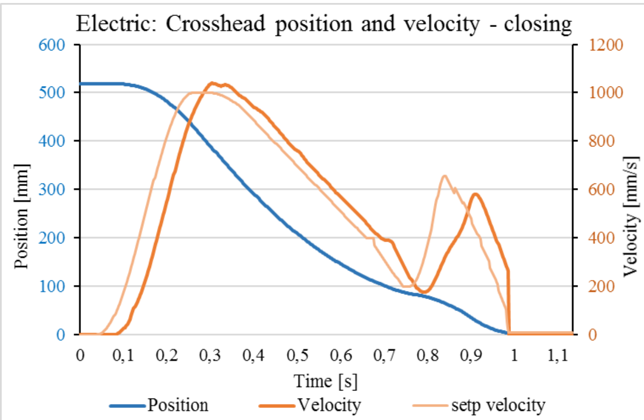

Figure 2.12, crosshead position and velocity while closing

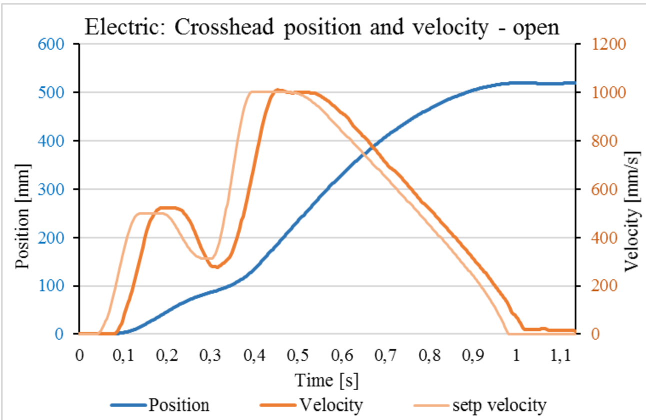

Figure 2.13, crosshead position and velocity while opening

Since the dynamic behavior is known, the control does not consist of a feedback-based control circuit, but is feedforward controlled. The desired crosshead speed is calculated to a corresponding motor rotation speed, which is linearly related to the added current to the motor. The speed follows the setpoint well (with a small time delay), the electrical velocity phases are equal compared to the hydraulic behavior in Figure 2.5 and Figure 2.6.

During the process, the crosshead (CH) and the mobile clamping plate (LSP) are driven. Phases either require (+) or generate energy (-), which is schematically shown in Figure 2.14. During deceleration, the LSP is overhauling. This kinetic type of energy must be braked or smartly reused.

	Accelerating CH/LSP	Decelerating CH/LSP	Locking CH	Injection molding	Unlocking CH	Accelerating CH/LSP	Decelerating CH/LSP
E_{rot}	+	-	+		+	+	-
E_{kin_CH}	+	-	+		+	+	-
E_{rot_LSP}	+	-				+	-
E_{strain}			+		-		

Figure 2.14, Energy usage per phase

2.3.2 Testing data reliability

The measured test data has been converted internally within the machine. The conversion factor is known, but is checked to validate the reliability of the experiment. Matlab is used to write a vector analysis code, that compares the data samples with data measured in the correct unit at random intervals. The code is added in Appendix B, the results can be seen in Figure 2.15. Besides one unreliable outlier and difficult measurable values around 0 Nm, the factor has been validated as 0.008 [-]. The measured test data is multiplied by this factor and further used in the analysis.

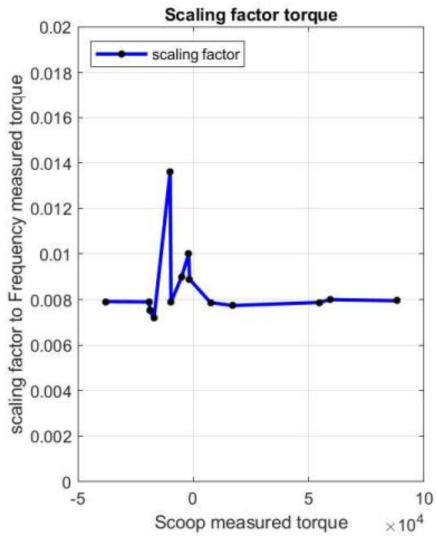

Figure 2.15, Scaling factor test data

2.3.3 Electric closing unit performance

The used electric motor is a Baumüller water-cooled three-phase synchronous motor with a nominal power P_{nom} of 70 kW. The nominal torque M_{nom} of 360 Nm is delivered at a nominal current I_{nom} of 135 A. The motor is overloaded to a maximum M_{max} 665 Nm at I_{max} of 300 A (Baumüller, 2013a, 2013b).

Different performances of the machine can be determined from the test data. The rotation speed of the motor n_m in rpm can be determined by dividing the crosshead speed v_c in m/s by the gear ratio i_g of 20,92 mm/rot, shown in equation 3. The total power P_{tot} in kW can be determined by using equation 4.

$$n_m = \frac{v_c * 10^3}{i_g} * 60 \quad (3), \qquad P_{tot} = T_m * n_m * \frac{2\pi}{6(10^4)} \quad (4)$$

The electric drive is known for its power-demanding inertia. To analyze the net energy on the crosshead, the rotational energy E_{rot} must be subtracted from the total energy. The rotation energy in J can be determined using equation (5). To obtain the rotation power, the energy is differentiated over time. To prevent a noisy graph characteristic of the data in vector form, a simple moving average is used to analyze the energy. The n_{th} rotational power $P_{rot\_MA\_n}$ sample is determined using the sum series over N = 12 periods in equation 6.

$$E_{rot} = \frac{1}{2} I_m \omega_m^2 = \frac{1}{2} I_m \left(\frac{n_m}{60} * 2\pi\right)^2 f \quad (5), \qquad P_{rot\_MA\_n} = \frac{1}{N} \sum_{k=0}^{N-1} \frac{dE}{dt}_{n-k} \quad (6)$$

The crosshead force F_c can either be determined by the crosshead power or the torque, both shown in equation 7. The energy used in a cycle can be determined by integrating the power over time, shown in equation 8.

$$F_c = \frac{1}{v_c}\left(P_{tot} - P_{rot\_MA\_n}\right) = \frac{P_c}{P_{tot}} * \frac{2\pi * T_m}{i_g} \quad (7), \qquad E_{tot,\ rot,\ ch} = \int_{\Delta t} P_{tot,\ rot,\ c}\, dt \quad (8)$$

The crosshead energy can be subtracted into two minor energy-demanding elements. The kinetic energy of the moving parts and the strain energy of the tie-bars, calculated using equation 9 and equation 10, respectively.

$$E_{kin} = \sum_{k=1}^{N} \left(\frac{1}{2} * m_c * ({v_n}^2 - {v_{n-1}}^2)\right)_n \quad (9), \qquad E_{strain} = \frac{F^2 * l_{tiebar}}{2 * Y_{young} * 4 A_{tiebar}} \quad (10)$$

The calculated time-dependent system properties can be seen in Figure 2.16 and Figure 2.17. A positive or negative force or power refers to the direction of the variable. A positive value indicates a parameter towards the crosshead, while a negative value indicates the direction away from the crosshead. The mold is moving forward during the closing movement, causing is positive power while accelerating. During opening, the mold is moving backwards, causing a negative power during acceleration. So, the negative energy during closing and the positive energy during opening can be regenerated.

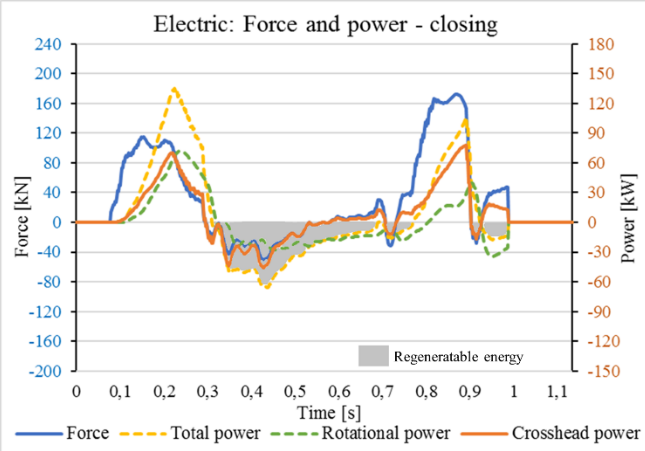

Figure 2.16, Electric force and power while closing

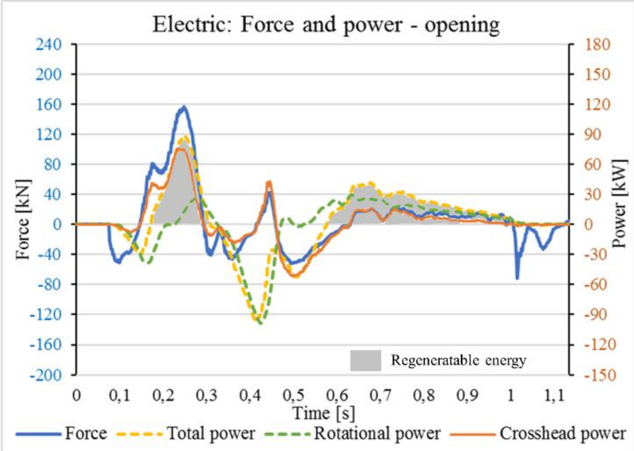

Figure 2.17, Electric force and power while opening

2.4 Minimal system performance

In conclusion from the research conducted in this paragraph, the maximum clamping force of the crosshead is 160 kN. The energy can be calculated using the earlier described equation 8. The required energy to perform one cycle is 32.1 kJ. The electric motor working as a generator during the recovery of kinetic and rotational energy is resulting in a energy regeneration of 81% (26.0 kJ). The rotational energy usage has a part of 28.3% with 9.08 kJ per cycle. The rest of the energy is used for the crosshead, wherein it is subdivided into kinetic energy, frictional energy loss, and strain energy.

3.Drive concept design

To design a good concept, the molding machine market and existing patents are researched first. Thereafter, the process is analyzed and functions are formed. Design parameters are researched, design considerations are examined using a morphological approach, and a concept is weighted out of three potential options. The general question answered in this chapter is: What is a suitable hybrid drive concept?

3.1 Market and patent research

Injection molding is an extensively used technique. As a result, there are also many manufacturers of injection molding machines. The market research looks at striking drives of competitor injection machine manufacturers.

3.1.1 Market research

The three most interesting findings from the market research are listed in the following summary, more about the market research can be found in Appendix C.

1. In ***ARBURG*** machines, the mold opening and closing are servo-electrically driven, the injection and secondary axis are hydraulically driven (ARBURG GmbH + Co KG, 2021a). Using an electrical drive, the kinetic breaking energy can relatively easily be regenerated. The system setup is 40 percent more energy efficient compared to a fully hydraulic driven machine (ARBURG GmbH + Co KG, 2021b).
1. ***HAITIAN Plastic Machinery*** produces full hydraulically driven machines. The hydraulic system (servomotor + gear pump) is claimed to be 70 percent more energy efficient compared to a classical hydraulic driven machine. The energy efficiency is achieved by not using accumulators. The direct drive connection between the servo-motor and the gear pump provides a combination of drive torque and required acceleration speeds (HAITIAN Plastic Machinery, 2021).
2. The ***NETSTAL ELIOS*** is using two additional hydraulic cylinders in addition to the electrical closing unit drive. The exact working and patent limitations are described in the next paragraph.

3.1.2 Patent limitations

The NETSTAL ELIOS machine is hybrid-driven. The particular type of drive is patented as a United States patent No.: US 10,112,331 B2 (Angst et al., 2018). The system setup is schematically sketched in Figure 3.1. The patent limits explicitly prohibit the use of an electric drive operatively connected with the crosshead **together** with a hydraulic drive including a piston cylinder which is operated by a pressure fluid (Angst et al., 2018). The kinetic energy during the braking flows into the electric motor and is converted into hydraulic energy by the hydraulic cylinders (KraussMaffei, 2021). The operation principle is further described in Appendix C.

Important system elements:

5. Cross clamp
10. electric drive with rod
11. piston cylinder system
13. hydraulic supply
14. control to hydr. and elec.
20-22. hydraulic valves
23. accumulator
24. pump
25. pressure medium source

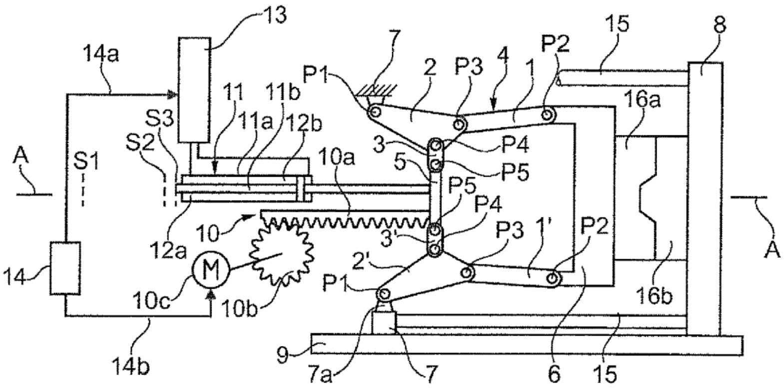

Figure 3.1, schematic overview NETSTAL ELIOS (Angst et al., 2018).

3.2 Design methodology

A suitable and appropriate design method must be selected for the design of a new closing unit drive. Due to the objective and the scope of the project, many parameters are out of interest. For example, energetic behavior is important, but many mechanical aspects are out of scope. At first, all the energy-related functions of the drive are examined, wherefrom three sub-functions emerge. Solutions are designed for the sub-functions: the behavior of the system in terms of delivery, recovery, and buffering of energy.

3.2.1 General function diagram

The design of the drive is based on the feed-forward controlled crosshead velocity. The function diagram is shown in Figure 3.2. A distinction is made in speed characteristics, energy transition, and energy release/supply, marked in blue, white, and yellow, respectively.

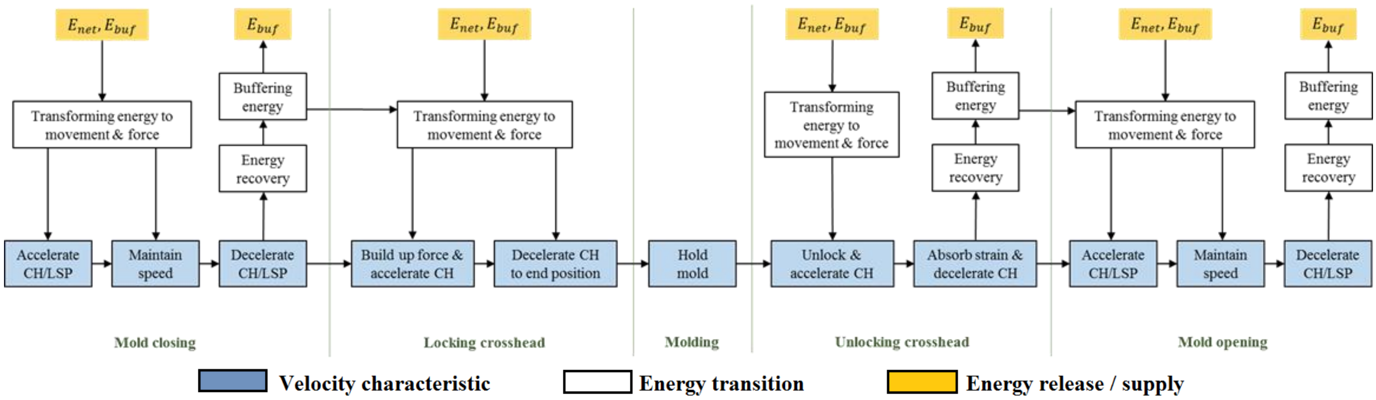

Figure 3.2, system function and energy analysis

3.2.2 Sub-functions

The functions related to energy transitions are summarized to three different basic functions: supplying energy, generating energy, and storing energy. Separate solutions can be devised for each of these latter described sub-functions. The sub-functions are shown in Figure 3.3, the figure recurs several times in this chapter and is constantly being expanded. The sub-functions are analyzed separately in the following three sections.

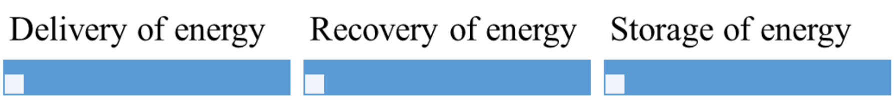

Figure 3.3, sub-functions

3.3 Sub-function analysis; Supply of energy

Considering the supply of energy to the system, five possible drive solutions are listed in Figure 3.4. However, purely hydraulic and electric are already being produced and are therefore not considered. A mechanical drive (usage of potential or kinetic energy) is judged as technically unfeasible because the movement/force takes place in two directions and happens in very short periods. Due to these factors, the research only focuses on a hybrid drive in terms of an electric and hydraulic combination. Unfeasible concepts are left out by making these choices in the initial stage of the research. This leaves sufficient time to develop a hybrid concept in a logical direction towards a promising concept. Concluding, only a combination of electric and hydraulic drives in series or parallel are further analyzed.

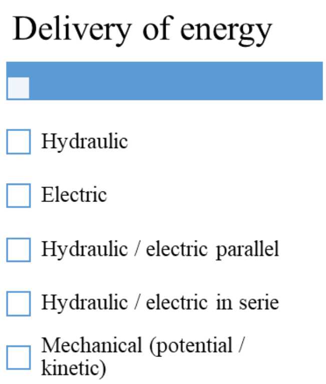

Figure 3.4, Delivery of energy

3.3.1 Hybridization

Generally, in hybrid systems, the braking energy loss is stored in an energy storage device, and the energy is reused effectively in the system (Chen, 2015). The hydraulic hybrid systems are subdivided into two categories: Parallel Hybrid (PH) and Series Hybrid (SH) (Ramakrishnan et al., 2012; K. E. Rydberg, 2009; Valente & Ferreira, 2008). This section covers both topics.

Parallel hybrid

PH allows both the electric motor and the hydraulic motor to deliver torque to the system, both the hydraulic pump and the electric motor are mounted on a single gearbox that drives a geared rack. The possible configurations during the displacement of the LSP and the locking process can be seen in Table 3.1. Selecting the appropriate drive configurations at the right phases can result in different working configurations. The PH has two impulsion devices, a hydraulic and an electric motor. Also, a smaller-sized electric motor can be used to obtain the same performance, wherein electric energy storage is worn out more slowly (Burke, 2007; Chan, 2007; Chan et al., 2010). Since the current electric motor on the molding machines is very large, purchase prices can drop significantly if the motor is slightly lighter in power.

Drive configurations – displacement of the LSP	*Drive configurations – force build-up*
1. Movement purely electric	1. Force build-up purely electric
2. Movement purely hydraulic	2. Force build-up purely hydraulic
3. Movement hybrid	3. Force build-up hybrid

Table 3.1, drive configurations during force build-up or the displacement of the LSP

Series hybrid

A search of the literature revealed some studies which focused on closed hydraulic circuits in vehicles to recover breaking energy. Although these processes take much longer than the braking period of the molding machine, it is worth researching the latest findings. In a series-designed drive, the hydraulic motor is controlled by the servo-driven hydraulic transmission (HT). A servo-electric drive can directly control the fixed-displacement hydraulic-pump speed instead of a traditional proportional valve (Tatiana Minav et al., 2014). Various system structures can be designed in which a combination of (variable) pumps/motors provide the drive.

The pump-controlled hydraulic system is categorized into two different systems: open-loop circuit type and closed-loop circuit type (Quan et al., 2014). An open-loop system can be combined with the other hydraulic systems on the injection machine, thus the system draws its fluid from the general reservoir and does not need an additional conditioning system. A secondary-controlled open-loop system is characterized by a high-pressure coupling, the flow is transferred without throttling from the primary side. By connecting a hydraulic accumulator on the high-pressure side, energy can be recovered when lowering or decelerating a load (Mahato & Ghoshal, 2020). Thus the flow and direction of the flow can be changed by controlling the displacement setting of the secondary unit "over zero" (K.-E. Rydberg, 2007). Figure 3.5 shows an open and a closed-loop system, wherein the inertia and the flywheel represent the kinetic behavior of the LSP.

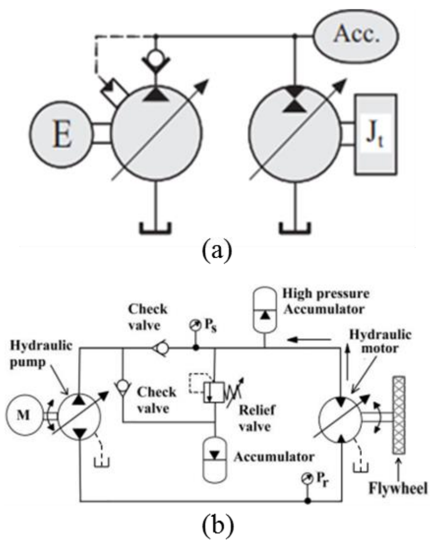

Figure 3.5 (Mahato & Ghoshal, 2020), *a. Open loop, secondary motor control; b. CPR-HST during braking*

In a closed hydrostatic transmission (HST), the torque can be transmitted in both directions, thus allowing hydrostatic braking. High stiffness, high efficiency, and controllability are the main advantages, but the need for active pump/motor control and cooling system still requires quite high power consumption (K.-E. Rydberg, 2007). This system is also known as a common pressure rail system CPR, wherein the system is connected by a high-pressure line and a low-pressure line. A high-pressure rail is directly connected with a high-pressure accumulator, whereas a low-pressure line is connected with the reservoir or a low-pressure accumulator. The pressure of the system is mainly controlled by the hydraulic pump, whereas the secondary unit controls the speed of the load by adjusting its displacement (Mahato & Ghoshal, 2020).

The hydraulic motor can either drive the load to accelerate and work as a pump to decelerate and store energy. Therefore, the rotary load can be controlled by the variable-displacement pump/motor. The accumulator is used for twin purposes, storing the recovered energy and generating system pressure as per the demand. The stated control principle is known as *Secondary Control* (Shen et al., 2013; Vael et al., 2000).

Research establishes that the energy recovery potential is dependent on the displacement of the pump/motor and varies from 32% to 66% (Mahato & Ghoshal, 2020). An improved CPR system is shown as b. in Figure 3.5 (Do & Ahn, 2011). Simulation results show that the regenerative efficiency of the stated system is about 63.4% as compared to the conventional HST system (Mahato & Ghoshal, 2020).

3.4 Sub-function analysis; Recovery of energy

It is desirable to recover energy with the same systems used to drive. Otherwise, additional expensive systems must be added, like a kinetic energy recovery system (KERS), making the concept unattractive and unfeasible. In addition, the recovered energy is re-used by the drives. Therefore only electric and hydraulic recovery of energy is considered.

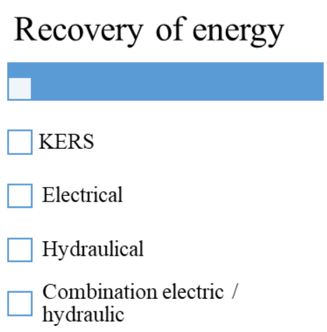

Figure 3.6, Recovery of energy

The basic idea of energy regeneration systems is to convert kinetic and potential energy to other types of energy (T. Minav et al., 2011). In this particular case, the kinetic energy of the LSP and the mold can be recovered. Parallel hybrid and series hybrid drive systems can both be divided into two categories. Namely, series electric hybrid (SHE), parallel electric hybrid (PEH), series hydraulic hybrid (SHH), and parallel hydraulic hybrid (PHH) (Mahato & Ghoshal, 2020).

3.4.1 Electric energy recovery

While lowering a mass in a potential energy recovery system, the potential energy forces a hydraulic motor to function as a pump, or an electric motor to act as a frequency-converter-controlled generator (T. Minav et al., 2011). A kinetic energy recovery system works the same, the load is overrunning compared to the controlled motor. For example, the LSP and the mold must decelerate before the mold closes, but due to the kinetic energy of the heavy weighting LSP, the rotor in the electromotor is overrunning on the controlling stator. The latter occurring process is generating a slip between the motor elements, resulting in a torque opposite to the direction of rotation. This torque can be converted by the motor as reverse current when the motor is used as a generator.

3.4.2 Hydraulic energy recovery

Since the 1990s, combinations of pressure valves, variable displacement pumps, and pump control have provided opportunities to reduce energy consumption in hydraulic systems (Liang, 2002). The accumulator used in a HH (hydraulic hybrid) system has high power density as well as faster charging capability of regenerated energy in comparison to the EH (electrical hybrid) system. Therefore an electrical system can have less energy recovery efficiency (K. E. Rydberg, 2009). Consideration must be given to the way electricity is reused. Electrical power is currently being returned to the grid.

3.5 Sub-function analysis; Storage of energy

Energy regeneration is possible by transferring energy to hydraulic accumulators, electric batteries (May, 2006), or a combination of different storages such as super capacitors and flywheels (Cross & Hilton, 2008). A direct application of the hydraulic accumulator has more limiting factors than the indirect recovery system (Juhala et al., 2009; Sinkkonen et al., 2011), the potential regeneration pressure from the crosshead is not continuously usable to charge hydraulic accumulators. However, an indirect recovery system contains more energy transversions and thus drops in efficiencies (Tatiana Minav et al., 2014).

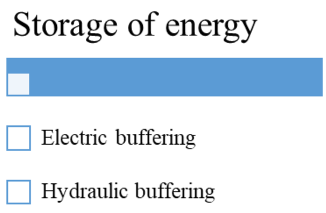

Figure 3.7, Storage of energy

Because of the relatively short recovery periods on the closing unit (milliseconds), recharging of conventional lead-acid batteries is considered inefficient (Isidor Buchmann, 2021). Besides, a super-capacitor is another energy storage device that provides higher power density and life longevity, but more expensive and comparatively less reliable as compared to the battery (Kim, 2008).

3.6 System drive concept

The sub-functions analysis leads to more in-depth knowledge and a theoretical basis to design a new drive. As a result of the sub-function analysis, a broad understanding and generation of design parameters originate. Important design parameters and realistic solutions are identified and summarized in a morphological scheme in Table 3.2. Hereafter, three concepts are formed by combining solutions for the parameters.

<table>
<tr><th>Design parameter</th><th colspan="6">Solutions</th></tr>
<tr><td>Type hybrid drive</td><td colspan="3">Elec. / hydr. parallel</td><td colspan="3">Elec. / hydr. series</td></tr>
<tr><td>Energy regeneration to</td><td colspan="2">Electric
Net</td><td colspan="2">Electric
Super capacitors</td><td colspan="2">Hydraulic
Accumulator</td></tr>
<tr><td>Hydraulic system</td><td colspan="3">Closed (separate)</td><td colspan="3">Open (combined injection)</td></tr>
</table>

Table 3.2, morphological scheme of the design parameters

Three concepts arise by combinations of system solutions, which are shown schematically in Figure 3.8. The three concepts combine electric and hydraulic drives. A hydraulic motor is used in consideration of the Netstal patent, which limits the use of an electric motor in combination with hydraulic cylinders. The concepts are explained individually after the figure.

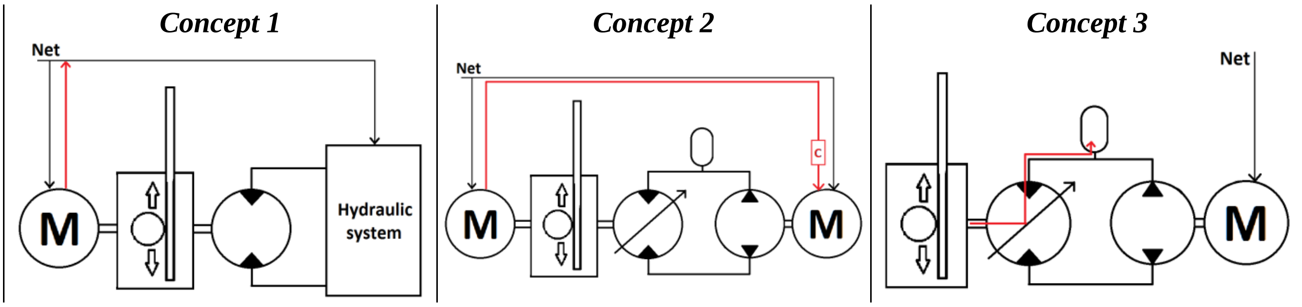

Figure 3.8, system drive concepts

- **Concept 1, Parallel** driven, **open** hydraulic system, **electric** regenerated, to **the net.**
  An electric and hydraulic drive both connected to the gearbox. Energy can be supplied both electrically and hydraulically. This makes it possible to move electrically in an energy-efficient manner and with powerful hydraulics in other phases. Energy is recovered by using the electric motor as a generator supplying to the net, the hydraulic system works from the net, using the energy directly.

- **Concept 2, Parallel** driven, **closed** hydraulic system, **electric** regenerated, to **a buffer.**
  The crosshead is driven in the same way as in concept 1, only the energy is electrically stabilized and hydraulically buffered. The hydraulic system functions as a closed hydraulic transmission.
- **Concept 3, Series** driven, **closed** hydraulic system, **hydraulic** regenerated, to **an accumulator.**
  Concept 3 uses a series electric and hydraulic drive, resulting in a servo-electrically driven hydraulic pump. In this concept, the low inertia of the hydraulic system is combined with the flexibility of the electrical system. Energy can be regenerated by changing the displacement of the pump 'over zero'.

3.7 Concept selection

To choose the most suitable concept for this particular machine, an S-diagram method is used, also known as a Kesselring method. By using this method, the three concepts are compared in a substantiated way. Choosing a concept is subjective. There is simply no time to thoroughly develop, test, and evaluate each concept objectively. However, by applying the method, a comparison is made on various weighted aspects, resulting in a substantiated final score. In the S-diagram, a distinction is made between functional aspects and realization aspects. Under functional aspects, the energy efficiency, the power possibilities, and the work configurations are taken into account. The costs, controllability, and system complexity are included under the realization aspects.

The analysis of the concepts and a completed assessment-criteria table are executed in Appendix D. Various conclusions can be drawn from the S-diagram in Figure 3.9. Concept 1 scores well on functionality due to the high power range of the dual drive and excellent energy efficiency. Concept 2 scores even better here due to less loss of efficiency in the fully variable hydraulic system. Concept 3 scores the least well in terms of functionality due to the loss of efficiency in the hydraulic storage of energy and due to the power limitations of the single drive. In terms of realization, concept 2 scores least well due to the high costs of both a separate hydraulic and an electrical system and the additional complexity. Concept 1 and 3 score equally well, while concept 1 is cheaper in terms of costs, and the simpler concept 3 scores better in controllability.

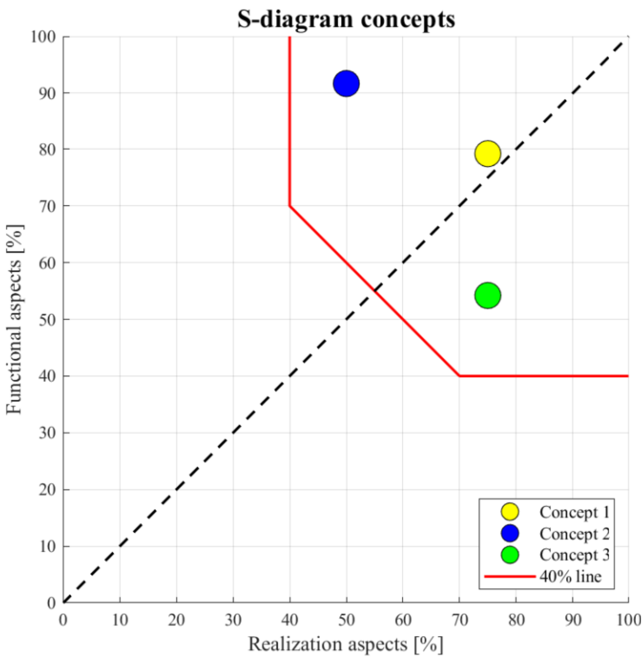

Figure 3.9, S-diagram concepts

3.8 Conclusion

The analysis had found that concept 1 fits the best for the new drive. A parallel drive where the hydraulic circuit is combined with the already present hydraulic system is concluded to be the best solution. The concept has high power capabilities and no extra costs of a separate hydraulic system. Also, the electric regenerated energy is not buffered but directly used by the hydraulic system. The concept is further specified and dimensioned in the next chapter.

4. Dynamic behavior in configurations

A larger or smaller electric and hydraulic drive results in different dynamic behavior. The third research question is answered in this chapter: How does a change in motor power affect the system behavior in speed, time, and energy? Therefore, the dynamic behavior is calculated in different drive configurations and the system properties are examined for different ratios between the electric and hydraulic motor. Also, effects in cycle time, energy consumption, and required power are calculated for variating speed characteristics. In this manner, ratios are examined between the electric and the hydraulic motor. A MathCad 15 model is used to simulate the process.

4.1 Approach strategy

First of all, a model is set up in which the tested speed data from the machines is serving as input for the model. This simulates the exact speed pattern of the current machines, like the green-colored line $v_v(i)$ in Figure 4.2. In this model, the powers are calculated and compared with the measured power. This step is crucial in validating the reliability of the calculation model. Secondly, a variable simulation model is created with an adjustable speed pattern that approximates reality. After this model is accurately built, the acceleration and deceleration speeds can be adjusted to analyze the dynamic behavior.

4.2 Ideal Physical Model

An Ideal physical model (IPM) of the machine is shown in Figure 4.1. The moving masses (m) and inertias (J) are displayed as blocks. The transmission ratios (i), moving directions (x), and energy directions (E) are displayed as well. In this paragraph, the transmission relation and the energy calculations are discussed.

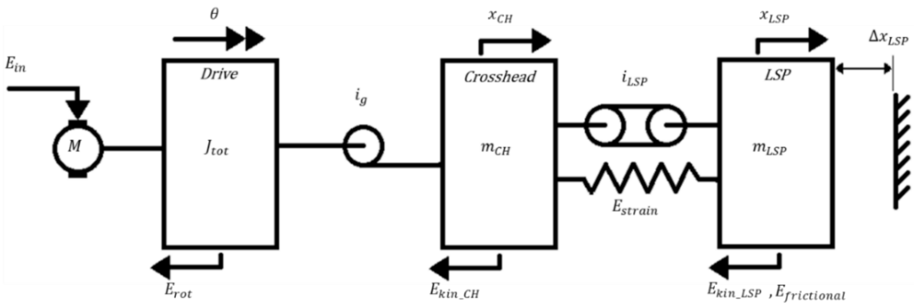

Figure 4.1, Ideal physical model

4.2.1 Transmission ratios

The gear ratio from the rack and pinion is 20.92 mm/rot, so the crosshead is linearly translated with 20.92 mm by every rotation of the electric motor. The gear ratio between the crosshead and the LSP is more complicated. However, it is important to precisely investigate the transmission ratio, the heavy LSP and the mold have a large share in the energy consumption. The speed of the crosshead $v_v(i)$ and the LSP $v_{LSP}(i)$ can be seen in Figure 4.2, together with the position of the crosshead $X_{ch}(i)$ and the LSP $X_5(i)$. A schematic representation of the transmission is shown in Figure 4.3, wherein the pivots are

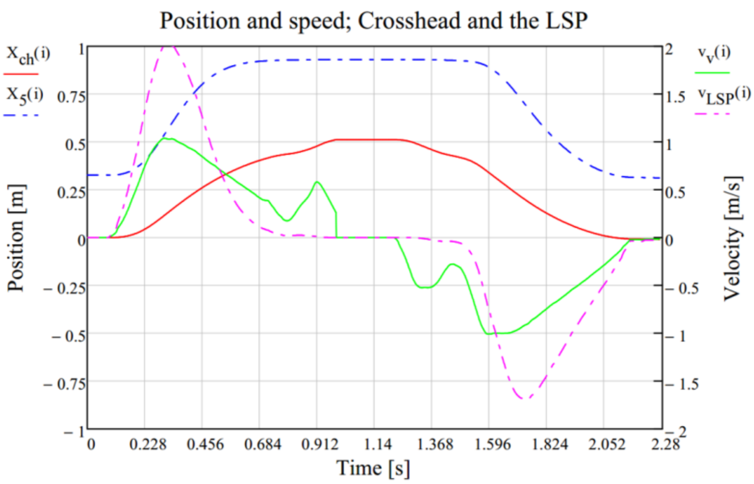

Figure 4.2, position and speed of the crosshead and the LSP

shown as black circles. Points 1 and 5 moves along the x-axis and represent the crosshead and the LSP, respectively. Point 4 is a static pivot point on the rear clamping plate. The toggles are represented by line 1-2, line 3-5, and triangle 2-3-4. The position of the LSP is set up as a function of the position of the crosshead using trigonometric calculations, this can be seen in Appendix E.

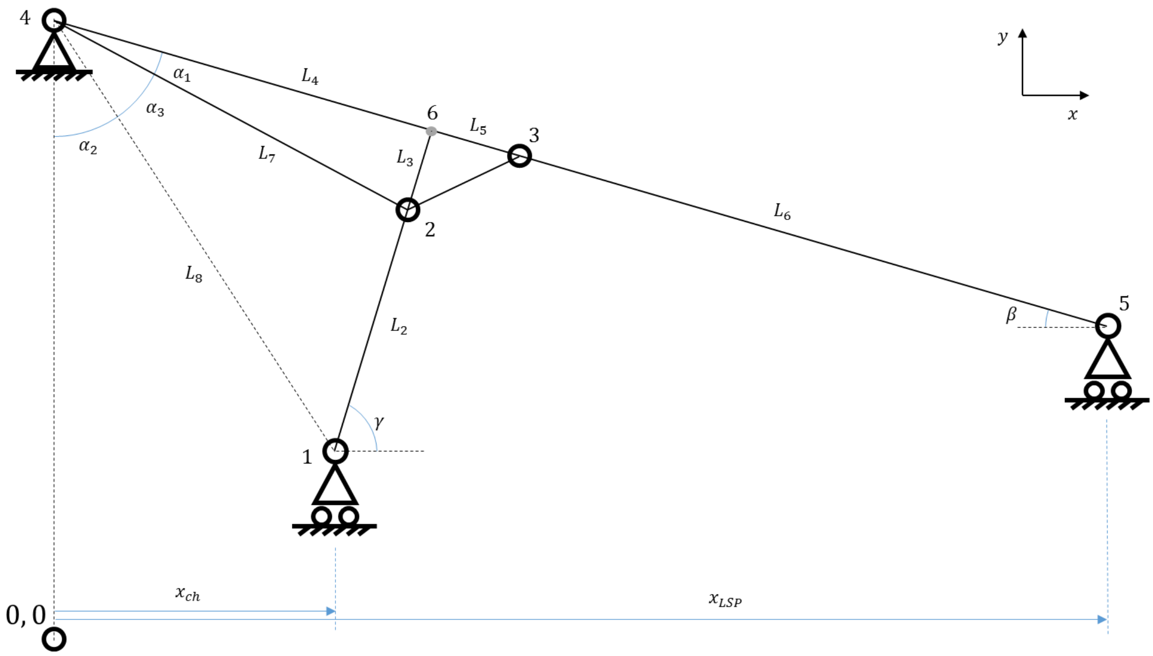

Figure 4.3, Schematic representation of the crosshead and the LSP

4.2.2 Rotational energy

The rotational energy can be calculated using equation 11. The rotational inertia of the electric motor I_m (valued as 0.178 kg·m^2 (Baumüller, 2013a)) is multiplied by a factor of 1.1 [-] for the unknown inertia of the gears in the gearbox. The direction of movement f is also included by multiplying the equation by 1 or -1.

$$E_{rot}(i) = \frac{1}{2} * I_m * n_m(i)^2 * f(i) \quad (11)$$

4.2.3 Kinetic energy

The kinetic energy is a result of the acceleration and deceleration of the crosshead and the LSP. In equation 12, these different masses m are multiplied by the corresponding velocity v. The LSP is not moving during closing, so in these time instances, this part of the formula is multiplied with 0 by the $status_{LSP}$.

$$E_{kin}(i) = \frac{1}{2} * (m_{ch} * v_{ch}(i)^2 + (m_{LSP} + m_{mold}) * status_{LSP} * v_{LSP}(i)^2) * f(i) \quad (12)$$

4.2.4 Strain energy

During closing, the tiebars are stretched considerably. Stretching the tiebars is in the end the force that keeps the mold parts together during the injection process. The required force and energy of this movement are simulated by a linear stretching spring up to the maximum strain in Figure 4.4.

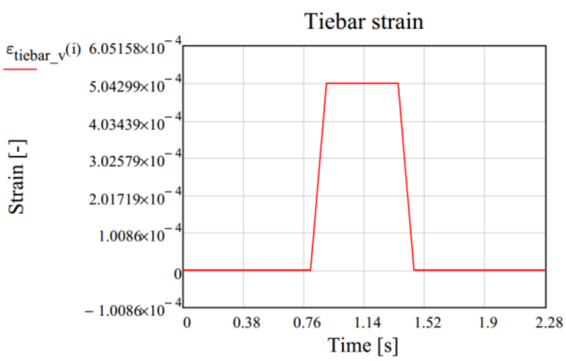

Figure 4.4, tiebar strain

The stretching Δl can be calculated by multiplying the original tiebar length l_{tb} with the strain, in this case, the force F_{tot} divided by four tiebar areas A_{tb} and Young's modulus Y of steel. The calculations are shown in eq. 13 and eq. 14.

$$\Delta l(i) = l_{tb}\, \varepsilon_{strain}(i) = l_{tb} * \frac{\sigma(i)}{Y} = l_{tb} * \frac{F_{tot(i)}}{4A_{tb}} \frac{1}{E} \quad (13), \qquad E_{strain}(i) = \frac{1}{2}\, 4A_{tb}\, l_{tb}\, Y * \left(\frac{\Delta l(i)}{l_{tb}}\right)^2 \quad (14)$$

4.2.5 Frictional energy loss

A frictional energy loss is estimated by comparing the calculated energy with the measured energy balance. Total frictional energy of 3 kJ is spread over the time instances where the LSP moves.

4.3 Power calculations

The required energy at every vector instance is calculated, so the power can now be obtained by calculating the change of energy over time. The energy signal is filtered first using a moving average in equation 15. Hereafter, the power is differentiated over time using equation 16. The weighted moving average prevents a noisy character and is crucial in the reliability of the result.

$$E_{x,\ MA}(i) = \frac{1}{w} * \sum_{j=i-w+1}^{i} E_x(j) \quad (15), \qquad P_x(i) = \frac{E_{xMA}(i) - E_{xMA}(i-1)}{t(i) - t(i-1)} \quad (16)$$

The rotation, kinetic, strain, and total power can be seen in Figure 4.5. The variating gear ratio is resulting in different weighting power effects. For example, during the closing movement, acceleration has a larger required power than deceleration as a result of the changing transmission ratio. As previously described in Figure 2.16 and Figure 2.17, a positive energy value during opening of the mold indicates regeneratable energy and a negative energy value during the opening movement represents required energy. This is the opposite during the closing movement of the mold

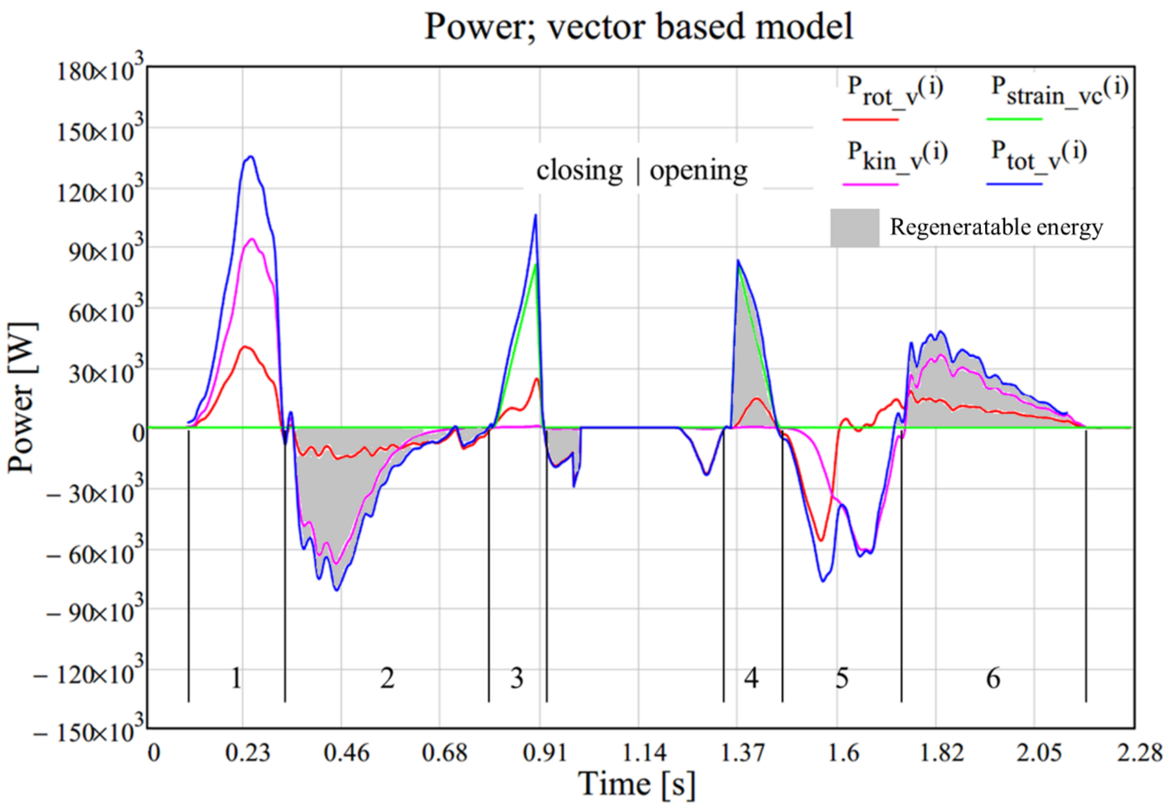

Figure 4.5, powers in the vector-based model

The indicated areas in Figure 4.5 represent the following phases:

1. Accelerating forward
2. Decelerating forward
3. Locking the crosshead
4. Unlocking the crosshead
5. Accelerating backward
6. Delerating backward

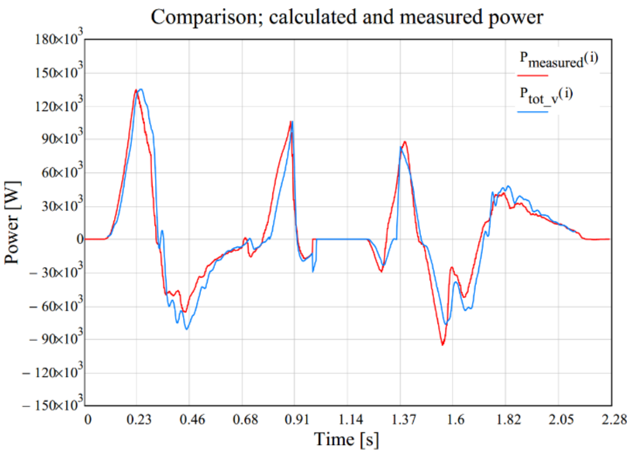

Figure 4.6, calculated and measured power

The calculated power is compared to the measured power in Figure 4.6. Similarities can be seen in the whole cycle, from which it can be concluded that the calculation is very reliable. No weight of the mold is included in this simulation. In the test setup, testing is also carried out without a mold, so this is necessary for the comparison.

The energy used in a certain time interval can be calculated by integrating the power over time. To obtain the energy from the vector-based result, the Riemann sum is used as shown in equation 17. The sum calculates the energy E_{tot} by summing the power P_x per sample time t_s between certain time units t_{start} and t_{end}. This form of calculation is reliable due to the weighted moving average of the characteristics taken earlier.

$$E_{tot} = \sum_{j=t_{start}}^{t_{end}} (P_x(i) * t_s) \qquad (17)$$

The required and generated energy per group and per phase are schematically shown in a table in Appendix E. The energy required for one closing movement within 1.86 s is 32.1 kJ. The distribution is as follows: rotational energy: 27.5%, kinetic energy: 47.9%, strain energy: 13.2%, and frictional losses: 11.4%.

4.4 Power characteristic variations

In the new drive concept, the available motor power changes, with the consequence that the cycle time and energy requirements also change. This section examines the effect of changing the accelerations during the closing and opening translation of the crosshead.

4.4.1 Model setup

A model is constructed in which the speed character can be adjusted by describing the speed as a function variating on time. First, a model has been tested wherein the speed approximates the tested crosshead speed. This speed is used in the previous calculation, wherefrom the results are reliable. The function-based model is the basis for the calculations wherein the accelerations are adjusted and is added in Appendix F.

4.4.2 Acceleration variations

If the drive is adjusted in power, less or more power is available to accelerate and decelerate during closing and opening. Since the recovery of energy is only performed with the electric motor, the deceleration speed is completely depending on the electric motor properties. The accelerations can be controlled both electric and hybrid, which opens up more drive configurations.

The variable calculation model is constructed in such a way that the acceleration speeds can be adjusted, without changing the travel distance of the crosshead. Iterations are performed with different accelerations, which can be seen in Appendix G. To properly analyze the results, a power-acceleration relation is shown in Figure 4.7 and the corresponding time-acceleration relation can be seen in Figure 4.8. Wherein acceleration 1/deceleration 1 stands for the closing movement, and acceleration 2/deceleration 2 represents the opening characteristics.

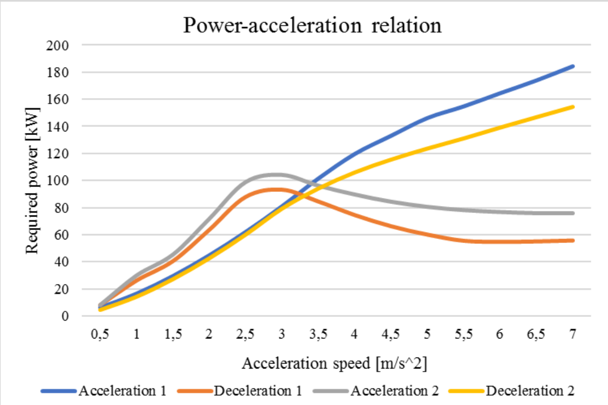

Figure 4.7, power-acceleration relation

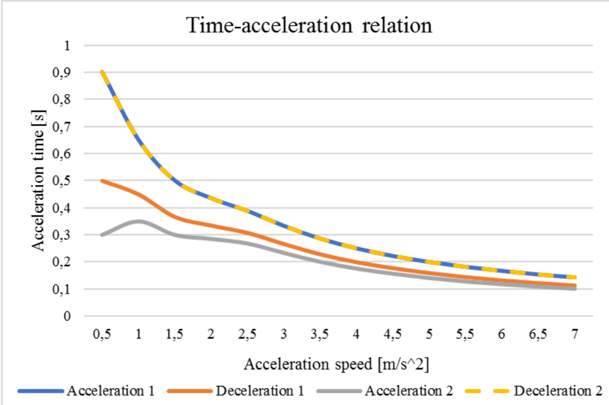

Figure 4.8, time-acceleration relation

A striking relationship can be seen during deceleration 1 (braking during closing) and acceleration 2 (accelerating during opening). By accelerating faster, less time and thus acceleration distance is required. This results in a different transmission ratio of the LSP to the crosshead. When accelerating/decelerating faster, the peaks of rotational energy and kinetic energy do not lie on top of each other, but consecutively. This reduces the required power. Acceleration 1 and decelration 2 has a linear relationship between increasing acceleration speed and power requirement.

The power is also compared directly against the effect in cycle time in Figure 4.9.

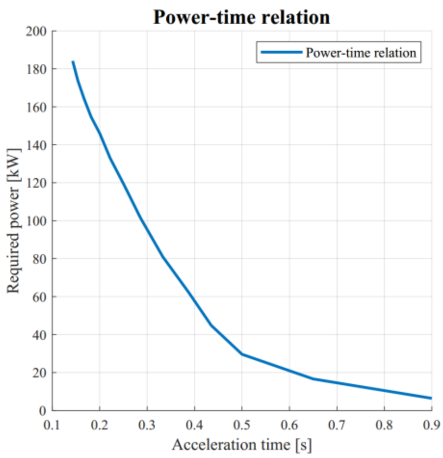

Figure 4.9, power-time relation

The machine must have the same or a faster cycle time than the current machine, but this is always possible in combination with a hydraulic motor. There is no fixed requirement in dry cycle time for the electric operating mode, in which the movement is only performed electrically. The latter is a trade-off for the customer between more efficient and slower versus less efficient and faster. The consequences of systems are tested in which electric motors are selected with a certain scaling percentage compared to the current electric motor (concept name: reference), further clarified in Table 4.1. The electric motors can be 80% overloaded, because they are not continuously under heavy loads and thus have time to cool down. The values in the table represent the available electrical power in the upcoming concepts.

Concept name	Percentage of current motor	Electrical motor power *[kW]*	+80% electrical overload *[kW]*
Reference	100%	70	126
$^{2}/_{3}$ concept	67%	55	99
$^{1}/_{2}$ concept	50%	35	63
$^{1}/_{3}$ concept	33%	23	41.4

Table 4.1, further evaluated configurations

4.5 Hydraulic system requirements

This section first discusses the structure of the hydraulic system. Hereafter, a calculation is performed to determine the hydraulic requirements.

4.5.1 Hydraulic system structure

The hydraulic system consists of a hydraulic motor with a fixed volume displacement. The flow is controlled by a proportional valve. In this case, the extra flexibility in the torque-speed ratio of a variable displacement motor is not profitable enough for the extra investment. This is partly due to the short operating time, and when it is used, almost the full power is used.

The hydraulic motor can function in two directions by the proportional valve. In addition, the hydraulic motor has an idle position. The hydraulic motor is permanently connected to the gearbox, so when the hydraulic motor is not in use, it rotates and displaces oil without a pressure difference. Here an idle power loss has to be taken into account.

4.5.2 Required hydraulic performance

During the locking process of the mold, a peak power of 100 kW is required. A safety factor *SF* of 1.2 [-] is taken to compensate for the uncertainties of the dual drive conjunction. A pressure drop over the pump Δp_{pump} is based on 200 bar. The rotation speeds are equal to the electric motor, assumed the hydraulic motor is connected to the first transmission step. The maximum rotation speed n_{max} is 2868 rpm, however, during closing this rotation speed is $n_{closing}$ 1651 rpm. The required hydraulic power P_{hydr} is calculated using equation 18. The required volume flow Q can now be calculated using equations 19 and 20. Equation 21 is used to approximate the motor displacement volume *vd*. The results and requirements are listed in Table 4.2.

$$P_{hydr} = P_{close} * SF - P_{elec} \quad (18),$$

$$Q\left(\frac{m^3}{hr}\right) = \frac{P_{hydr}(kW) * 3.6\ 10^6}{\Delta p_{pump}(Pa)} \quad (19)$$

$$Q\left(\frac{l}{\min}\right) = Q\left(\frac{m^3}{hr}\right) * \frac{10^3}{60} \quad (20),$$

$$vd\left(\frac{cc}{rot}\right) = Q\left(\frac{l}{\min}\right) * \frac{10^3}{n_{closing}\left(\frac{rot}{\min}\right)} \quad (21)$$

Concept name	Electrical motor power	+80% electrical overload	Required hydraulic power	Required volume flow	Required volume flow	Minimal volume displacement
	[kW]	*[kW]*	*[kW]*	*[m^3/hr]*	*[l/min]*	*[cc/rot]*
Reference	70	126.0	-	-	-	-
$^2/_3$ concept	55	99.0	21.0	3.8	63.0	38.2
$^1/_2$ concept	35	63.0	57.0	10.3	171.0	103.6
$^1/_3$ concept	23	41.4	78.6	14.1	235.8	142.8

Table 4.2, hydraulic motor requirements

4.5.3 Discussion on the hydraulic system

In the calculation, no mechanical and volumetric efficiencies are taken into account. Therefore, the motor must not be selected smaller than calculated. The safety factor ensures enough closing power, adding to this, the electric motor can still be more overloaded. Also, the pressure difference over the pump is assumed on 200 bar, which can be slightly higher or lower. Lastly, the idle power of the motor is not known, so the dry cycle time can deviate a few hundreds of a second.

4.6 Drive ratio configurations

Concluding from the analysis performed in this chapter, three concepts emerged, shown in Table 4.2. The relation between drive power, the possible speed characteristics, and cycle times are thoroughly examined. The concepts are further examined in a technical feasibility analysis in the next chapter, where aspects like costs, technical integration, and energy efficiency are researched.

5.Technical feasibility analysis

A technically feasible concept performs to a certain expectation within the machine. In this chapter, the last research question is researched: What is the technical feasibility of the concept in terms of technical integration in the machine, energy efficiency, and compenent costs?

5.1 Technical integration

The technical integration studies the integration of the concept in the system, the working modes, and the effects on the cycle time.

5.1.1 Component selection

A schematic representation of the system is shown in Figure 5.1. Three sections are indicated in the schematic representation. These sections are discussed individually in the following listing:

- **Section I, the electric drive;** The electric drive consists of an electric motor and a frequency converter. Compared to the previous drive, the recovery unit and electric brake are left out. The recovered energy is passed directly through the bus voltage between the frequency converters of the electric motor and the servo motor of the hydraulic system. The brake is superfluous, by closing the valves of the hydraulic motor an emergency brake is already present.
- **Section II, the hydraulic drive**; The hydraulic drive consists of a hydraulic motor with a fixed displacement volume in combination with a fully controllable proportional valve. It should be noted that in the neutral position of the proportional valve in Figure 5.1, the hydraulic oil on the motor side can flow freely. After all, this is necessary for the proper functioning of the neutral position if the hydraulic motor is idling.
- **Section III, The Hydraulic System.** The hydraulic system remains unchanged from the current drive. An electrically controlled hydro pump charges the accumulators. The recovered energy is recycled via the frequency converter bus voltage. This bus voltage can be supplemented with energy from the grid.

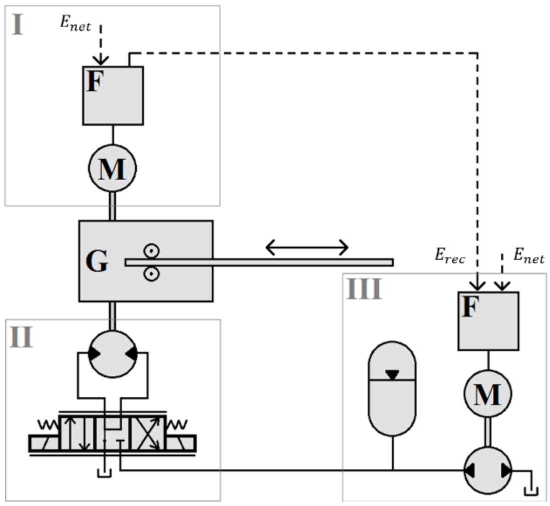

Figure 5.1, drive system structure

The drive has two possible operating modes:

1. **Electric mode;** Moving the crosshead purely electric. Higher forces are required during locking the mold, for which it is supported hydraulically.
2. **Hybrid mode;** Provide hydraulic support during the movement of the crosshead when accelerating. Thus, more power is available for acceleration, which results in shorter cycle times. The braking is done purely electric to enable the highest energy efficiency.

5.1.2 Behavioral characteristics

Earlier in Table 4.2, combinations of electric motors and hydraulic motors were calculated. Simulations have been performed for the three concept options, in which the properties in electric mode and hybrid mode have been simulated. An example of the outcome is shown in Figure 5.2, which shows the speed and power of concept 2, electrical mode. All evaluations are shown in Appendix H. The results are further compared in this chapter.

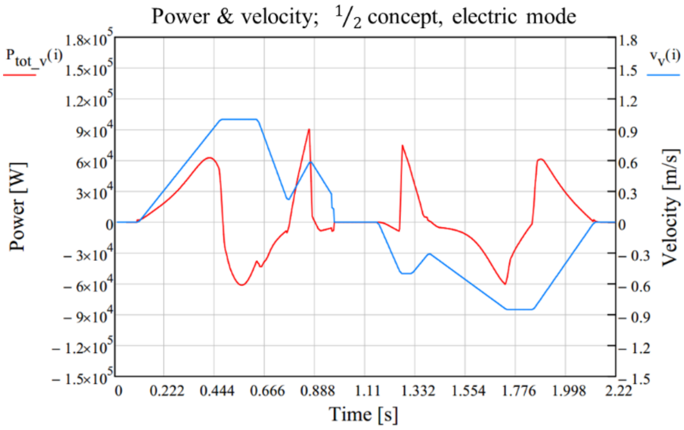

Figure 5.2, Evaluation figure

The dry cycle time depends on the acceleration and deceleration during the closing and opening of the mold. The acceleration and deceleration are depending on the available engine power, but cannot be infinitely large to keep the heavy mass of the LSP controllable. In addition, it is desirable to brake purely electric, so the majority of the used energy can be regenerated. The difference between the electric mode and the hybrid mode is thus the accelerations of the LSP. The dry cycle times are shown in Table 5.1. The concept 'reference' is the current electrical driven mold drive.

Concept name	Dry cycle time electric mode	Dry cycle time hybrid
	[s]	*[s]*
Reference	1.86	
$^2/_3$ concept	1.63	1.62
$^1/_2$ concept	1.82	1.65
$^1/_3$ concept	2.12	1.93

Table 5.1, dry cycle times of the drive concepts

It can be concluded from the table that less power for the drive has a little effect on the cycle time. By making better use of full power of the drive during all acceleration and deceleration actions, a faster cycle time can be achieved with less power. Consideration must be given to the occupation of the current pump. Depending on the applied concept, the hydraulic energy demand increases.

5.2 Energy efficiency

Energy usage is an important parameter. Therefore, it is important to investigate energy usage, energy regeneration, and grid load.

5.2.1 Energy usage per cycle

The three concepts are simulated for both the electric and hybrid mode. The simulation results are added in Appendix H. The results are summarized in Figure 5.3. Almost no differences are observed between the electric (E) and hybrid (H) mode in the $^2/_3$ concept. In this concept, the accelerations are already very high. To accelerate even faster, much more added power has less effect. In addition, it is not possible to slow down faster without any certainty that the molds do not hit each other too hard. A better alternative to speed up the cycle time is to increase the maximum speed, and thus the gear ratio. Assumptions have been made on hydraulic (throttling) losses to give an appropriate indication with a lack of knowledge on the hydraulic throttle loss. A loss of 0.25 on the strain energy and 0.5 on the hydraulic energy usage are taken into account, an expectation based on the control behavior and system structure. Recommendations to further research the hydraulic behavior are reviewed in chapter 7, Discussion and recommendations.

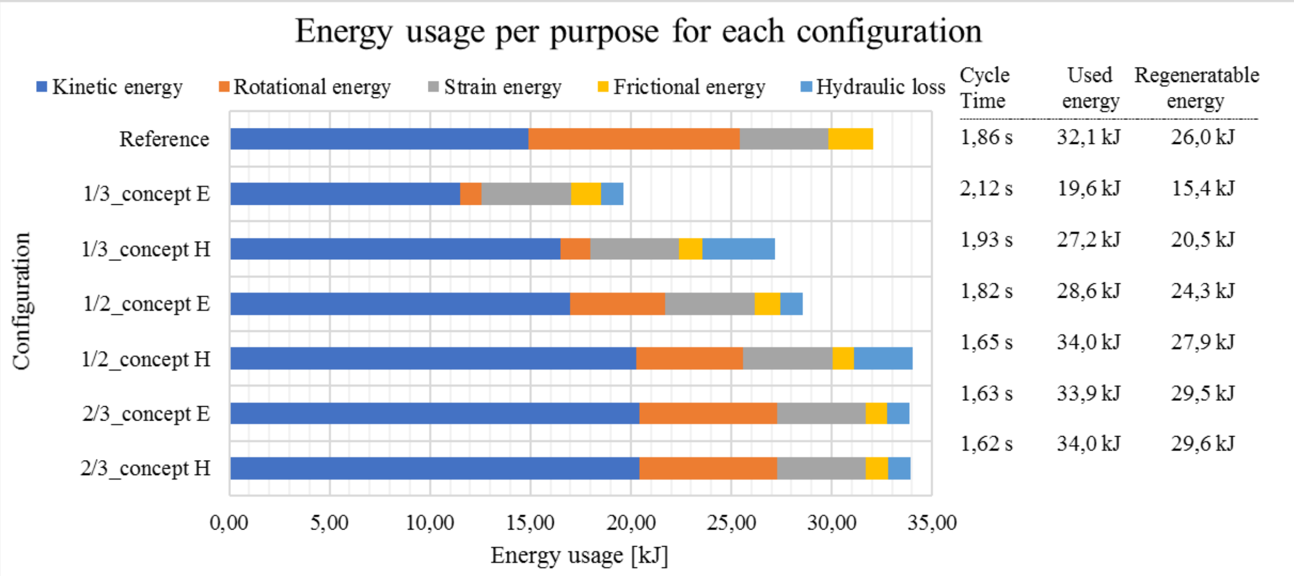

Figure 5.3, Energy usage per concept

Figure 5.3 clearly shows that the energy consumption per cycle increases when accelerating with higher accelerations. The share of the rotational energy of the drive itself also increases with bigger electric motors. The higher accelerations have a big effect on this rotational inertia. The cycle times, used, and regenerated energy of the concepts in Figure 5.3 can be compared to the current electric model (named ‘reference’ in the figure). The change in cycle time and energy usage are shown in Table 5.2. An energy regeneration efficiency of 94.6% is assumed, as a loss in energy transformations in the frequency converter and mechanical efficiencies. The value is estimated based on the remaining energy of the measured vector based calculation (reference), including frictional energy loss.

	Cycle time *[%]*	Energy usage *[%]*
Reference	-	-
$^1/_3$ concept E	13.8%	-17.7%
$^1/_3$ concept H	3.5%	28.2%
$^1/_2$ concept E	-2.2%	-7.7%
$^1/_2$ concept H	-11.3%	25.7%
$^2/_3$ concept E	-12.2%	7.5%
$^2/_3$ concept H	-13.2%	7.8%

Table 5.2, change in cycle time and energy usage

Concept $^1/_2$ electric mode has the greatest effect. The concept is a little bit faster and above all more energy efficient. With this concept, the customer is given a choice to operate energy-efficiently at an acceptable speed, or much faster but less energy-efficient. Concept $^1/_3$ does not meet the required cycle time. Concept $^2/_3$ has advantages in terms of cycle time, but uses more energy.

5.3 Costs

It has previously been found that the injection molding machine market is very tight. It is important as a manufacturer to keep the purchase price of the injection molding machines as low as possible.

5.3.1 Initial costs

The change in drive costs is related to a few factors. Firstly, the electric motor is smaller, which makes a difference in costs. On the other hand, an expensive hydraulic system is added. Table 5.3 shows the costs of motors. It is striking that the combination of electric and hydraulic motors does not differ very much. A hybrid drive is more expensive than a single driving motor.

Concept name	Electrical motor power	Electric drive costs	Hydraulic volume displacement	Hydraulic drive costs	Total drive costs	Costs difference
	[kW]	*[€]*	*[cc/rot]*	*[€]*	*[€]*	*[€]*
Reference	70	*4358,-*	-	-	*4358,-*	-
$^{2}/_{3}$ concept	55	*3907,-*	38.2	*1862,-*	*5769,-*	*1411,-*
$^{1}/_{2}$ concept	35	*2747,-*	103.6	*2975,-*	*5722,-*	*1364,-*
$^{1}/_{3}$ concept	23	*1825,-*	142.8	*3878,-*	*5703,-*	*1345,-*

Note! All the prices regarding electric parts are internally known at the Stork IMM, prices regarding hydraulic parts are derived from comparable parts from Parker (Parker Hannifin Corp, 2021).

Table 5.3, drive motor costs

The remaining changes to the system do weigh opposite to the more expensive hybrid drives. Table 5.4 shows that the removal of the recovery unit and the brake reduces the costs of the system. However, a proportional valve is required to control the hydraulic motor.

Part	Costs
	[€]
Regeneration unit + add-ons	*-2578,-*
Electromotor brake	*-500,-*
Proportional valve (range)	*1165,-*
Piping and connection material	*800,-*
Total	*-1113,-*

Note! All the prices are internally known at the Stork IMM

Table 5.4, Changing system part costs

5.4 Concept selection advice

Research in this paragraph showed that the concept can relatively easily be combined with the current machine parts. In the $^{1}/_{3}$ concept, not enough power is available to achieve the desired cycle times. The $^{1}/_{2}$ concept is able to achieve the current cycle time, and is more energy efficient compared to the $^{2}/_{3}$ concept. Therefore, the research leads to the advice to use the $^{1}/_{2}$ concept. An extra investment of 251,- is quickly recouped due to the more energy-efficient properties. Conclusions on the hybrid drive feasibility compared to the current electric drive are summaryzed:

Hybrid properties compared to electric:

+ Less mass inertia is resulting in less peak energy
+ 7.7% more energy efficient (wherein the hydraulic motor inertia, conditioning (cooling and filtering) are not taken into account and the hydraulic efficiency is estimated)
+ Option to operate 11.3% faster
- Less reliable due to more complex system components
- In fast mode, which is a common mode, a poor efficiency of +25.7%
- More complex, besides mechanical, in control and software too

6. Conclusion

The present study was designed to determine the effect of a hybrid drive for the Stork IMM injection molding machine closing unit. The study emphasized four phases, wherein the current machine has been analyzed, a new concept has been designed, various concepts have been analyzed iteratively, and the final concept has been tested for technical feasibility. The conclusion is based on the research questions.

1. **What are the current hydraulic and electric drive performances?**

The current drives are thoroughly analyzed. Research has shown that the mold drive must be able to deliver a force of 160 kN. A cycle requires 32.1 kJ of energy from which 81% can be recovered. The dry cycle time is currently 1.86 s and is a minimum requirement of the design. The reliability of the measurements has been taken into account and checked several times in the calculation.

2. **What is a suitable hybrid drive concept?**

An appropriate design method has led to a targeted study, in which the focus has remained on the relevant criteria. In the design, a distinction has been made between delivery, recovery, and storage of energy. The concept does not exceed existing patents. In the concept, energy is regenerated purely electrically. Hydraulic regeneration is unfavourable due to a maximum efficiency of 63%, and the additional costs of a required variable-displacement hydraulic motor.

3. **How does a change in motor power affect the system behavior in speed, time, and energy?**

Three concepts, in which the current electric motor was reduced by 33%, 50%, or 66%, have been simulated with a calculation model that has been successively tested against practical measured results. In the calculation model, the transmission ratio between the crosshead and the LSP has led to interesting conclusions. For example, regarding kinetic energy, it has been found that faster braking requires less peak power because the transmission ratio changes favorably in these processes. With the help of iterations in different acceleration speeds in different phases, a clear analysis has emerged in terms of consequences for speed, time, and power requirement. The concepts have two operating modes, in which the movement of the mold is carried out purely electrically or hybrid. Braking is always done electrically to achieve the highest possible energy efficiency. In the so-called $^{1}/_{3}$ concept, the electric motor has too little power to achieve the required cycle times. The advice is to use the $^{1}/_{2}$ concept, which is 2.2% faster and 7.7% more energy efficient in electric mode, but 11.3% faster and 25.7 less efficient in hybrid mode. Besides the energy efficiency conclusions, the grid load is in both cases halved using smart energy handle techniques. The $^{2}/_{3}$ concept is faster, but also consumes more energy.

4. **What is the technical feasibility of the concept in terms of technical integration in the machine, energy efficiency, and component costs?**

A hybrid drive is technically feasible and relatively easy to integrate into the current hydraulic system. The cost of the drive is about 251,- higher, which is only 2.6% of the drive costs. In the electrical field, the recovery unit and the electric brake are saved, while in the hydraulic field a hydro motor, proportional valve, and system components such as piping are added. The regenerated energy can directly be used to load the hydraulic accumulators. The energy is transmitted through the bus voltage of the coupled frequency converters.

7. Discussion and recommendations

- **Reliability of the measurements**

The reliability of the measurements is checked in paragraph 2.3.2. The measurements were taken during the commissioning of the machine. During the tests, the machine was running according to operating conditions. However, there was no mold attached to the machine, only a trial mold, fixedly attached to the fixed clamping plate (VSP). In reality, the machine runs slightly heavier due to the mass of the mold. This is a factor of 1.05 on the mass.

- **Faster operting in the current electric drive**

The electric motor of the current injection molding machine is not using its full capacity during the cycle. Thus, by optimizing the process, current cycle times could be reduced. Also, the research has shown that a certain window of decelerations is unfavorable during braking, when the motor and the LSP experience their most unfavorable transmission ratio. When braking faster, and thus later, less power is needed, as previously proofed in Figure 4.7, power-acceleration relation. However, it must also be done in a controlled manner: it is not desirable for the mold halves to hit each other hard. To avoid a crash, the LSP has to achieve a desired velocity a few millimeters before the molds hit each other, a safety distance of for example 5-10 mm is appropriate. Or, the hydraulic motor can be used to brake more quickly at the end. Although this is unfavorable for energy recovery, this is not needed under normal conditions of use, i.e. 100% electrical deceleration. Improvement on the current drive is calculated in Figure 7.1 and Figure 7.2. Improvements in three phases are shown in terms of time, the dry cycle time is 0.2 s (11%) faster. The same system components are used.

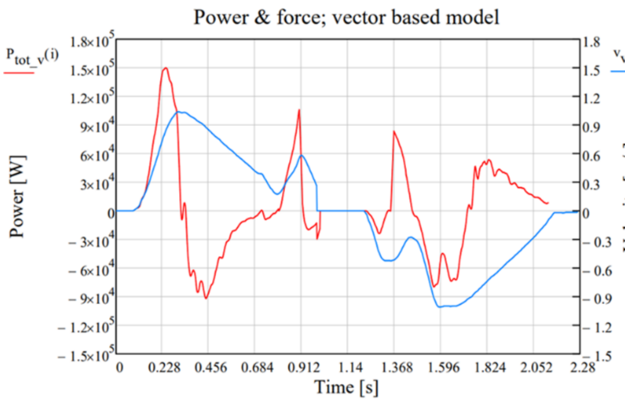

Figure 7.1, current electric drive behavior

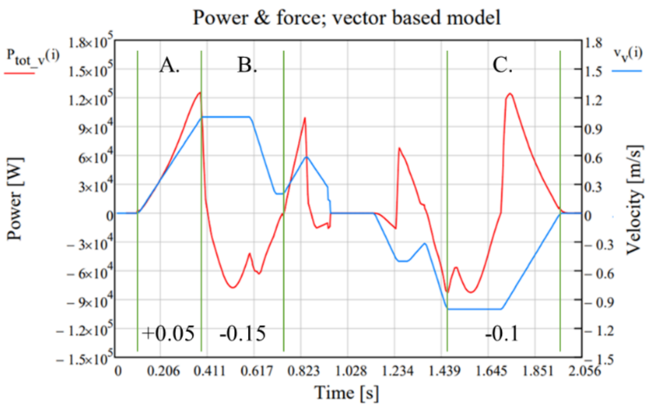

Figure 7.2, improvement on current drive

The evaluation sheet of the calculation of the improvement on the current electric drive is added in Appendix I.

- **Costs saving on the current electric drive**

Research has shown that the development of frequency converters is undergoing a spurt. Possible improvements to the current electric injection molding machine could be made by connecting the bus voltage of the closing and the injection unit frequency converters, making the recovery unit superfluous. This results in a cost-saving of approximately 2500,- in parts.

- **Grid demand**

Compared to the more constant energy-demanding hydraulic machine, the electric injection molding machine has a noisy grid load with high peaks. User peaks of the closing and injection unit, as well as peaks in energy return, are processed in the grid. By applying the concept, the user peak of the injection unit and the return peak of the closing unit cancel each other out, but the grid load can be reduced even further.

By having several injection molding machines interact with each other in a factory, the energy demand of the grid can be stabilized continuously. In this way concepts such as Industrial Internet of Things (IIoT), industry 4.0, and smart energy grid are applied. If there are many injection molding machines in the factory, it is even possible to place a kinetic energy buffer in the circuit. Due to the kinetic energy buffer, the energy demand of the grid can be leveled.

- **Bigger closing units**

It currently appears that the change to hybrid is slightly more expensive/almost as expensive. However, the concept can turn out cheaper if it is applied to larger machines for which the costs increase exponentially. The calculation has been carried out for a closing unit with an available force of 4,400 kN, but Stork IMM already manufactures closing units with a capacity of 11,000 kN, for which the concept could be more interesting.

- **Decreasing cycle time**

The current accelerations are already high. To accelerate even faster, a lot more power is needed, but the effect in required time to accelerate decreases. If the cycle times have to be even shorter, increasing the top speed has more effect. The transmission ratio of the gearbox has to be adjusted.

- **Hybrid concept controllability**

A possible follow-up study concerns the control of the hybrid concept. The behavior of both drives on such a type of machine is yet unknown. The input of the electric motor is a current and a voltage, due to the constant voltage, the input current is proportional to the rotation speed. The input to the hydraulic motor is a input flow and differential pressure across the motor. The input flow is proportional to the rotation speed, so the differential pressure across the motor is the only input value that can be used to control power.

A suggestion is to calculate the required differential pressure across the motor at a desired speed. Then control the electric motor on the real time measured rotation of the hydraulic motor, because the drives must drive with an exactly equal speed. In this way, the controllability is done as quickly as possible, using the fast reaction time of the simpler electric drive. Conversely, it is difficult to tune the hydraulic motor equally to the electric drive, because of several dependent variables that take care of the rotation.

With regard to the hydraulic efficiency, it is advantageous to drive the hydraulic motor directly on the hydraulic pump. Resulting in less throttling loss from the accumulators. The system itself is expected to find its balance in this way, but due to the lack of knowledge about this behavior, further research in this area is necessary.

8. Literature list

Angst, A., Fuchs, M., Hausammann, M., Hautle, M., & Jenny, D. (2018). *U.S. Patent No. 10,112,331 B2* (Patent No. 10,112,331).

ARBURG GmbH + Co KG. (2021a). *HYBRID ALLROUNDERS*. https://www.arburg.com/fileadmin/redaktion/mediathek/prospekte/arburg_hybrid_allrounders_680343_en_us.pdf

ARBURG GmbH + Co KG. (2021b). *Hybrid machines*. https://www.arburg.com/us/us/products-and-services/injection-molding/injection-molding-machines/hybrid-machines/

Baumüller. (2013a). *DS2-160KO54W-25-5*. https://www.baumueller-services.com/de/downloads/motors/send/3-doc-motors/

Baumüller. (2013b). *Three-phase synchronous motors DS2 100-200*. https://www.baumueller-services.com/de/downloads/motors/send/3-doc-motors/167-ds2-100-200-en

Burke, A. F. (2007). Batteries and ultracapacitors for electric, hybrid, and fuel cell vehicles. *Proceedings of the IEEE, 95:806-820.* https://doi.org/10.1109/JPROC.2007.892490

Chan, C. C. (2007). The state of the art of electric, hybrid, and fuel cell vehicles. *Proceedings of the IEEE, 95:704-718.* https://doi.org/10.1109/JPROC.2007.892489

Chan, C. C., Bouscayrol, A., & Chen, K. (2010). Electric, hybrid, and fuel-cell vehicles: Architectures and modeling. *IEEE Transactions on Vehicular Technology, 59:589-598.* https://doi.org/10.1109/TVT.2009.2033605

Chen, J. S. (2015). Energy efficiency comparison between hydraulic hybrid and hybrid electric vehicles. *Energies, 8:4697-4723.* https://doi.org/10.3390/en8064697

Cross, D., & Hilton, J. (2008). *'High speed flywheel based hybrid systems for low carbon vehicles.'* Hybrid and Eco-Friendly Vehicle Conf., IET HEVC 2008.

Do, H. T., & Ahn, K. K. (2011). A study on a closed-loop hydraulic braking energy regeneration system driven by a sliding mode controller. *International Conference on Control, Automation and Systems (ICCAS-2011), IEEE 1594-1599*. https://ieeexplore.ieee.org/document/6106248

Engel Machinery INC. (2021). *Injection molding machines - e-speed*. https://www.engelglobal.com/en/us/products/injection-molding-machines/e-speed.html

HAITIAN Plastic Machinery. (2021). *The Mars technology - energy saving drive systems*. http://haitianpm.com/en/products/the-mars-technology/

Husky Injection Molding Systems Ltd. (2021). *Engineered solutions - Our systems*. https://www.husky.co/en/solutions/systems/

Interempresas Media. (2019). *Anales sectoriales Plastico*. https://www.interempresas.net/Plastico/Articulos/9274-Husky-va-mas-alla-de-las-palabras-en-el-moldeo-por-inyeccion.html

Isidor Buchmann. (2021). *Charging Lead Acid*. https://batteryuniversity.com/index.php/learn/article/charging_the_lead_acid_battery

Juhala, J., Kauranne, H., Kajaste, J., & M., P. (2009). Improving energy efficiency of work machine with digital hydraulics and pressure accumulator. *Proceedings of the 11th Scandinavian International Conference on Fluid Power, Linköping.*

KEB Automation KG. (2016). *Application manual KEB Combivert F5 multi servo*. https://www.keb.co.uk/drive-technology/drive-controller-for-your-drive-tasks/application-drive-combivert-f5

KEB Automation KG. (2017a). *Combivert R6 instruction manual*. https://www.keb.co.uk/drive-technology/supplyregen-solutions/block-shaped-supplyregen

KEB Automation KG. (2017b). *Combivert R6 line regen systems*. https://www.keb.co.uk/drive-technology/supplyregen-solutions/block-shaped-supplyregen

Kim, Y. J. (2008). Integrated modeling and hardware-in-the-loop study for systematic evaluation of hydraulic hybrid propulsion options. *A Dissertation Thesis for Doctor of Philosophy. The University of Michigan.* http://hdl.handle.net/2027.42/58396

KraussMaffei. (2021). *Netstal Elios (4500 - 10000 kN)*. https://www.kraussmaffei.com/en/our-products/netstal-elios-4500-10000-kn

Liang, X. (2002). *On improving energy utilization in hydraulic booms*. Espoo, PhD Thesis.

Mahato, A. C., & Ghoshal, S. K. (2020). Energy saving strategies on power hydraulic system: An overview,. *Proceedings of the Institution of Mechanical Engineers, Part I: Journal of Systems and Control Engineering, IF 2020: 1.166.* https://doi.org/10.1177%2F0959651820931627

May, G. (2006). *'Battery options for hybrid electric vehicles.'* Conf. IET The Institution of Engineering and Technology.

Minav, T., Immonen, P., Laurila, L., Vtorov, V., Pyrhönen, J., & Niemelä, M. (2011). Electric energy recovery system for a hydraulic forklift - theoretical and experimental evaluation. *IET Electric Power Applications*, *5*(4), 377–385. https://doi.org/10.1049/iet-epa.2009.0302

Minav, Tatiana, Hänninen, H., Sinkkonen, A., Laurila, L., & Pyrhönen, J. (2014). Electric or hydraulic energy recovery systems in a reach truck- A comparison. *Strojniski Vestnik/Journal of Mechanical Engineering*, *60*(4), 232–240. https://doi.org/10.5545/sv-jme.2013.1581

Parker Hannifin Corp. (2021). *Hydraulic Pumps*. https://ph.parker.com/nl/en/hydraulic-pumps

Quan, Z., Quan, L., & Zhang, J. (2014). Review of energy efficient direct pump controlled cylinder electro-hydrualic technology. *Renewable and Sustainable Energy Reviews, 35:336-346.* https://doi.org/10.1016/j.rser.2014.04.036

Ramakrishnan, R., Hiremath, S. S., & Singaperumal, M. (2012). Theoretical investigations on the effect of system parameters in series hydraulic hybrid system with hydrostatic regenerative braking. *Journal of Mechanical Science and Technology, 26:1321-1331.* https://doi.org/10.1007/s12206-012-0321-y%0D

Rydberg, K.-E. (2007). No Title. *Division of Fluid and Mech. Eng. Systems. Dept. of Management and Engineering Linkoping University; SE-581 83.*

Rydberg, K. E. (2009). Energy Efficient Hydraulic Hybrid Drives: *Scandinavian International Conference on Fluid Power, SICFP-09, Linkoping, Sweden*. http://www.diva-portal.org/smash/get/diva2:373607/FULLTEXT01.pdf

Shen, W., Jiang, J., Su, X., & Karimi, H. R. (2013). Energy-saving analysis of hydraulic hybrid excavator based on common pressure rail. *The Scientific World Journal, 2013, Article ID 560694.* http://dx.doi.org/10.1155/2013/560694

Sinkkonen, A., Kauranne, H., Hänninen, H., & Pietola, M. (2011). Analysis of energy balance in electrohydraulic forklift. *Proceedings of the 12th Scandinavian International Conference on Fluid Power, Tampere*.

Stork IMM. (2021). *S+ Injection Moulding Machine User & Service Manual*.

Vael, G. E., Achten, P. A., & Fu, Z. (2000). Theinnas hydraulic transformer the key to the hydrostatic common pressure rail. *SAE Technical Paper, Paper No. 2000-01-2561.* https://doi.org/10.4271/2000-01-2561

Valente, S., & Ferreira, H. (2008). Braking energy regeneration using hydraulic systems. *Polytechnic Institute of Porto (IPP)*, *8*. https://doi.org/Portugal 2008;

Appendices

Appendix A. Machine test data

To understand the current machines properly, tests have been carried out on the machine. The test data used has been added in this appendix.

The hydraulic test data can be found in the document: ‘Hydraulic_closing_unit_test_measurements.xls’

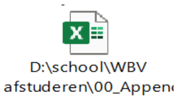

Figuur 0.1

The used sensors in the document are:

- Tijd Time sample
- /TR251 Pressure sensor on piston side
- /TR252 Pressure sensor on rod side
- /RY251 Control voltage proportional valve
- /clp/m/VYcrh_abs Absolute speed sensor crosshead
- /clp/i/PO Absolute position sensor crosshead
- Differentiaal Differential valve status
- Bewegingsrichting Movement direction

The electric test data can be found in the document: ‘Electric_closing_unit_test_measurements.xls’

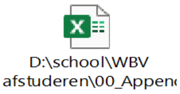

Figuur 0.2

The used sensors in the document are:

- /clp/o/VY Control voltage
- /clp/o/PR Setpoint torque as percentage of motor maximum
- /clp/m/VYsetp_tmp Setpoint speed
- /clp/m/VYcrh_abs Absolute speed
- /clp/m/POsetp Setpoint position
- /clp/i/PO Absolute position
- /clp/i/PR Measured torque

A simplified hydraulic scheme, including sensor names:

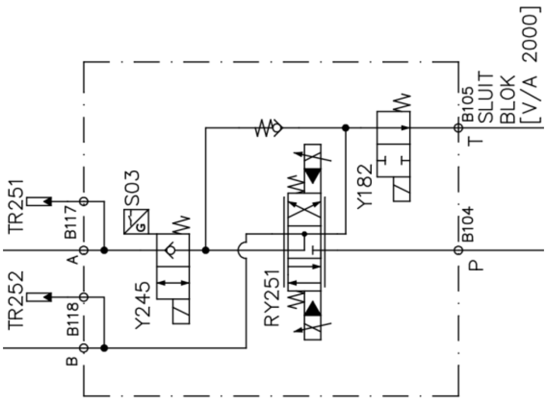

Appendix B. Measurement data Matlab analysis code

The reliability of the measurements has been validated by comparing different measurements. For this, a vector analysis code was created in Matlab to calculate and represent the deviation and the scaling factors.

```
clear,clc
format shortG

%input of RAW test data:
RAW_clp_i_PR = [-1575, -18900, 59388, -37900, 16933, 54618, -16965,...
    88200, -10000, 7500, -9643, -19000, -2000, -5000]'
RAW_RU_12 = [-14, -142, 474.9, -299.8, 131, 430, -122, 701, -136,...
    59, -76, -150, -20, -45]'
RAW_clp_o_PR = [20000, 200001, 80000, 200000, 210000, 180000]'
RAW_CS_18 = [9.5, 95.25, 38.1, 95.2, 100, 85.7]

%Sort comlumns
Scoop_torque = sort(RAW_clp_i_PR)
Scoop_demand = sort(RAW_clp_o_PR)

%Create matrix space
Indice_torque = zeros([1, length(RAW_clp_i_PR)])
Indice_demand = zeros([1, length(RAW_clp_o_PR)])


%Sorting program based on indice position (to prevent mixing up not...
    % accurate measured data);
%program to sort torque matrix:
for k = 1:length(RAW_clp_i_PR)  %Execute loop for every value of matrix.
    Indice_torque(k) = find(RAW_clp_i_PR==Scoop_torque(k))
                                %Find corresponing indice location.
    Freq_torque(k) = RAW_RU_12(Indice_torque(k))
                                %Create new matrix based on index location.
end

%program to sort motor demand setpoint matrix:
for k = 1:length(RAW_clp_o_PR)  %Execute loop for every value of matrix.
    Indice_demand(k) = find(RAW_clp_o_PR==Scoop_demand(k))
                                %Find corresponing indice location.
    Freq_demand(k) = RAW_CS_18(Indice_demand(k))
                                %Create new matrix based on index location.
end

Scoop_demand_table = Scoop_demand; Scoop_demand_table([7:14],1) = NaN
Freq_demand_table = Freq_demand; Freq_demand_table(1,[7:14]) = NaN

%creating table:
columnnames = {'Scoop torque', 'Freq_torque', 'Scoop demand', 'Freq demand'}
data = [Scoop_torque Freq_torque' Scoop_demand_table Freq_demand_table']
disp(array2table(data,'Variablenames',columnnames))

%calculating scaling factor:
Scaling_factor_torque = Freq_torque./Scoop_torque'  %scaling factor torque
Scaling_factor_demand = Freq_demand./Scoop_demand'  %scaling factor demand
Scaling_factor_torque_mean = mean(Scaling_factor_torque)
Scaling_factor_demand_mean = mean(Scaling_factor_demand)

%Figure:
figure(1), clf(1), hold on
```

```
subplot(2,2,[1 3]);           %subplot 1
plot(Scoop_torque,Scaling_factor_torque,'-*b',...
    'LineWidth',2,'MarkerEdgeColor','k','MarkerSize',4) %plot variables
ylim([0 0.02]);               %limit y-axis to personalized values
grid on;                      %gridlines on
legend('scaling factor','Location','NorthWest');     %add legend
xlabel('Scoop measured torque');                     %asix lables
ylabel('scaling factor to Frequency measured torque')
title('Scaling factor torque','FontSize',10)         %add title

subplot(2,2,[2 4]);           %subplot 2
plot(Scoop_demand,Scaling_factor_demand,'-*b',...
    'LineWidth',2,'MarkerEdgeColor','k','MarkerSize',4); %plot variables
ylim([4.6*10^(-4) 4.9*10^(-4)]);      %limit y-axis to personalized values
grid on;                              %gridlines on
legend('scaling factor','Location','NorthWest');     %add legend
xlabel('Scoop measured demand');                     %add axis lables
ylabel('scaling factor to Frequency measured demand')
title('Scaling factor demand','FontSize',10)         %add title
hold off
```

Scoop torque	Freq_torque	Scoop demand	Freq demand
-37900	-299.8	20000	9.5
-19000	-150	80000	38.1
-18900	-142	1.8e+05	85.7
-16965	-122	2e+05	95.2
-10000	-136	2e+05	95.25
-9643	-76	2.1e+05	100
-5000	-45	NaN	NaN
-2000	-20	NaN	NaN
-1575	-14	NaN	NaN
7500	59	NaN	NaN
16933	131	NaN	NaN
54618	430	NaN	NaN
59388	474.9	NaN	NaN
88200	701	NaN	NaN

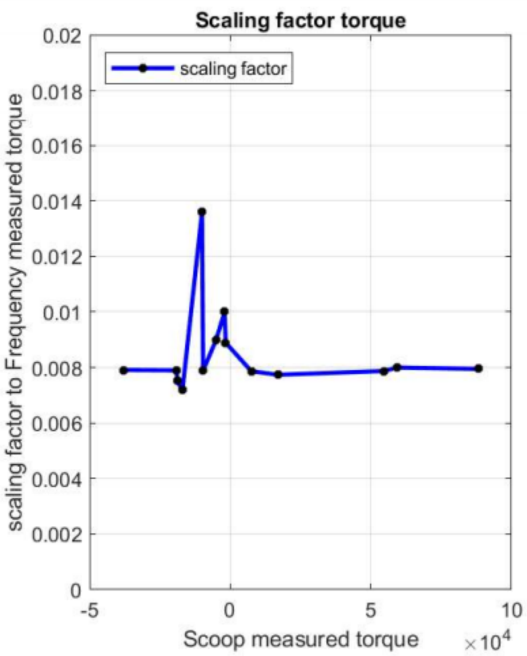

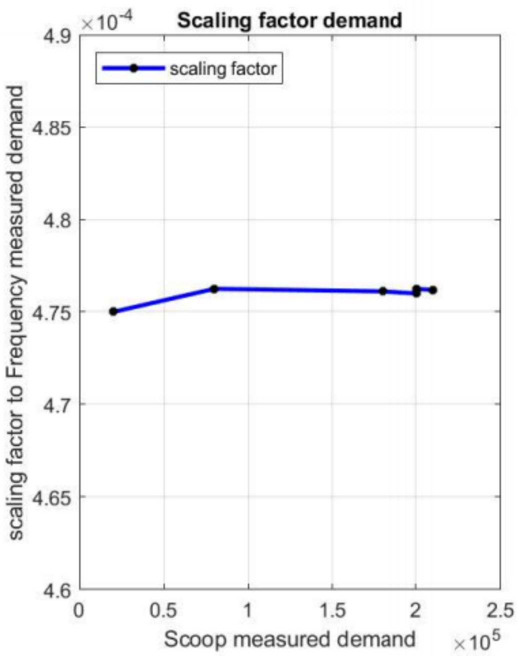

Appendix C. Market research

Injection molding is a very widely used technique. As a result, there are also many manufacturers of injection molding machines. The market research looks at striking drives of competitor injection molding machines. The market research lists the remarkable features of competitors. The remarks are listed in the following table.

Company	**Remarks**
Arburg GmbH + Co KG	*Arburg GmbH + Co KG* claims to produce hybrid injection molding machines. Although, the term hybrid, therefore, refers to a combination of both drives within the machine. The mold opening and closing are servo-electrically driven, the injection and secondary axis are hydraulically driven (ARBURG GmbH + Co KG, 2021a). Using an electrical closing unit drive, the kinetic braking energy can relatively easily be regenerated. The combination of electrical and hydraulic system elements is close to the current drive of Stork IMM. The system setup is 40 percent more energy efficient compared to a fully hydraulic driven machine (ARBURG GmbH + Co KG, 2021b).
ENGEL Group	*ENGEL AUSTRIA GmbH* produces e-speed series molding machines, highly comparable to the Stork IMM injection molding machines. The servo-electric mold drive differs on the linearization of the rotating motor by a spindle, versus a rack and pinion from Stork IMM. The claimed energy recovery system is presumably constructed with an energy recovery unit, as a part of the full electric closing unit. The hydraulic system contains hydraulic accumulators and the injection and nozzle stroke are driven servo-hydraulic, named eco-drive (Engel Machinery INC., 2021).
HAITIAN Plastic Machinery	*HAITIAN Plastic Machinery* produces full hydraulically driven machines. The hydraulic system (servomotor + gear pump) is claimed to be 70 percent more energy efficient. The direct drive connection between the servo-motor and the gear pump provides a combination of drive torque and required acceleration speeds (HAITIAN Plastic Machinery, 2021).
Husky Injection Molding Systems Ltd.	The two-platen drive technology (no toggle system but a single direct driven platen) has been expanded by *Husky Injection Molding Systems Ltd.* with a multimold system. Due to an arm construction, both sides of the middle clamping platen can be used, the construction can be seen in Figure 0.1. The closing unit is electrically driven and reduces energy consumption by 30 percent (Husky Injection Molding Systems Ltd., 2021). 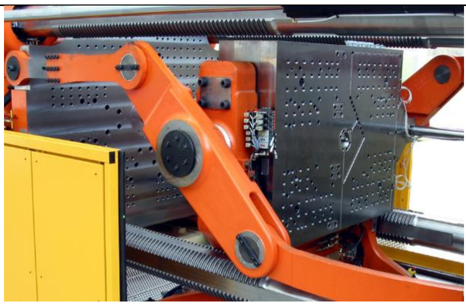 *Figure 0.1, Husky multimold* (Interempresas Media, 2019)
Krauss-Maffei GmbH	The *NETSTAL ELIOS* is using two additional hydraulic cylinders in addition to the electrical closing unit drive. The kinetic energy during the braking flows into the electric motor and is converted into hydraulic energy by the hydraulic cylinders (KraussMaffei, 2021). The exact working and patent limitations are described in the next paragraph.

Table 0.1, competitors remarkable drive systems

Patent limitations

The NETSTAL ELIOS machine is hybrid-driven. In this paragraph, the construction and the patent limitations are examined. The type of drive is patented as a United States patent No.: US 10,112,331 B2 on October 30, 2018. The patent owner is Netstal-Maschinen AG, Näfels (CH). Also, the patent is published in Europe as patent No.: PCT/EP2016/060854. A schematic overview of the system can be seen in Figure 0.2.

Important system elements:

5.	Cross clamp
10.	electric drive with rod
11.	piston cylinder system
13.	hydraulic supply
14.	control to hydr. and elec.
20-22	hydraulic valves
23.	accumulator
24.	pump
25.	pressure medium source

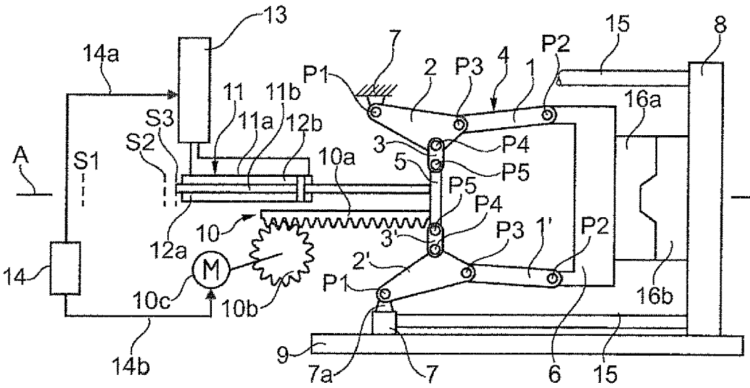

Figure 0.2, schematic overview NETSTAL ELIOS (Angst et al., 2018).

The schematic control diagram in Figure 0.3 indicates the working principles of the machine. The electric drive mainly ensures the reciprocating movement of the crosshead. The electric drive is always linked to the crosshead. The hydraulic drive system can function the same, however, in addition to the forward and reverse drive positions, the system has an idle stand. The hydraulic pressure relief valve (22) allows the oil to flow from one to the other side of the piston. The accumulator can be recharged by operating the hydraulic control valve (21). The patent limits explicitly the use of an electric drive operatively connected with the crosshead **together** with a hydraulic drive including a piston-cylinder which is operated by a pressure fluid (Angst et al., 2018). Depending on their size, the drive components can function in any ratio.

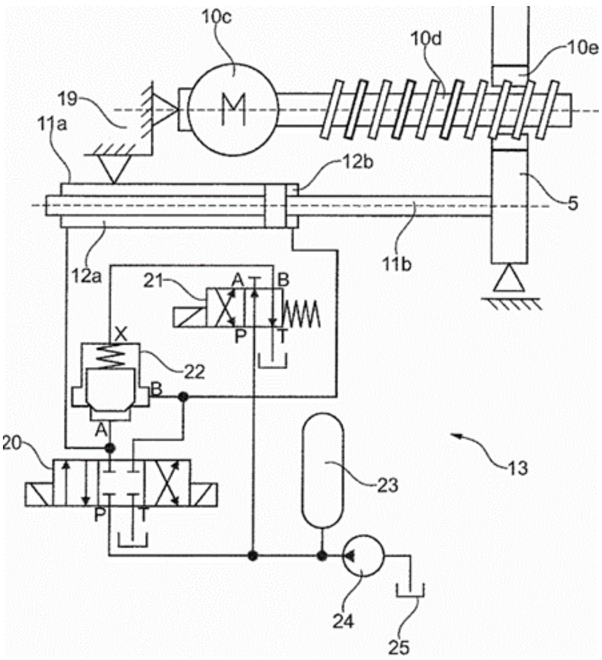

Figure 0.3, NETSTAL ELIOS drive setup (Angst et al., 2018)

Appendix D. Concept design

Reference to the realization of the assessment method is shown in Table 0.2 and Table 0.3. The weighting factor WF is scaled between 1 and 3, the concept examination is scaled from 1 to 4.

		Weighting (1-3)	lower scale (1)	Concept 1	Concept 2	Concept 3	Max scale (4)
Functional aspects	Energy efficiency	3	Low	3	4	2	High
	Power capability	3	Low	4	4	3	High
	Work configurations	2	One	3	3	3	More
Realization aspects	Component costs	2	High	4	3	3	Low
	Controllability	1	Difficult	2	2	3	Easy
	System complexity	1	Big	3	2	4	Small

Table 0.2, S-diagram assessment table

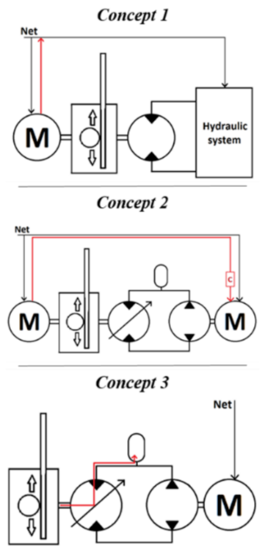

	Concept 1	**Concept 2**	**Concept 3**
Energy efficiency	Elec drive good, Energy regen. Good, Little hydraulic loss	Elec drive good, Energy regen. Good, Hydraulic variable	Regeneration loss to accumulator.
Power capability	Elec/Hydr parallel, boost	Elec/Hydr parallel, boost	Only hydraulic, has to be dimensioned bigger
Work configurations	Elec/Hydr variable	Elec/Hydr variable	Hydr variable
Component costs	Elec system, Small hydr system	Elec system Big hydr system	Big hydr system
Controllability	Dual drive	Dual drive	Single variable drive
System complexity	Two existing systems	Complex closed hydr. Transmission, energy buffered	Closed hydraulic system, variable flow/pressure.

Table 0.3, S-diagram assessment desctiption

The weighted average of i aspects of concept j $\overline{x_j}$ in percentages can be calculated using the following. The equation is set up to calculate a percentage between 0% and 100%. The results are shown in Table 0.4.

$$\overline{x_j} = \sum_{i=1}^{n} \left(\left(x_{i,j} - 1 \right) * WF_i \right) * \frac{100}{n * \sum_{i=1}^{n} WF_i}$$

	Functionality	**Realization**
Concept 1	79,2	75,0
Concept 2	91,7	50,0
Concept 3	54,2	75,0

Table 0.4, S-diagram concept input

Appendix E. Vector-based calculation model

MathCad model calculation on the crosshead during the opening and closing movement
Vector based model

This MathCad15 model is set up to calculate the power and energy usage in different stages.
The data is feed-forward controlled on a pre-defined speed, which also serves as the input for this calculation.
The test data is obtained as data in time samples, thus a vector / matrix form. Firstly, the raw test data is analyzed. Hereafter, a function based model is set up to approach the vector based model.
The function based model comes in handy if the acceleration or deceleration speeds are varied and adjusted.
The latter process is very hard to do with a vector based model.

<u>The table of contents:</u>

A IPM (Ideal Physical Model) has been made of the situation. All the gear ratios, masses, forces and energy directions are included in the model. The IPM can be seen in the following figure:

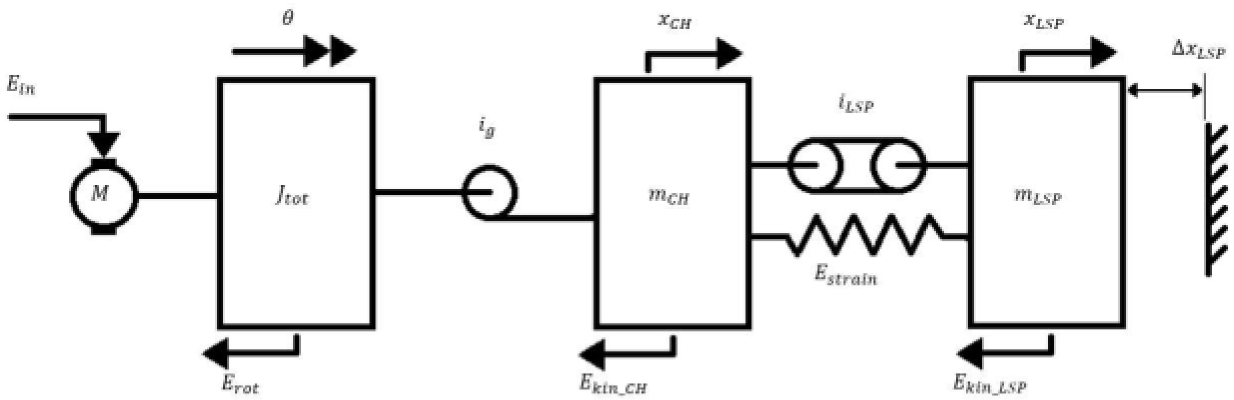

General input data:

Motor properties:

Motor intertia: $I_{motor} := 0.084 kg \cdot m^2$

Multiplication factor: $I_{sv} := 1.1$

Rotation inertia: $I_m := I_{motor} \cdot I_{sv} = 0.092 \, kg \cdot m^2$

Gearing: $i_g := \frac{20.92}{2 \cdot \pi} \frac{mm}{rad}$

Masses:

Multiplication factor mass: $m_{sv} := 0.95$

Mass crosshead: $m_{ch} := m_{sv} \cdot 275kg$

Mass LSP $m_{LSP} := m_{sv} \cdot 4060kg$

Mass mold $m_{mold} := m_{sv} \cdot 1533kg$

Closing unit properties:

$F_{tot} := 4400kN$

$l_{tiebar} := 3987mm$

$d_{tiebar} := 115mm$

$E_{steel} := 210GPa$

Vector based model:

1. input data

Several tests are performed on the machine to fully understand the dynamic behavior. The tests are inserted via the Excel sheet.

$Extdata :=$ ..\Measurements_electric.xls

Making the data suitable for this MathCad sheet:

direction: $d_v(i) := Extdata_{i,2}$

Time: $t_v(i) := Extdata_{i,0} \cdot s$

Velocity: $v_v(i) := Extdata_{i,1} \cdot 10^{-3} \cdot \frac{m}{s} \cdot d_v(i)$

Torque measured: $T_m(i) := Extdata_{i,3} \cdot (N \cdot m)$

Samples: $samples := 1140$

Vector: $i := 0 .. samples - 1$

$t_{start} := 0s$ $\quad t_{end} := samples \cdot 0.002s = 2.28\,s$ $\quad t_s := 0.002s$

Motor rpm: $n_{m\_v}(i) := \frac{v_v(i)}{i_g}$

$n_{m\_v}(10) = 0 \cdot rpm$

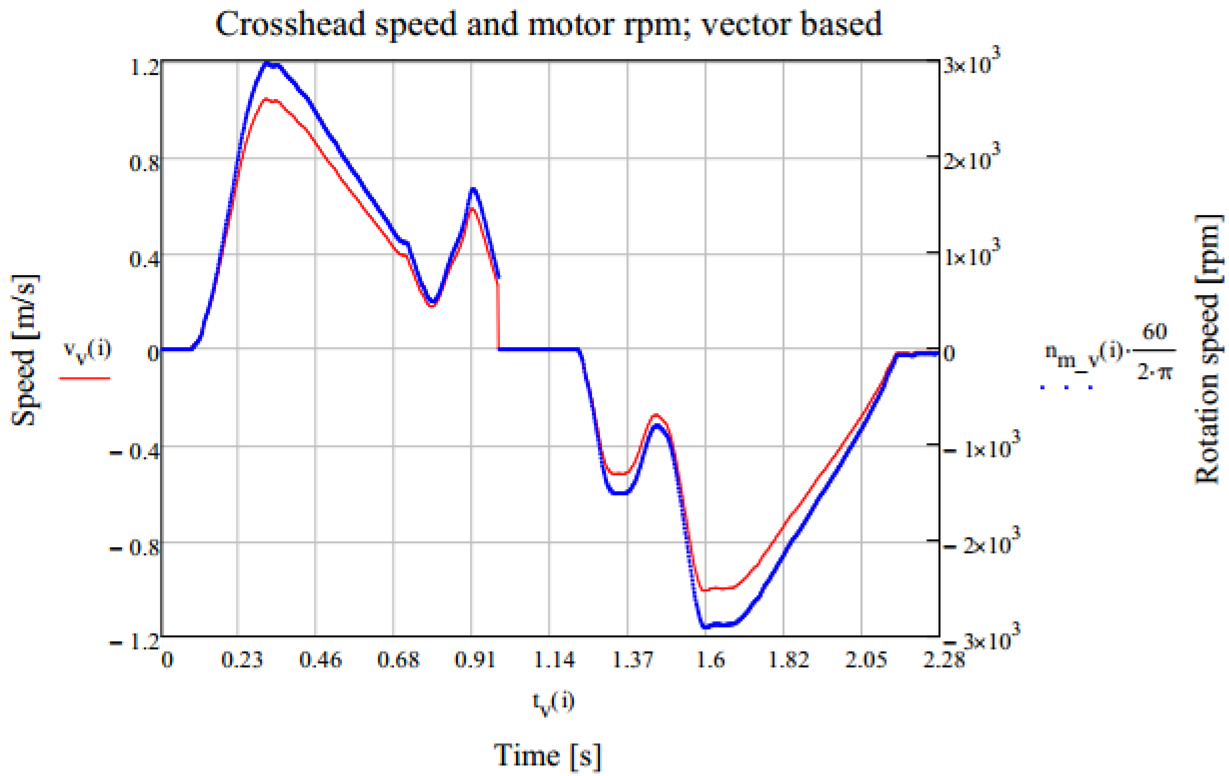

Distance: $$s_{tot\_v} := \sum_{i=2}^{\frac{s}{t_s}} \left(v_v(i)\,t_s\right) = 0.512\,m$$

2. Ratio between the LSP and the crosshead:

The lsp moves at a different speed relative to the crosshead. In order to properly map the kinetic energy of the heavy LSP, it is important to consider the transmission ratio.
Point 1 (crosshead) and point 5 (LSP) only move horizontally. The black circles are the rotation points. So triangle 2-3-4 represents a toggle, line 1-2 and line 3-5 represent the other toggles.

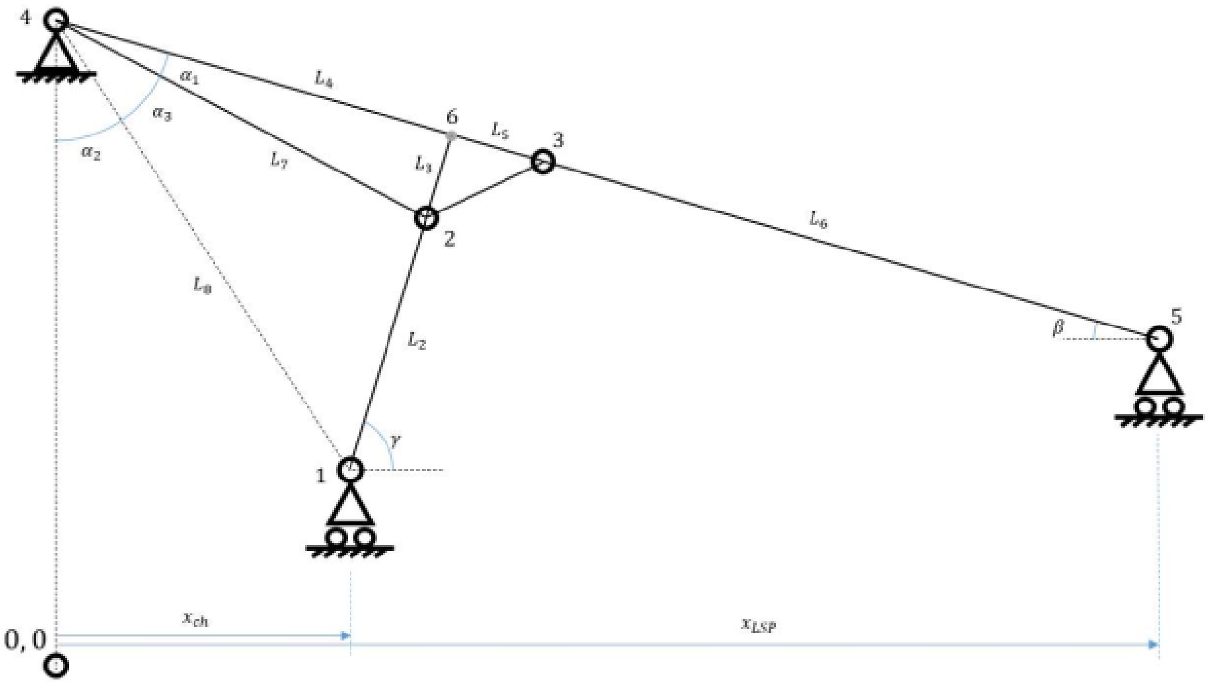

$L_1 := 255mm$ $\quad L_3 := 85mm$ $\quad L_5 := 175mm$ $\quad Y_4 := 535mm$ $\quad Y_1 := L_1$

$L_2 := 169.7mm$ $\quad L_4 := 260mm$ $\quad L_6 := 500mm$ $\quad Y_5 := 440mm$

Max angle:

Max angle if toggles are alligned: $$\alpha_{totmax} := acos\left(\frac{Y_4 - Y_5}{L_4 + L_5 + L_6}\right) = 84.168 \cdot deg$$

Max range LSP: $$X_{LSPmax} := \sin(\alpha_{totmax}) \cdot (L_4 + L_5 + L_6) = 930.161 \cdot mm$$

Position 6: $X_6 := \sin(\alpha_{totmax}) \cdot L_4$ $\qquad Y_6 := Y_4 - \cos(\alpha_{totmax}) \cdot L_4$

Position 2: $X_2 := X_6 - \cos(\alpha_{totmax}) \cdot L_3$ $\qquad Y_2 := Y_6 - \sin(\alpha_{totmax}) \cdot L_3$

Gamma: $$\gamma_o := asin\left(\frac{Y_2 - Y_1}{L_2}\right) = 84.88 \cdot deg$$

Max crosshead pos relative to gonio zero $$X_{chmax} := X_2 - \cos(\gamma_o) \cdot L_2 = 234.872 \cdot mm$$

Crosshead position relative to goniometric sketch origin:

Crosshead position: $$X_{ch}(i) := \sum_{i=2}^{1} \left(v_v(i)\,t_s\right)$$

$$X_1(i) := X_{ch}(i) - \left(X_{ch}(500) - X_{chmax}\right)$$

<u>LSP position as a function of the crosshead position:</u>

Length L7: $$L_7 := \sqrt{L_3^{\,2} + L_4^{\,2}}$$

Length L8: $$L_8(i) := \sqrt{X_1(i)^2 + \left(Y_4 - Y_1\right)^2}$$

Angle α1: $$\alpha_{o1} := \operatorname{atan}\left(\frac{L_3}{L_4}\right)$$

Angle α2: $$\alpha_{o2}(i) := \operatorname{atan}\left(\frac{X_1(i)}{Y_4 - Y_1}\right)$$

Angle α3: $$\alpha_{o3}(i) := \operatorname{acos}\left[\frac{-\left(L_2^{\,2}\right) + L_7^{\,2} + L_8(i)^2}{2 \cdot L_7 \cdot L_8(i)}\right]$$

Position 3: $$X_3(i) := \sin\left(\alpha_{o1} + \alpha_{o2}(i) + \alpha_{o3}(i)\right) \cdot \left(L_4 + L_5\right)$$

$$Y_3(i) := Y_4 - \cos\left(\alpha_{o1} + \alpha_{o2}(i) + \alpha_{o3}(i)\right) \cdot \left(L_4 + L_5\right)$$

Angle L6: $$\beta_o(i) := \operatorname{asin}\left(\frac{Y_3(i) - Y_5}{L_6}\right)$$

The position of the LSP as a function of the position of the crosshead:

Position LSP: $$X_5(i) := X_3(i) + \cos\left(\beta_o(i)\right) \cdot L_6$$

$$v_{LSP}(i) := \frac{X_5(i) - X_5(i-1)}{t_v(i) - t_v(i-1)}$$

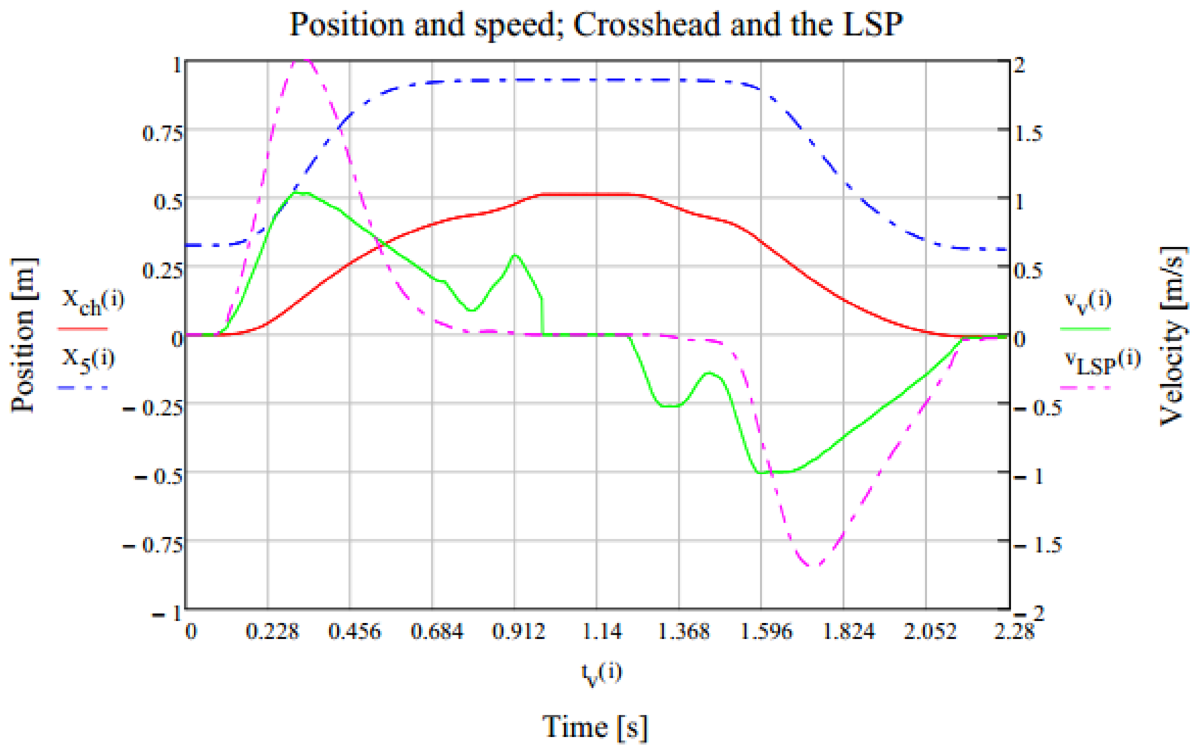

3. Phase times

Several phases have been created in which the speed pattern of the machine changes. Later on, the speed characteristics of the machine during the phases are approached. The phases are shown in the figure:

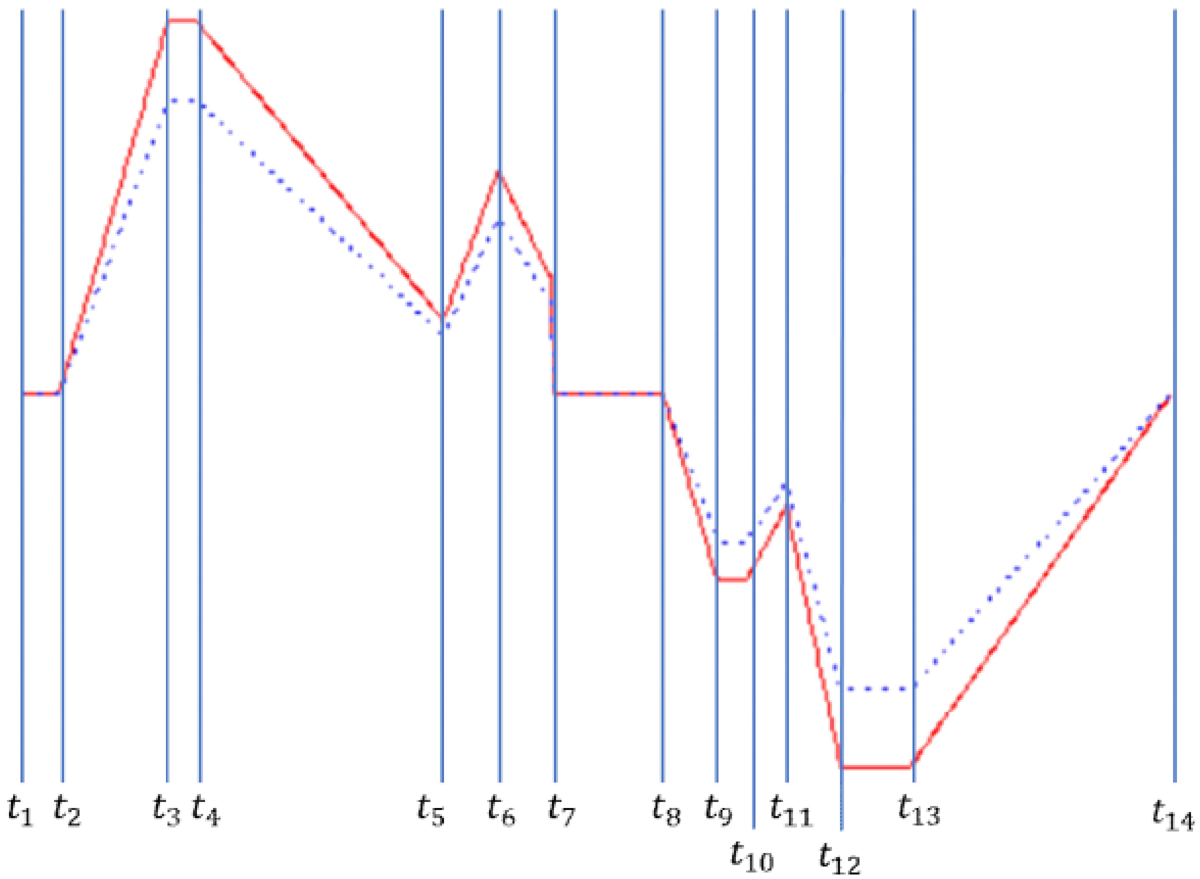

Time instances:

Starting time: $t_{start} = 0$

Ending time: $t_{end} = 2.28\,s$

Sample time: $t_s = 2 \cdot ms$

Accelerating 1: $t_{acc1} := 0.2s$

Decelerating 1: $t_{dec1} := 0.45s$

Accelerating 2: $t_{acc2} := 0.1s$

Decelerating 2: $t_{dec2} := 0.475s$

Timeslots as defined in figure 2:

$t_1 := t_{start}$ $\quad t_2 := t_1 + 0.1s$

$t_3 := t_2 + t_{acc1}$ $\quad t_4 := t_3 + 0.05s$

$t_5 := t_4 + t_{dec1}$ $\quad t_6 := t_5 + 0.1s$

$t_7 := t_6 + 0.1s$ $\quad t_8 := t_7 + 0.2s$

$t_9 := t_8 + 0.1s$ $\quad t_{10} := t_9 + 0.05s$

$t_{11} := t_{10} + 0.075s$ $\quad t_{12} := t_{11} + t_{acc2}$

$t_{13} := t_{12} + 0.125s$ $\quad t_{14} := t_{13} + t_{dec2}$

$t_{15} := t_{end}$

4. Rotational energy

Rotational energy of the vector based model:

Rotational energy formula: $E_{rot\_v}(i) := \frac{1}{2} \cdot I_m \cdot \left(n_{m\_v}(i)\right)^2 \cdot d_v(i)$

To prevent a shocky character after differentiating over small time intervals, a moving average is taken.

Moving average range: $w := 8$

Moving average:
$$E_{rot\_v\_MA}(i) := \text{if}\left(i < w, \frac{\sum_{j=0}^{i} E_{rot\_v}(j)}{i+1}, \frac{\sum_{j=i-w+1}^{i} E_{rot\_v}(j)}{w}\right)$$

Rotational power:
$$P_{rot\_v}(i) := \frac{\left(E_{rot\_v\_MA}(i) - E_{rot\_v\_MA}(i-1)\right)}{t_v(i) - t_v(i-1)}$$

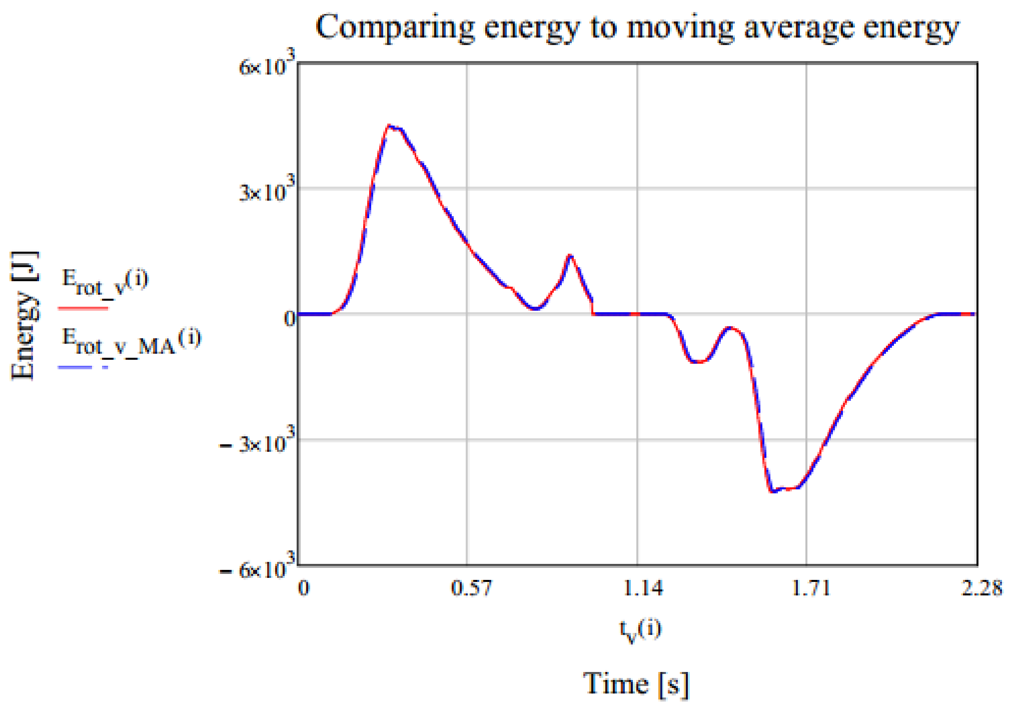

5. kinetic energy

Kinetic energy of the vector based model:

Defining when the LSP & the mold are moving:

$$Status_{LSP\_mold\_v}(i) := \begin{cases} 1 & \text{if } i \geq \frac{t_{start}}{t_s} \wedge i < \frac{0.8s}{t_s} \\ 0 & \text{if } i \geq \frac{0.8s}{t_s} \wedge i < \frac{1.425s}{t_s} \\ 1 & \text{if } i \geq \frac{1.425s}{t_s} \wedge i < \frac{t_{end}}{t_s} \end{cases}$$

Kinetic energy:

$$E_{kin\_v}(i) := d_v(i)\cdot\left[\frac{1}{2}\cdot m_{ch}\cdot v_v(i)^2 + \frac{1}{2}\cdot\left(m_{LSP} + m_{mold}\right)\cdot Status_{LSP\_mold\_v}(i)\cdot v_{LSP}(i)^2\right]$$

Moving average range: $w_2 := 8$

Moving average:

$$E_{kin\_v\_MA}(i) := \text{if}\left(i < w, \frac{\sum_{j=0}^{i} E_{kin\_v}(j)}{i+1}, \frac{\sum_{j=i-w_2+1}^{i} E_{kin\_v}(j)}{w_2}\right)$$

Rotational power:

$$P_{kin\_v}(i) := \frac{\left(E_{kin\_v\_MA}(i) - E_{kin\_v\_MA}(i-1)\right)}{t_v(i) - t_v(i-1)}$$

6. Strain energy

the strain energy is approached by a linear build-up strain form 0 to it's maximum strain in the desired time period. Firstly, the maximum strain is calculated:

Tie bar area: $A_{tiebar} := \frac{\pi}{4} \cdot d_{tiebar}^2 = 0.01\,m^2$

Potential strain energy: $E_{strain} = \frac{1}{2} \cdot V \cdot \sigma \cdot \varepsilon = \frac{1}{2} \cdot V \cdot E \cdot \varepsilon^2 = \frac{1}{2} \cdot \frac{V}{E} \cdot \sigma^2$

$$E_{strain} = \frac{1}{2} \cdot \left(A_{tiebar} \cdot 4 \cdot l_{tiebar}\right) \cdot E \cdot \left(\frac{l_\Delta}{l_{tiebar}}\right)^2$$

Strain: $\varepsilon_{test} := \frac{F_{tot}}{A_{tiebar} \cdot 4} \cdot \frac{1}{E_{steel}} = 5.043 \times 10^{-4}$

Strain in length: $l_\Delta := l_{tiebar} \cdot \varepsilon_{test} = 2.011 \cdot mm$

$$kJ := 10^3 J$$

Strain energy: $E_{strain} := \frac{1}{2} \cdot \left(A_{tiebar} \cdot 4 \cdot l_{tiebar}\right) \cdot E_{steel} \cdot \left(\frac{l_\Delta}{l_{tiebar}}\right)^2 = 4.423 \cdot kJ$

Linear strain formulas on the desired time slots:

$$\varepsilon_{tiebar\_v}(i) := \begin{cases} 0 & \text{if } i \geq \frac{0s}{t_s} \wedge i < \frac{0.8s}{t_s} \\ \frac{\varepsilon_{test}}{0.1 \cdot s} \cdot i \cdot t_s - \frac{\varepsilon_{test} \cdot 0.8}{0.1} & \text{if } i \geq \frac{0.8s}{t_s} \wedge i < \frac{0.9s}{t_s} \\ \varepsilon_{test} & \text{if } i \geq \frac{0.9s}{t_s} \wedge i < \frac{1.35s}{t_s} \\ \frac{-\varepsilon_{test}}{0.1 \cdot s} \cdot i \cdot t_s + \frac{\varepsilon_{test} \cdot 1.45}{0.1} & \text{if } i \geq \frac{1.35s}{t_s} \wedge i < \frac{1.45s}{t_s} \\ 0 & \text{if } i \geq \frac{1.45s}{t_s} \wedge i < \frac{t_{end}}{t_s} \end{cases}$$

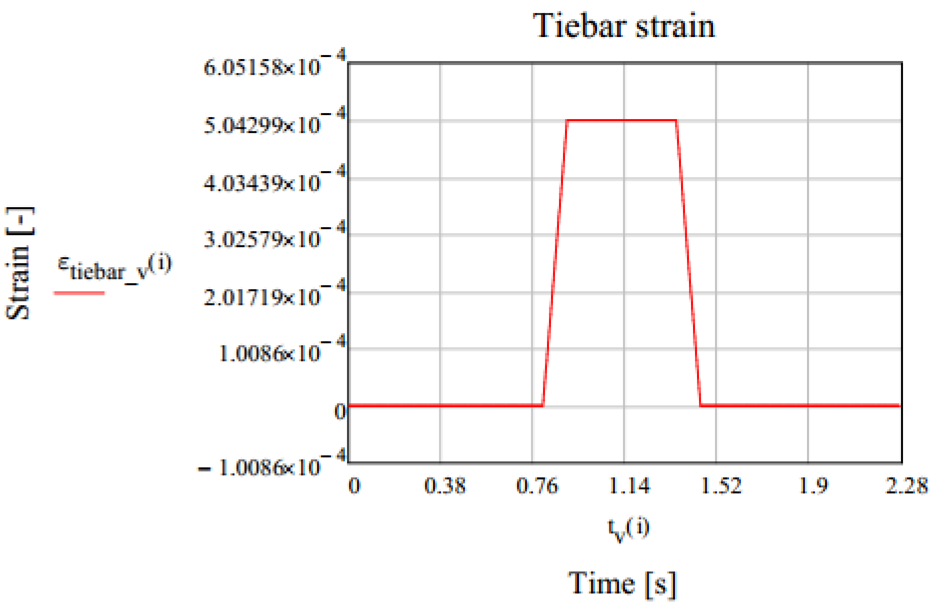

Strain energy formula: $E_{strain\_v}(i) := \frac{1}{2}\cdot\left(A_{tiebar}\cdot 4\cdot l_{tiebar}\right)\cdot E_{steel}\cdot\left(\varepsilon_{tiebar\_v}(i)\right)^2\cdot d_v(i)$

Moving average range: $w_3 := 8$

Moving average:

$$E_{strain\_v\_MA}(i) := \mathrm{if}\left(i < w, \frac{\sum_{j=0}^{i} E_{strain\_v}(j)}{i+1}, \frac{\sum_{j=i-w_3+1}^{i} E_{strain\_v}(j)}{w_3}\right)$$

Rotational power:

$$P_{strain\_v}(i) := \frac{\left(E_{strain\_v\_MA}(i) - E_{strain\_v\_MA}(i-1)\right)}{t_v(i) - t_v(i-1)}$$

7. Frictional energy loss

The total frictional loss is estimated by comparing the calculated and measured energy balance. A this way, the friction loss can be approached.

$E_{friction} := 3kJ$

$$P_{friction} := \frac{E_{friction}}{t_5 - t_2 + t_{14} - t_{11}} = 2.143\cdot kW$$

$$P_{friction\_v}(i) := \begin{cases} P_{friction} & \text{if } i \ge \frac{t_2}{t_s} \wedge i < \frac{t_5}{t_s} \\ 0 & \text{if } i \ge \frac{t_5}{t_s} \wedge i < \frac{t_{11}}{t_s} \\ -P_{friction} & \text{if } i \ge \frac{t_{11}}{t_s} \wedge i < \frac{t_{14}}{t_s} \end{cases}$$

8. Energy conclusion

Anti-overshoot by flipping over 0

$$\text{Status}_{neutral}(i) := \begin{cases} 1 & \text{if } i \geq \dfrac{t_{start}}{t_s} \wedge i < \dfrac{t_7 + 0.01s}{t_s} \\ 0 & \text{if } i \geq \dfrac{t_7 + 0.01s}{t_s} \wedge i < \dfrac{t_8 - 0.01s}{t_s} \\ 1 & \text{if } i \geq \dfrac{t_8 - 0.01s}{t_s} \wedge i < \dfrac{t_{end}}{t_s} \end{cases}$$

Total power:

$$P_{tot\_v}(i) := \left(P_{rot\_v}(i) + P_{kin\_v}(i) + P_{strain\_v}(i) + P_{friction\_v}(i)\right) \cdot \text{Status}_{neutral}(i)$$

Corrected strain power:

$$P_{strain\_vc}(i) := P_{strain\_v}(i) \cdot \text{Status}_{neutral}(i)$$

Crosshead force:

$$F_{ch\_v}(i) := \frac{1}{v_v(i) \cdot d_v(i)} \cdot \left(P_{tot\_v}(i) - P_{rot\_v}(i)\right)$$

$$P_{rotkin}(i) := P_{rot\_v}(i) + P_{kin\_v}(i) + P_{friction\_v}(i)$$

Measured power:

$$P_{measured}(i) := n_{m\_v}(i) \cdot T_m(i) \cdot d_v(i)$$

$$\Delta P_{strain}(i) := P_{measured}(i) - P_{rotkin}(i)$$

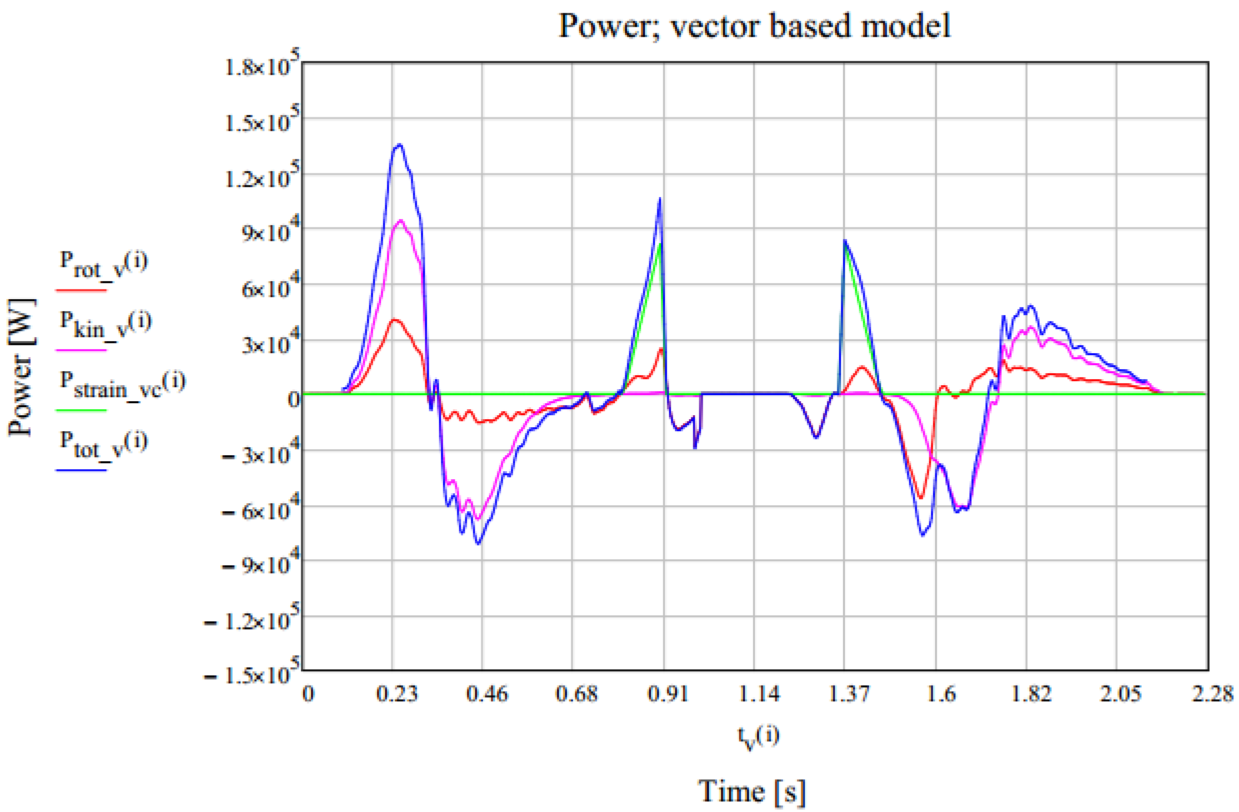

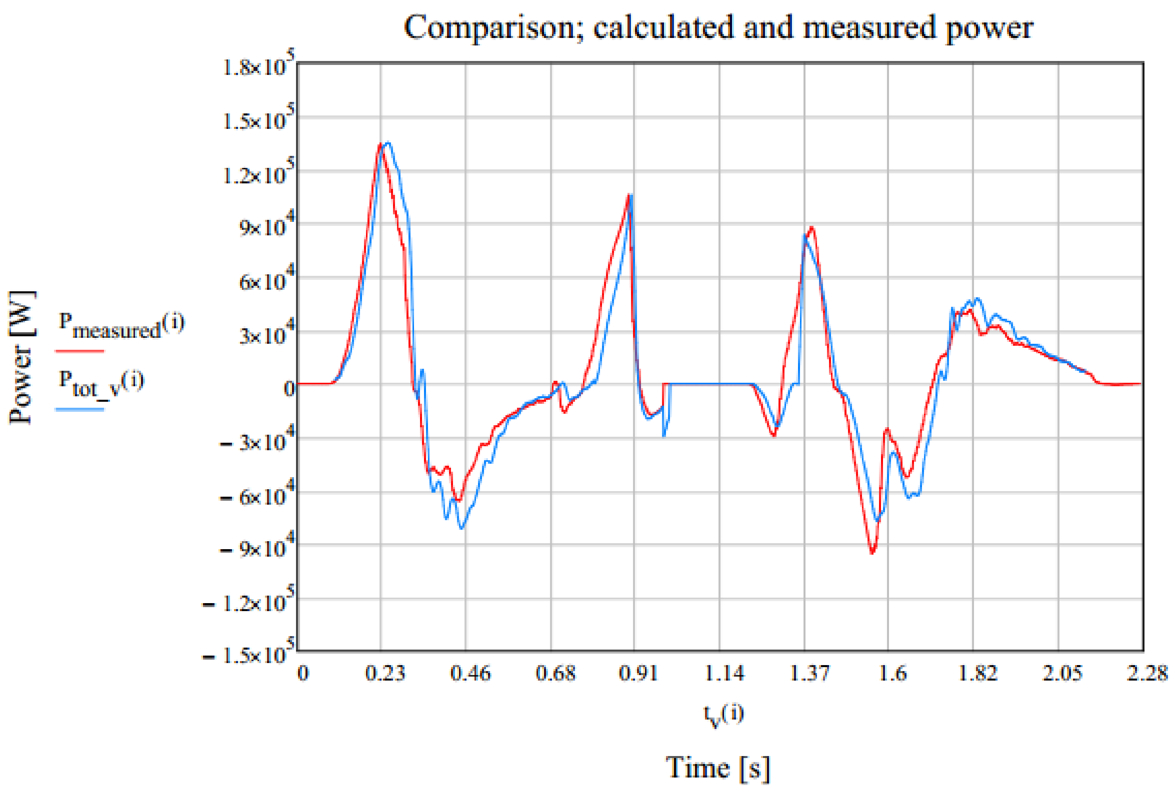

Change of energy:

$$\Delta E_{rot\_v}(i) := P_{rot\_v}(i)\, t_s$$

$$\Delta E_{kin\_v}(i) := P_{kin\_v}(i)\, t_s$$

$$\Delta E_{strain\_v}(i) := P_{strain\_v}(i)\, t_s$$

$$\Delta E_{tot\_v}(i) := P_{tot\_v}(i)\, t_s$$

Energy balances can be created to calculate the used energy (integrating the power over time):

Rotational energy:

$$E_{rot\_v\_in} := \sum_{j=\frac{t_2}{t_s}}^{\frac{t_4}{t_s}} \Delta E_{rot\_v}(j) + \sum_{j=\frac{t_5}{t_s}}^{\frac{t_6}{t_s}} \Delta E_{rot\_v}(j) - \sum_{j=\frac{t_8-0.5s}{t_s}}^{\frac{t_9}{t_s}} \Delta E_{rot\_v}(j) - \sum_{j=\frac{t_{11}}{t_s}+0.5}^{\frac{t_{13}}{t_s}} \Delta E_{rot\_v}(j)$$

$$E_{rot\_v\_rec} := \sum_{j=\frac{t_4}{t_s}}^{\frac{t_5}{t_s}} \Delta E_{rot\_v}(j) + \sum_{j=\frac{t_6}{t_s}}^{\frac{t_7+0.5s}{t_s}} \Delta E_{rot\_v}(j) - \sum_{j=\frac{t_{10}}{t_s}}^{\frac{t_{11}}{t_s}+0.5} \Delta E_{rot\_v}(j) - \sum_{j=\frac{t_{13}}{t_s}}^{\frac{t_{14}+0.001s}{t_s}} \Delta E_{rot\_v}(j)$$

Kinetic energy:

$$E_{kin\_v\_in} := \sum_{j=\frac{t_2}{t_s}}^{\frac{t_4}{t_s}} \Delta E_{kin\_v}(j) + \sum_{j=\frac{t_5}{t_s}}^{\frac{t_6}{t_s}} \Delta E_{kin\_v}(j) - \sum_{j=\frac{t_8-0.5s}{t_s}}^{\frac{t_9}{t_s}} \Delta E_{kin\_v}(j) - \sum_{j=\frac{t_{11}}{t_s}+0.5}^{\frac{t_{13}}{t_s}} \Delta E_{kin\_v}(j)$$

$$E_{kin\_v\_rec} := \sum_{j=\frac{t_4}{t_s}}^{\frac{t_5}{t_s}} \Delta E_{kin\_v}(j) + \sum_{j=\frac{t_6}{t_s}}^{\frac{t_7+0.5s}{t_s}} \Delta E_{kin\_v}(j) - \sum_{j=\frac{t_{10}}{t_s}}^{\frac{t_{11}}{t_s}+0.5} \Delta E_{kin\_v}(j) - \sum_{j=\frac{t_{13}}{t_s}}^{\frac{t_{14}+0.001s}{t_s}} \Delta E_{kin\_v}(j)$$

Strain energy:

$$E_{strain\_v\_in} := \sum_{j=\frac{t_5}{t_s}}^{\frac{(t_7+0.05s)}{t_s}} \Delta E_{strain\_v}(j) \qquad E_{strain\_v\_rec} := \sum_{j=\frac{t_8-0.01s}{t_s}}^{\frac{t_{11}+0.001s}{t_s}} -\Delta E_{strain\_v}(j)$$

Total energy:

$$E_{tot\_v\_in} := \sum_{j=\frac{t_2}{t_s}}^{\frac{t_4}{t_s}} \Delta E_{tot\_v}(j) + \sum_{j=\frac{t_5}{t_s}}^{\frac{t_6}{t_s}} \Delta E_{tot\_v}(j) - \sum_{j=\frac{t_8}{t_s}}^{\frac{t_9}{t_s}} \Delta E_{tot\_v}(j) - \sum_{j=\frac{t_{11}}{t_s}+0.5}^{\frac{t_{13}}{t_s}} \Delta E_{tot\_v}(j) + E_{friction}$$

$$E_{tot\_v\_rec} := \sum_{j=\frac{t_4}{t_s}}^{\frac{t_5}{t_s}} \Delta E_{tot\_v}(j) + \sum_{j=\frac{t_6}{t_s}}^{\frac{t_7}{t_s}} \Delta E_{tot\_v}(j) - \sum_{j=\frac{t_{10}}{t_s}}^{\frac{t_{11}}{t_s}+0.5} \Delta E_{tot\_v}(j) - \sum_{j=\frac{t_{13}}{t_s}}^{\frac{t_{14}-0.001s}{t_s}} \Delta E_{tot\_v}(j)$$

Concluding:

	Energy in:	Theoretical regeneratable energy:
Rotational:	$E_{rot\_v\_in} = 10.485\cdot kJ$	$E_{rot\_v\_rec} = -10.665\cdot kJ$
Kinetic:	$E_{kin\_v\_in} = 14.918\cdot kJ$	$E_{kin\_v\_rec} = -14.735\cdot kJ$
Strain:	$E_{strain\_v\_in} = 4.423\cdot kJ$	$E_{strain\_v\_rec} = -3.989\cdot kJ$
Total:	$E_{tot\_v\_in} = 32.045\cdot kJ$	$E_{tot\_v\_rec} = -25.967\cdot kJ$

Appendix F. Acceleration variable calculation model

MathCad model calculation on the crosshead during the opening and closing movement
Variable model

A reliable model has been built up in the vector-based model. Now the goal is to adapt the model, so the accelerations can be adjusted. By making the model variable in acceleration and speeds, it can be researched what the possibilities are in the behavior of the machine.

The table of contents:

A IPM (Ideal Physical Model) has been made of the situation. All the gear ratios, masses, forces and energy directions are included in the model. The IPM can be seen in the following figure:

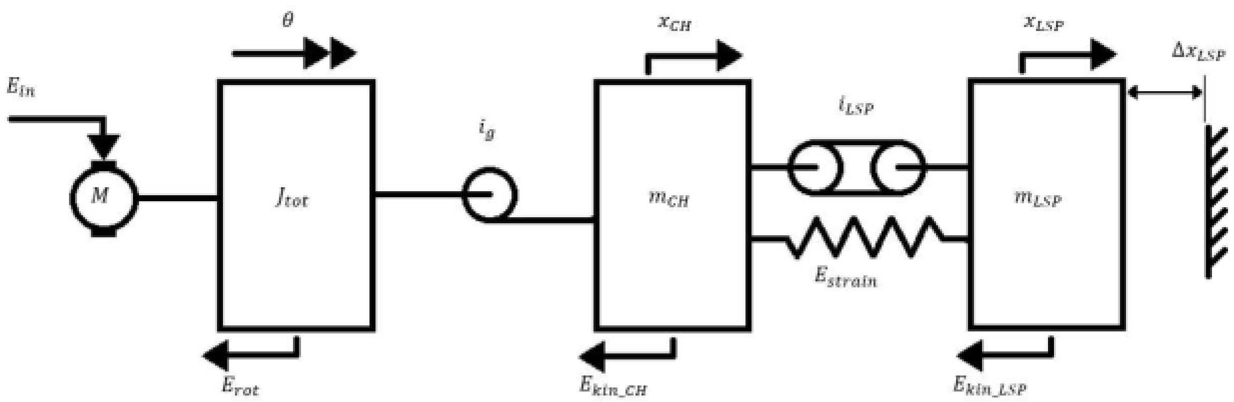

1. General input data:

Motor properties:

Motor intertia: $I_{motor} := 0.058\,kg \cdot m^2$

Multiplication factor: $I_{sv} := 1.1$

Rotation inertia: $I_m := I_{motor} \cdot I_{sv} = 0.064\,kg \cdot m^2$

Gearing: $i_g := \frac{20.92}{2 \cdot \pi} \frac{mm}{rad}$

Masses:

Multiplication factor mass: $m_{sv} := 0.95$

Mass crosshead: $m_{ch} := m_{sv} \cdot 275kg$

Mass LSP $m_{LSP} := m_{sv} \cdot 4060kg$

Mass mold $m_{mold} := m_{sv} \cdot 1533kg$

Closing unit properties:

$F_{tot} := 4400kN$ $d_{tiebar} := 115mm$

$l_{tiebar} := 3987mm$ $E_{steel} := 210GPa$

Time properties:

$t_{start} := 0s$

$t_{step} := 0.0025s$

$t_s := t_{step}$

2. Phase times

Several phases have been created in which the speed pattern of the machine changes. Later on, the speed characteristics of the machine during the phases are approached. The phases are shown in the figure:

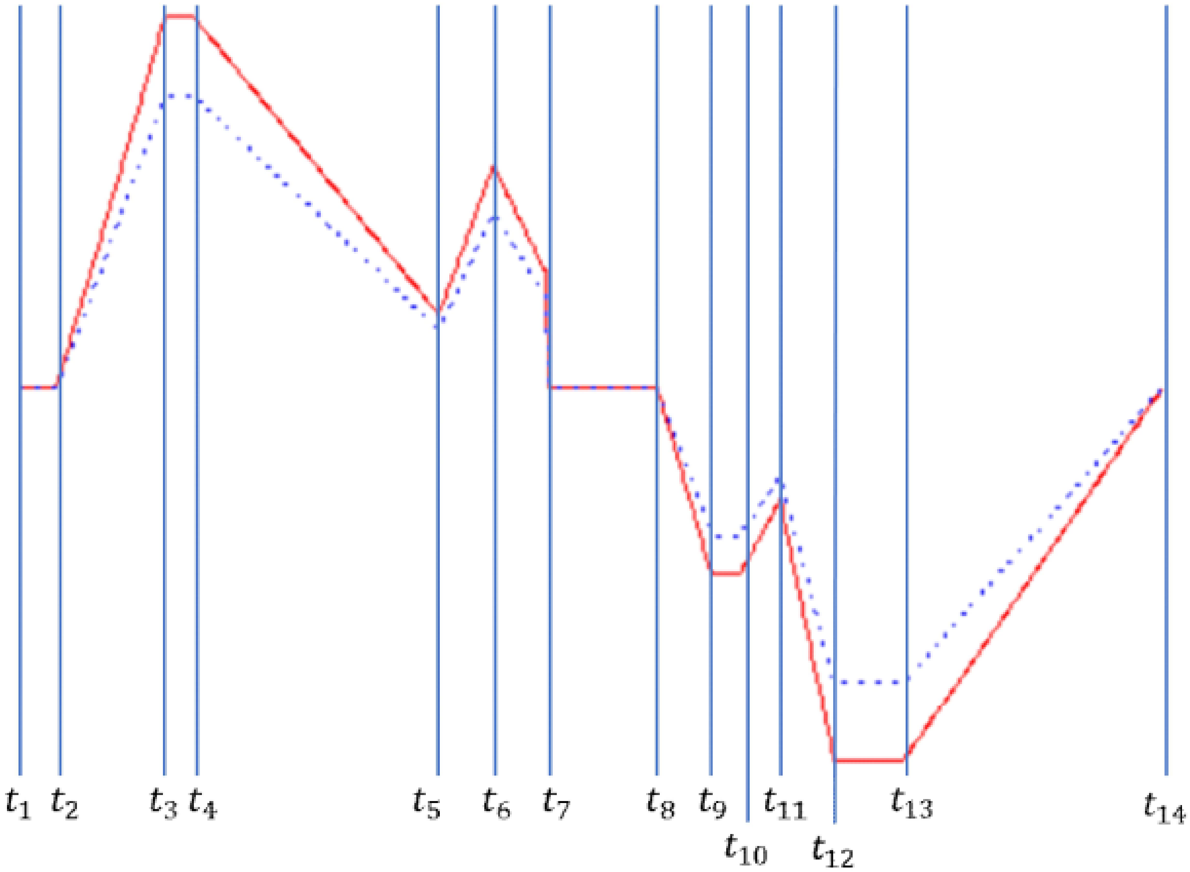

$v_{max} := 1\frac{m}{s}$ $a_{acc1} := 5\frac{m}{s^2}$ $a_{dec1} := \frac{16}{9}\frac{m}{s^2}$ $a_{acc2} := 7\frac{m}{s^2}$ $a_{dec2} := 2.1\frac{m}{s^2}$ $s_{stroke} := 0.512m$

Starting time: $t_1 := t_{start}$

Time before & after acceleration: $t_2 := t_1 + 0.1s$ $t_3 := t_2 + \frac{v_{max}}{a_{acc1}}$

Assuming constant acceleration: $s = v_{gem} \cdot t = v_{gem} \cdot \frac{\Delta v}{a_c}$

Distance without t3-t4:

$$s_{const} := \frac{v_{max}}{2} \cdot \frac{v_{max}}{a_{acc1}} + \frac{v_{max} + 0.2\frac{m}{s}}{2} \cdot \frac{v_{max} - 0.2\frac{m}{s}}{a_{dec1}} + \frac{(0.6 + 0.2)\frac{m}{s}}{2} \cdot 0.1s + \frac{(0.6 + 0.3)\frac{m}{s}}{2} \cdot 0.1s$$

Time before & after deceleration: $t_4 := t_3 + \frac{s_{stroke} - s_{const}}{v_{max}}$ $t_5 := t_4 + \frac{v_{max} - 0.2\frac{m}{s}}{a_{dec1}}$

Locking crosshead: $t_6 := t_5 + 0.1s$ $t_7 := t_6 + 0.1s$

Starting to open: $t_8 := t_7 + 0.2s$

$t_9 := t_8 + 0.1s$ $t_{10} := t_9 + 0.05s$ $t_{11} := t_{10} + 0.075s$

Time after acceleration: $t_{12} := t_{11} + \dfrac{v_{max} - 0.3\frac{m}{s}}{a_{acc2}}$

$$s_{const2} := \frac{0.5\frac{m}{s}}{2}\cdot 0.1s + 0.5\frac{m}{s}\cdot 0.05s + \frac{(0.5+0.3)\frac{m}{s}}{2}\cdot 0.075s + \frac{v_{max} + 0.3\frac{m}{s}}{2}\cdot\frac{v_{max} - 0.3\frac{m}{s}}{a_{acc2}} + \frac{v_{max}}{2}\cdot\frac{v_{max}}{a_{dec2}}$$

Time before & after deceleration: $t_{13} := t_{12} + \dfrac{s_{stroke} - s_{const2}}{v_{max}}$ $\quad t_{14} := t_{13} + \dfrac{v_{max}}{a_{dec2}}$

Ending time: $t_{15} := t_{14} + 0.1s$ $\quad t_{end} := t_{15}$

Speed in function over time:

$$v_{f1}(t) := \begin{cases} 0\frac{m}{s} & \text{if } t \ge t_1 \wedge t < t_2 \\ a_{acc1}\cdot t - a_{acc1}\cdot t_2 & \text{if } t \ge t_2 \wedge t < t_3 \\ v_{max} & \text{if } t \ge t_3 \wedge t < t_4 \\ -a_{dec1}\cdot t + 0.2\frac{m}{s} + a_{dec1}\cdot t_5 & \text{if } t \ge t_4 \wedge t < t_5 \\ 4\frac{m}{s^2}t + 0.2\frac{m}{s} - 4\frac{m}{s^2}\cdot t_5 & \text{if } t \ge t_5 \wedge t < t_6 \\ -3.5\frac{m}{s^2}t + 0.6\frac{m}{s} + 3.5\frac{m}{s^2}\cdot t_6 & \text{if } t \ge t_6 \wedge t < t_7 \\ 0\frac{m}{s} & \text{if } t \ge t_7 \wedge t < t_8 \\ -5\frac{m}{s^2}t + 5\frac{m}{s^2}\cdot t_8 & \text{if } t \ge t_8 \wedge t < t_9 \\ -0.5\frac{m}{s} & \text{if } t \ge t_9 \wedge t < t_{10} \\ \frac{8}{3}\frac{m}{s^2}t - 0.5\frac{m}{s} - \frac{8}{3}\cdot\frac{m}{s^2}\cdot t_{10} & \text{if } t \ge t_{10} \wedge t < t_{11} \\ -a_{acc2}t + a_{acc2}\cdot t_{11} - 0.3\frac{m}{s} & \text{if } t \ge t_{11} \wedge t < t_{12} \\ -v_{max} & \text{if } t \ge t_{12} \wedge t < t_{13} \\ a_{dec2}t - a_{dec2}\cdot t_{14} & \text{if } t \ge t_{13} \wedge t < t_{14} \\ 0\frac{m}{s} & \text{if } t \ge t_{14} \wedge t < t_{15} \end{cases}$$

Speed average: $v_f(t) := \dfrac{v_{f1}(t - 0.01s) + v_{f1}(t)}{2}$

Time intervals: $t := t_{start}, t_{step} .. t_{end}$

Motor rpm: $n_{m\_f}(t) := \dfrac{v_f(t)}{i_g}$

Direction in a function:

$$d_f(t) := \begin{cases} 1 & \text{if } t \ge 0s \wedge t < \frac{t_7 + t_8}{2} \\ (-1) & \text{if } t \ge \frac{t_7 + t_8}{2} \wedge t < t_{end} \end{cases}$$

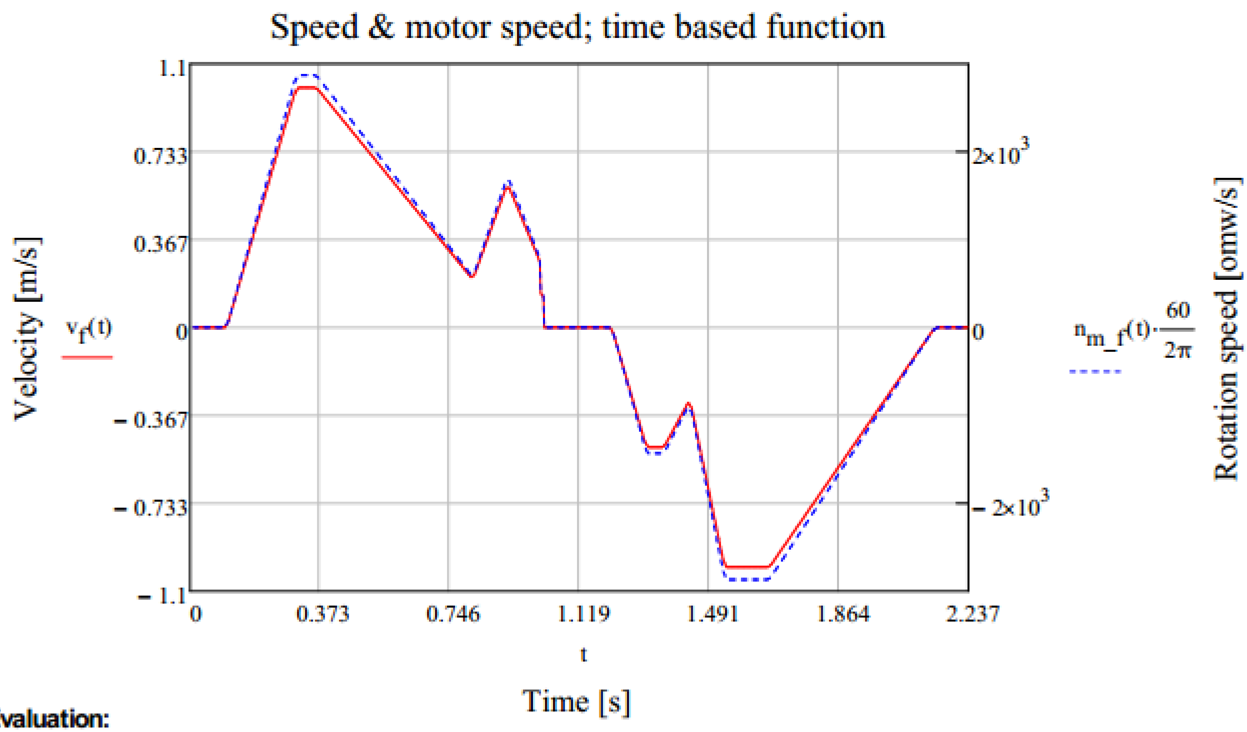

Evaluation:

Closing: Acceleration time: $t_{acc1} := t_3 - t_2 = 0.2\,s$

Constant speed: $t_4 - t_3 = 0.057\,s$

Deceleration time: $t_{dec1} := t_5 - t_4 = 0.45\,s$

Opening: Acceleration time: $t_{acc2} := t_{12} - t_{11} = 0.1\,s$

Constant speed: $t_{13} - t_{12} = 0.129\,s$

Deceleration time: $t_{dec2} := t_{14} - t_{13} = 0.476\,s$

Dry cycle time: $t_{dry} := t_{14} - t_8 + t_7 - t_2 = 1.837\,s$

Converting function based model to vector based model:

$$\text{Integers} := \text{round}\left(\frac{t_{end} - t_{step}}{t_{step}}\right) = 894$$

$$i := 0 .. \text{Integers}$$

$$v_v(i) := v_f(i\cdot t_{step})$$

$$t_v(i) := i\cdot t_{step}$$

$$n_{m\_v}(i) := \frac{v_v(i)}{i_g}$$

$$d_v(i) := d_f(i\cdot t_{step})$$

3. Ratio between the LSP and the crosshead:

The lsp moves at a different speed relative to the crosshead. In order to properly map the kinetic energy of the heavy LSP, it is important to consider the transmission ratio.
Point 1 (crosshead) and point 5 (LSP) only move horizontally. The black circles are the rotation points. So triangle 2-3-4 represents a toggle, line 1-2 and line 3-5 represent the other toggles.

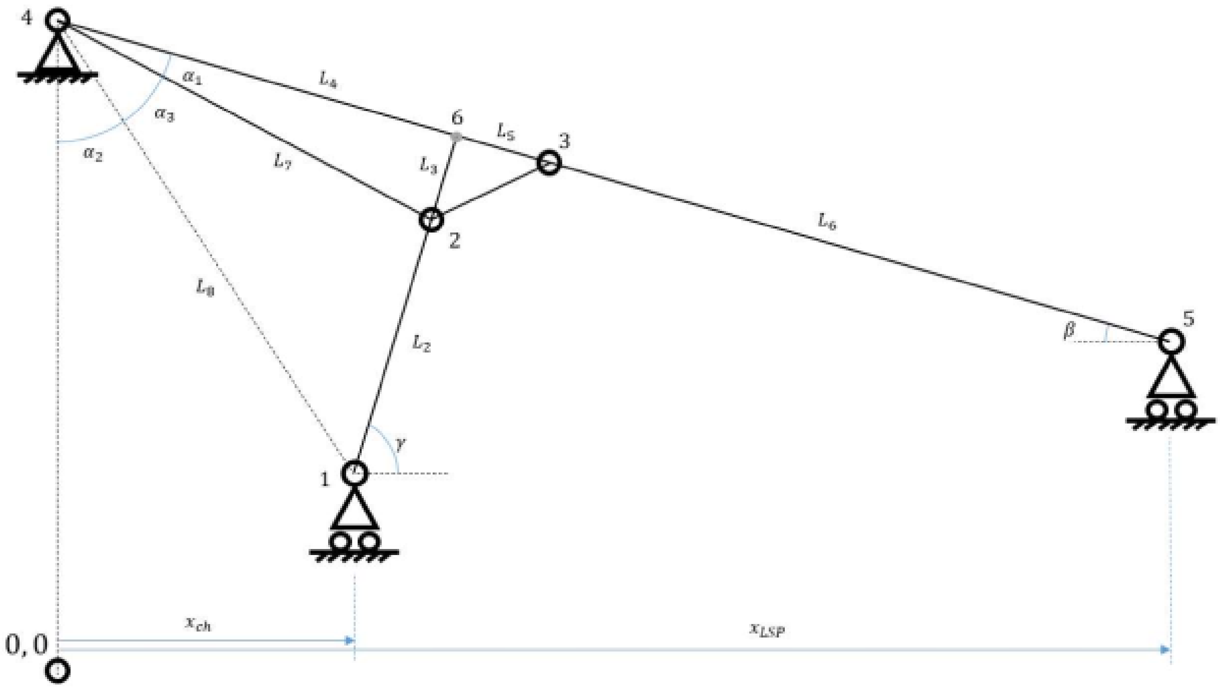

$L_1 := 255mm$ $L_3 := 85mm$ $L_5 := 175mm$ $Y_4 := 535mm$ $Y_1 := L_1$

$L_2 := 169.7mm$ $L_4 := 260mm$ $L_6 := 500mm$ $Y_5 := 440mm$

Max angle:

Max angle if toggles are alligned: $\alpha_{totmax} := \operatorname{acos}\left(\frac{Y_4 - Y_5}{L_4 + L_5 + L_6}\right) = 84.168 \cdot deg$

Max range LSP: $X_{LSPmax} := \sin(\alpha_{totmax}) \cdot (L_4 + L_5 + L_6) = 930.161 \cdot mm$

Position 6: $X_6 := \sin(\alpha_{totmax}) \cdot L_4$ $Y_6 := Y_4 - \cos(\alpha_{totmax}) \cdot L_4$

Position 2: $X_2 := X_6 - \cos(\alpha_{totmax}) \cdot L_3$ $Y_2 := Y_6 - \sin(\alpha_{totmax}) \cdot L_3$

Gamma: $\gamma_o := \operatorname{asin}\left(\frac{Y_2 - Y_1}{L_2}\right) = 84.88 \cdot deg$

Max crosshead pos relative to gonio zero: $X_{chmax} := X_2 - \cos(\gamma_o) \cdot L_2 = 234.872 \cdot mm$

Crosshead position relative to goniometric sketch origin:

Crosshead position: $X_{ch}(i) := \sum_{i=4}^{i} \left(v_v(i)\, t_{step}\right)$

$$X_1(i) := X_{ch}(i) - \left(s_{stroke} - X_{chmax}\right)$$

LSP position as a function of the crosshead position:

Length L7: $L_7 := \sqrt{L_3^{\,2} + L_4^{\,2}}$

Length L8: $L_8(i) := \sqrt{X_1(i)^2 + (Y_4 - Y_1)^2}$

Angle α1: $\alpha_{o1} := \operatorname{atan}\left(\frac{L_3}{L_4}\right)$

Angle α2: $\alpha_{o2}(i) := \operatorname{atan}\left(\frac{X_1(i)}{Y_4 - Y_1}\right)$

Angle α3: $\alpha_{o3}(i) := \operatorname{acos}\left[\frac{-\left(L_2^{\,2}\right) + L_7^{\,2} + L_8(i)^2}{2 \cdot L_7 \cdot L_8(i)}\right]$

Position 3:

$$X_3(i) := \sin\left(\alpha_{o1} + \alpha_{o2}(i) + \alpha_{o3}(i)\right) \cdot (L_4 + L_5)$$

$$Y_3(i) := Y_4 - \cos\left(\alpha_{o1} + \alpha_{o2}(i) + \alpha_{o3}(i)\right) \cdot (L_4 + L_5)$$

Angle L6: $\beta_o(i) := \operatorname{asin}\left(\frac{Y_3(i) - Y_5}{L_6}\right)$

The position of the LSP as a function of the position of the crosshead:

Position LSP: $X_5(i) := X_3(i) + \cos\left(\beta_o(i)\right) \cdot L_6$

Speed LSP: $v_{LSP}(i) := \frac{X_5(i) - X_5(i-1)}{t_v(i) - t_v(i-1)}$

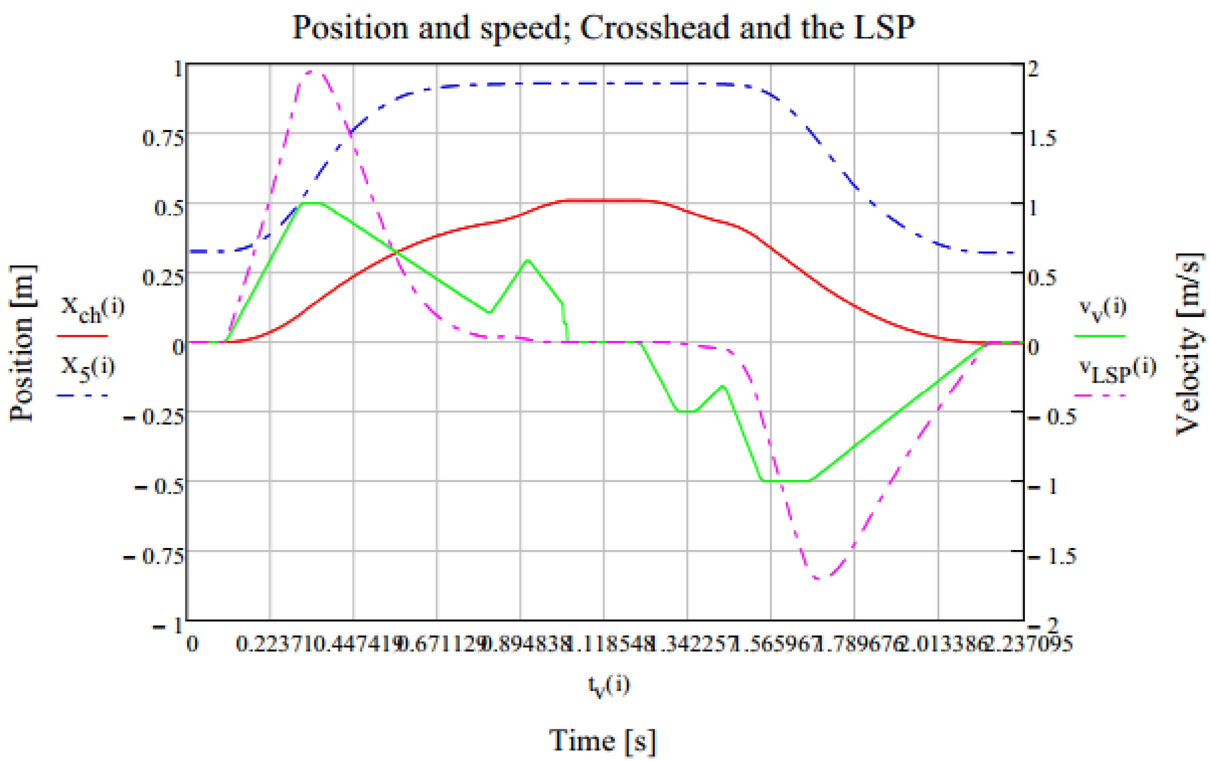

The working speeds and gear ratios are know. So, the energy can be calculated.
The energy to close/open the closing unit is splitted into 4 parts, namely:
1. Rotational energy of the motor
2. Kinetic energy of the crosshead, the LSP and the mold
3. Strain energy of the tie-bars as a reaction of the clamping force
4. Frictional energy loss

4. Rotational energy

Rotational energy of the vector based model:

Rotational energy formula: $E_{rot\_v}(i) := \frac{1}{2} \cdot I_m \cdot \left(n_{m\_v}(i)\right)^2 \cdot d_v(i)$

To prevent a shocky character after differentiating over small time intervals, a moving average is taken.

Moving average range: $w := 16$

Moving average: $$E_{rot\_v\_MA}(i) := \text{if}\left(i < w, \frac{\sum_{j=0}^{i} E_{rot\_v}(j)}{i+1}, \frac{\sum_{j=i-w+1}^{i} E_{rot\_v}(j)}{w} \right)$$

Rotational power: $$P_{rot\_v}(i) := \frac{\left(E_{rot\_v\_MA}(i) - E_{rot\_v\_MA}(i-1)\right)}{t_v(i) - t_v(i-1)}$$

5. Kinetic energy

The LSP and the mold are not moving along with the crosshead at the whole cylce, therefore a function is made to describe the status of the LSP and the mold:

Defining when the LSP & the mold are moving: $$Status_{LSP\_mold\_v}(i) := \left| \begin{array}{l} 1 \ \text{ if } i \geq \frac{t_{start}}{t_s} \wedge i < \frac{t_5}{t_s} \\ 0 \ \text{ if } i \geq \frac{t_5}{t_s} \wedge i < \frac{t_{11}}{t_s} \\ 1 \ \text{ if } i \geq \frac{t_{11}}{t_s} \wedge i < \frac{t_{end}}{t_s} \end{array} \right.$$

Kinetic energy: $$E_{kin\_v}(i) := d_v(i) \cdot \left[\frac{1}{2} \cdot m_{ch} \cdot v_v(i)^2 + \frac{1}{2} \cdot \left(m_{LSP} + m_{mold}\right) \cdot Status_{LSP\_mold\_v}(i) \cdot v_{LSP}(i)^2 \right]$$

Moving average range: $w_2 := 5$

Moving average: $$E_{kin\_v\_MA}(i) := \text{if}\left(i < w, \frac{\sum_{j=0}^{i} E_{kin\_v}(j)}{i+1}, \frac{\sum_{j=i-w_2+1}^{i} E_{kin\_v}(j)}{w_2} \right)$$

Rotational power: $$P_{kin\_v}(i) := \frac{\left(E_{kin\_v\_MA}(i) - E_{kin\_v\_MA}(i-1)\right)}{t_v(i) - t_v(i-1)}$$

6. Strain energy

Strain energy of the function based model:

Tie bar area: $A_{tiebar} := \frac{\pi}{4} \cdot d_{tiebar}^{2} = 0.01\,m^{2}$

Potential strain energy: $E_{strain} = \frac{1}{2} \cdot V \cdot \sigma \cdot \varepsilon = \frac{1}{2} \cdot V \cdot E \cdot \varepsilon^{2} = \frac{1}{2} \cdot \frac{V}{E} \cdot \sigma^{2}$

$$E_{strain} = \frac{1}{2} \cdot (A_{tiebar} \cdot 4 \cdot l_{tiebar}) \cdot E \cdot \left(\frac{l_{\Delta}}{l_{tiebar}}\right)^{2}$$

Strain: $\varepsilon_{test} := \frac{F_{tot}}{A_{tiebar} \cdot 4} \cdot \frac{1}{E_{steel}} = 5.043 \times 10^{-4}$

Strain in length: $l_{\Delta} := l_{tiebar} \cdot \varepsilon_{test} = 2.011 \cdot mm$

$kJ := 10^{3} J$

Strain energy: $E_{strain} := \frac{1}{2} \cdot (A_{tiebar} \cdot 4 \cdot l_{tiebar}) \cdot E_{steel} \cdot \left(\frac{l_{\Delta}}{l_{tiebar}}\right)^{2} = 4.423 \cdot kJ$

Linear strain formulas on the desired time slots:

$$\varepsilon_{tiebar\_v}(i) := \begin{cases} 0 & \text{if } i \geq \frac{0s}{t_s} \wedge i < \frac{t_5}{t_s} \\ \frac{\varepsilon_{test}}{0.1 \cdot s} \cdot i \cdot t_s - \frac{\varepsilon_{test} \cdot t_5}{0.1s} & \text{if } i \geq \frac{t_5}{t_s} \wedge i < \frac{t_6}{t_s} \\ \varepsilon_{test} & \text{if } i \geq \frac{t_6}{t_s} \wedge i < \frac{t_9}{t_s} \\ \frac{-\varepsilon_{test}}{0.1 \cdot s} \cdot i \cdot t_s + \frac{\varepsilon_{test} \cdot (t_9 + 0.1s)}{0.1s} & \text{if } i \geq \frac{t_9}{t_s} \wedge i < \frac{t_9 + 0.1s}{t_s} \\ 0 & \text{if } i \geq \frac{t_9 + 0.1s}{t_s} \wedge i < \frac{t_{end}}{t_s} \end{cases}$$

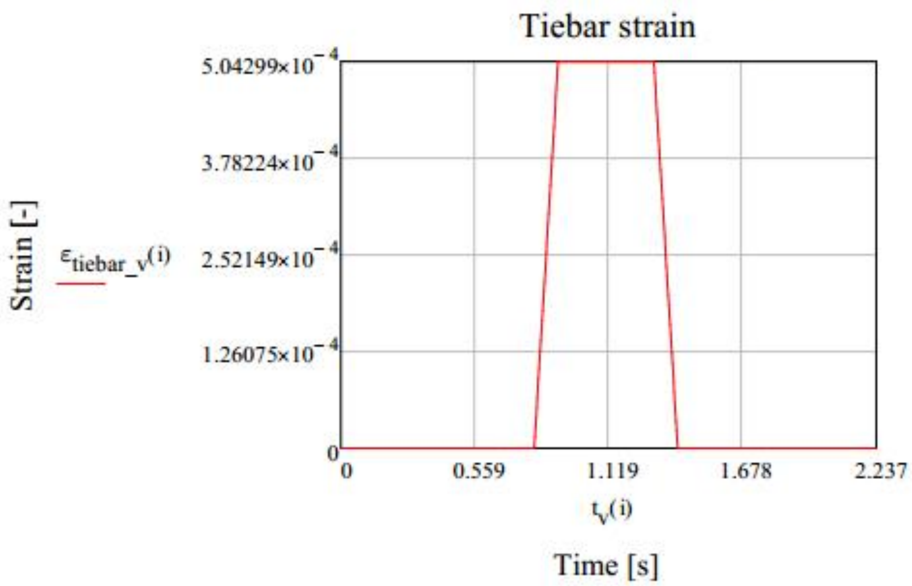

Anti-overshoot by flipping over 0

$$Status_{neutral}(i) := \begin{cases} 1 & \text{if } i \geq \frac{t_{start}}{t_s} \wedge i < \frac{t_7 + 0.01s}{t_s} \\ 0 & \text{if } i \geq \frac{t_7 + 0.01s}{t_s} \wedge i < \frac{t_8 - 0.01s}{t_s} \\ 1 & \text{if } i \geq \frac{t_8 - 0.01s}{t_s} \wedge i < \frac{t_{end}}{t_s} \end{cases}$$

Strain energy formula:

$$E_{strain\_v}(i) := \frac{1}{2} \cdot \left(A_{tiebar} \cdot 4 \cdot l_{tiebar}\right) \cdot E_{steel} \cdot \left(\varepsilon_{tiebar\_v}(i)\right)^2 \cdot d_v(i)$$

Moving average range:

$$w_3 := 5$$

Moving average:

$$E_{strain\_v\_MA}(i) := \text{if}\left(i < w, \frac{\sum_{j=0}^{i} E_{strain\_v}(j)}{i+1}, \frac{\sum_{j=i-w_3+1}^{i} E_{strain\_v}(j)}{w_3} \right)$$

Rotational power:

$$P_{strain\_v}(i) := \frac{\left(E_{strain\_v\_MA}(i) - E_{strain\_v\_MA}(i-1)\right)}{t_v(i) - t_v(i-1)} \cdot Status_{neutral}(i)$$

7. Frictional energy loss

The total frictional loss is estimated by comparing the calculated and measured energy balance.

$$E_{friction} := 3kJ$$

$$P_{friction} := \frac{E_{friction}}{t_5 - t_2 + t_{14} - t_{11}} = 2.125 \cdot kW$$

$$P_{friction\_v}(i) := \begin{cases} 0 & \text{if } i \geq \frac{t_1}{t_s} \wedge i < \frac{t_2}{t_s} \\ P_{friction} & \text{if } i \geq \frac{t_2}{t_s} \wedge i < \frac{t_5}{t_s} \\ 0 & \text{if } i \geq \frac{t_5}{t_s} \wedge i < \frac{t_{11}}{t_s} \\ -P_{friction} & \text{if } i \geq \frac{t_{11}}{t_s} \wedge i < \frac{t_{14}}{t_s} \\ 0 & \text{if } i \geq \frac{t_{14}}{t_s} \wedge i < \frac{t_{end}}{t_s} \end{cases}$$

8. Total power

For a smooth gradient of the power curves, a weighted average is taken over a time interval

Total power:

$$P_{tot\_v}(i) := \left(P_{rot\_v}(i) + P_{kin\_v}(i) + P_{strain\_v}(i) + P_{friction\_v}(i)\right) \cdot Status_{neutral}(i)$$

Crosshead force:

$$F_{ch\_v}(i) := \frac{1}{v_v(i) \cdot d_v(i)} \cdot \left(P_{tot\_v}(i) - P_{rot\_v}(i)\right)$$

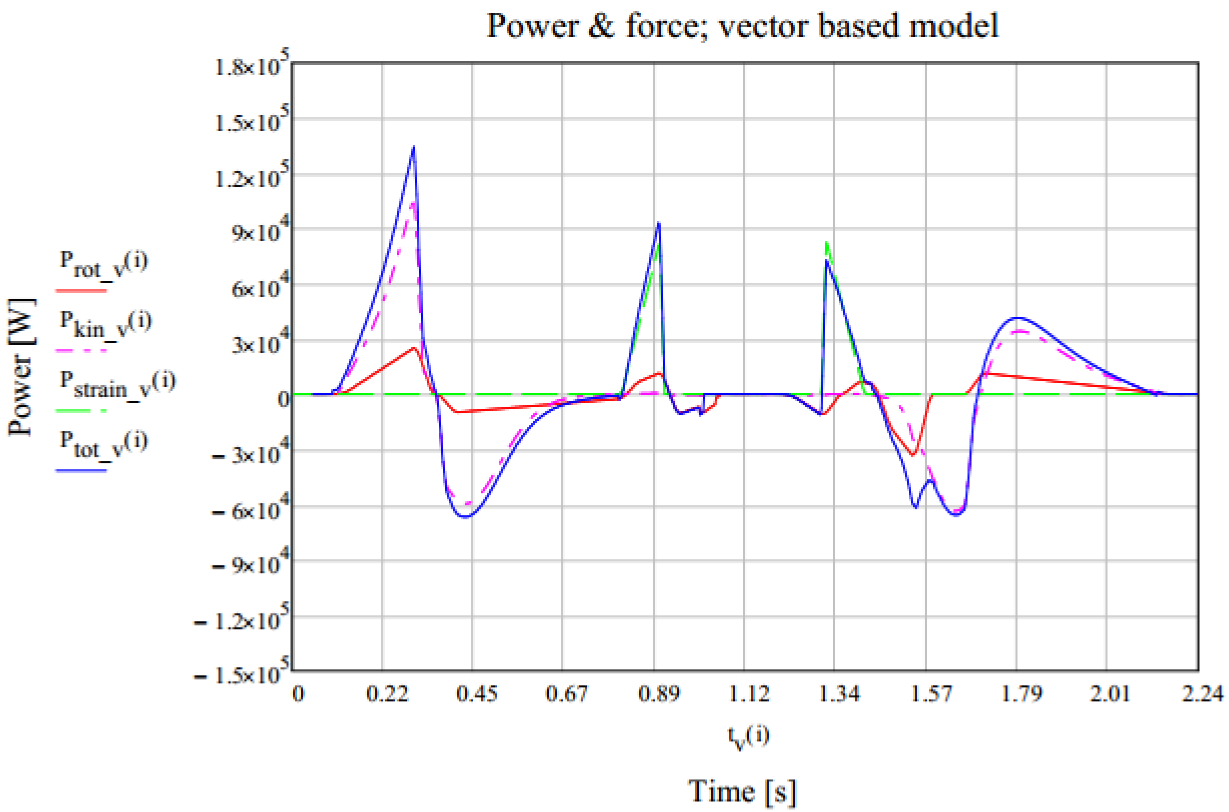

Change of energy:

$$\Delta E_{rot\_v}(i) := P_{rot\_v}(i)\,t_s$$

$$\Delta E_{kin\_v}(i) := P_{kin\_v}(i)\,t_s$$

$$\Delta E_{strain\_v}(i) := P_{strain\_v}(i)\,t_s$$

$$\Delta E_{tot\_v}(i) := P_{tot\_v}(i)\,t_s$$

Program loops for energy calculations:

Energy in while closing:

$$Energy = \sum_{j=t_{end}}^{t_{start}} \Delta E_{x\_v}(j)$$

$$Energy_{in\_close}(x) := \left| \begin{array}{l} mx \leftarrow 0 \\ sum \leftarrow 0 \\ \text{for } i \in 20..\,round\left[0.5\cdot\frac{(t_7 + t_8)}{t_s}\right] \\ \quad \left| \begin{array}{l} \delta \leftarrow x(i) \\ sum \leftarrow sum + \delta \ \text{ if } \ \delta > mx \\ sum \end{array} \right. \end{array} \right.$$

Energy regeneration while closing:

$$Energy = \sum_{j=t_{end}}^{t_{start}} \Delta E_{x\_v}(j)$$

$$Energy_{reg\_close}(x) := \left| \begin{array}{l} mx \leftarrow 0 \\ sum \leftarrow 0 \\ \text{for } i \in 20..\,round\left[0.5\cdot\frac{(t_7 + t_8)}{t_s}\right] \\ \quad \left| \begin{array}{l} \delta \leftarrow x(i) \\ sum \leftarrow sum + \delta \ \text{ if } \ \delta < mx \\ sum \end{array} \right. \end{array} \right.$$

Energy in while opening:

$$Energy = \sum_{j = t_{end}}^{t_{start}} \Delta E_{x\_v}(j)$$

$$Energy_{in\_open}(x) := \left| \begin{array}{l} mx \leftarrow 0 \\ sum \leftarrow 0 \\ \text{for } i \in round\left[0.5 \cdot \frac{(t_7 + t_8)}{t_s}\right] .. \frac{t_{end}}{t_s} \\ \quad \left| \begin{array}{l} \delta \leftarrow x(i) \\ sum \leftarrow sum + \delta \text{ if } \delta < mx \\ sum \end{array} \right. \end{array} \right.$$

Energy regeneration while opening:

$$Energy = \sum_{j = t_{end}}^{t_{start}} \Delta E_{x\_v}(j)$$

$$Energy_{reg\_open}(x) := \left| \begin{array}{l} mx \leftarrow 0 \\ sum \leftarrow 0 \\ \text{for } i \in round\left[0.5 \cdot \frac{(t_7 + t_8)}{t_s}\right] .. \frac{t_{end}}{t_s} \\ \quad \left| \begin{array}{l} \delta \leftarrow x(i) \\ sum \leftarrow sum + \delta \text{ if } \delta > mx \\ sum \end{array} \right. \end{array} \right.$$

Energy balances can be created to calculate the used energy (integrating the power over time):

Rotational energy:

$$E_{rot\_v\_in} := Energy_{in\_close}(\Delta E_{rot\_v}) - Energy_{in\_open}(\Delta E_{rot\_v}) = 6.894 \cdot kJ$$

$$E_{rot\_v\_rec} := Energy_{reg\_close}(\Delta E_{rot\_v}) - Energy_{reg\_open}(\Delta E_{rot\_v}) = -6.894 \cdot kJ$$

Kinetic energy:

$$E_{kin\_v\_in} := Energy_{in\_close}(\Delta E_{kin\_v}) - Energy_{in\_open}(\Delta E_{kin\_v}) = 18.074 \cdot kJ$$

$$E_{kin\_v\_rec} := Energy_{reg\_close}(\Delta E_{kin\_v}) - Energy_{reg\_open}(\Delta E_{kin\_v}) = -18.074 \cdot kJ$$

Strain energy:

$$E_{strain\_v\_in} := Energy_{in\_close}(\Delta E_{strain\_v}) - Energy_{in\_open}(\Delta E_{strain\_v}) = 4.423 \cdot kJ$$

$$E_{strain\_v\_rec} := Energy_{reg\_close}(\Delta E_{strain\_v}) - Energy_{reg\_open}(\Delta E_{strain\_v}) = -4.423 \cdot kJ$$

Total energy:

$$E_{tot\_v\_in} := Energy_{in\_close}(\Delta E_{tot\_v}) - Energy_{in\_open}(\Delta E_{tot\_v}) = 30.005 \cdot kJ$$

$$E_{tot\_v\_rec} := Energy_{reg\_close}(\Delta E_{tot\_v}) - Energy_{reg\_open}(\Delta E_{tot\_v}) = -26.76 \cdot kJ$$

9. Energy conclusion:

Energy per destination:

	Energy in:	Theoretical regeneratable energy:
Rotational:	$E_{rot\_v\_in} = 6.894 \cdot kJ$	$E_{rot\_v\_rec} = -6.894 \cdot kJ$
Kinetic:	$E_{kin\_v\_in} = 18.074 \cdot kJ$	$E_{kin\_v\_rec} = -18.074 \cdot kJ$
Strain:	$E_{strain\_v\_in} = 4.423 \cdot kJ$	$E_{strain\_v\_rec} = -4.423 \cdot kJ$
Total:	$E_{tot\_v\_in} = 30.005 \cdot kJ$	$E_{tot\_v\_rec} = -26.76 \cdot kJ$

10. Calculations regarding the model evaluation

Energy per phase:

$$E_{acc1} := \sum_{j = \mathrm{round}\left(\frac{t_2}{t_s}\right)}^{\mathrm{round}\left(\frac{t_4}{t_s}\right)} \Delta E_{tot\_v}(j) \qquad E_{acc2} := \sum_{j = \mathrm{round}\left(\frac{t_{11}}{t_s}\right)}^{\mathrm{round}\left(\frac{t_{13}}{t_s}\right)} \Delta E_{tot\_v}(j)$$

$$E_{dec1} := \sum_{j = \mathrm{round}\left(\frac{t_4}{t_s}\right)}^{\mathrm{round}\left(\frac{t_5}{t_s}\right)} \Delta E_{tot\_v}(j) \qquad E_{dec2} := \sum_{j = \mathrm{round}\left(\frac{t_{13}}{t_s}\right)}^{\mathrm{round}\left(\frac{t_{14}}{t_s}\right)} \Delta E_{tot\_v}(j)$$

Max power per phase:

$$P_{acc1} := \left| \begin{array}{l} mx \leftarrow 0 \\ \text{for } i \in \mathrm{round}\left(\frac{t_2}{t_s}\right) .. \mathrm{round}\left(\frac{t_4}{t_s}\right) \\ \quad \left| \begin{array}{l} \delta \leftarrow P_{tot\_v}(i) \\ mx \leftarrow \delta \ \text{ if } \ \delta > mx \end{array} \right. \\ mx \end{array} \right.$$

$$P_{acc2} := \left| \begin{array}{l} mx \leftarrow 0 \\ \text{for } i \in \mathrm{round}\left(\frac{t_{11}}{t_s}\right) .. \mathrm{round}\left(\frac{t_{13}}{t_s}\right) \\ \quad \left| \begin{array}{l} \delta \leftarrow P_{tot\_v}(i) \\ mx \leftarrow \delta \ \text{ if } \ \delta < mx \end{array} \right. \\ mx \cdot -1 \end{array} \right.$$

$$P_{dec1} := \left| \begin{array}{l} mx \leftarrow 0 \\ \text{for } i \in \mathrm{round}\left(\frac{t_4}{t_s}\right) .. \mathrm{round}\left(\frac{t_5}{t_s}\right) \\ \quad \left| \begin{array}{l} \delta \leftarrow P_{tot\_v}(i) \\ mx \leftarrow \delta \ \text{ if } \ \delta < mx \end{array} \right. \\ mx \end{array} \right.$$

$$P_{dec2} := \left| \begin{array}{l} mx \leftarrow 0 \\ \text{for } i \in \mathrm{round}\left(\frac{t_{13}}{t_s}\right) .. \mathrm{round}\left(\frac{t_{14}}{t_s}\right) \\ \quad \left| \begin{array}{l} \delta \leftarrow P_{tot\_v}(i) \\ mx \leftarrow \delta \ \text{ if } \ \delta > mx \end{array} \right. \\ mx \cdot -1 \end{array} \right.$$

Evaluation sheet:

Total dry cycle time: $t_{dry} = 1.837\,s$

	Acceleration	time	Energy in/out	Peak power
Acceleration to close	$a_{acc1} = 5\,\frac{m}{s^2}$	$t_{acc1} = 0.2\,s$	$E_{acc1} = 13.605 \cdot kJ$	$P_{acc1} = 134.295 \cdot kW$
Deceleration to close	$a_{dec1} = 1.778\,\frac{m}{s^2}$	$t_{dec1} = 0.45\,s$	$E_{dec1} = -11.927 \cdot kJ$	$P_{dec1} = -66.539 \cdot kW$
Acceleration to open	$a_{acc2} = 7\,\frac{m}{s^2}$	$t_{acc2} = 0.1\,s$	$E_{acc2} = -9.835 \cdot kJ$	$P_{acc2} = 65.479 \cdot kW$
Deceleration to open	$a_{dec2} = 2.1\,\frac{m}{s^2}$	$t_{dec2} = 0.476\,s$	$E_{dec2} = 8.577 \cdot kJ$	$P_{dec2} = -41.434 \cdot kW$

Energy per destination:

	Energy in:	Theoretical regeneratable energy:
Rotational:	$E_{rot\_v\_in} = 6.894 \cdot kJ$	$E_{rot\_v\_rec} = -6.894 \cdot kJ$
Kinetic:	$E_{kin\_v\_in} = 18.074 \cdot kJ$	$E_{kin\_v\_rec} = -18.074 \cdot kJ$
Strain:	$E_{strain\_v\_in} = 4.423 \cdot kJ$	$E_{strain\_v\_rec} = -4.423 \cdot kJ$
Total:	$E_{tot\_v\_in} = 30.005 \cdot kJ$	$E_{tot\_v\_rec} = -26.76 \cdot kJ$

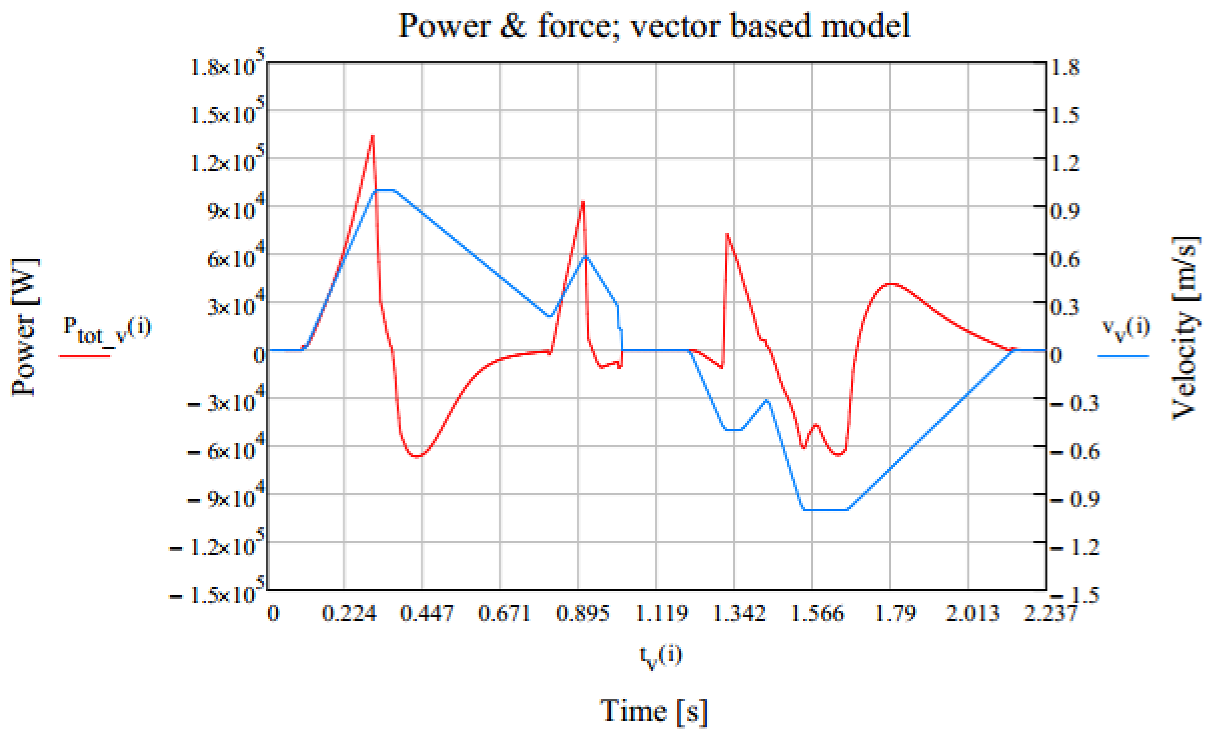

Appendix G. Calculation iterations acceleration speed

In the new concept, the available drive power changes during acceleration and deceleration. It is important to identify the consequences of a faster or slower speed change. Therefore, several iterations have been performed, in which the acceleration varies between 0.5 and 7 m/s². The results of the calculation (exactly the same calculation as in the previous appendix, but with adjusted acceleration speeds) are displayed using an evaluation sheet. Herein, the peak powers, energy consumption, and times are displayed.

Acceleration speed: 0.5 m/s²

Evaluation sheet:

Total dry cycle time: $t_{dry} = 3.423\,s$

Max locking power: $P_{max\_lock} := 100kW$

	Acceleration	time	Energy in/out	Peak power
Acceleration to close	$a_{acc1} = 0.5\,\frac{m}{s^2}$	$t_{acc1} = 0.9\,s$	$E_{acc1} = 3.109 \cdot kJ$	$P_{acc1} = 6.41 \cdot kW$
Deceleration to close	$a_{dec1} = 0.5\,\frac{m}{s^2}$	$t_{dec1} = 0.5\,s$	$E_{dec1} = -1.383 \cdot kJ$	$P_{dec1} = -7.971 \cdot kW$
Acceleration to open	$a_{acc2} = 0.5\,\frac{m}{s^2}$	$t_{acc2} = 0.3\,s$	$E_{acc2} = -2.632 \cdot kJ$	$P_{acc2} = 8.004 \cdot kW$
Deceleration to open	$a_{dec2} = 0.5\,\frac{m}{s^2}$	$t_{dec2} = 0.9\,s$	$E_{dec2} = 1.75 \cdot kJ$	$P_{dec2} = -4.515 \cdot kW$

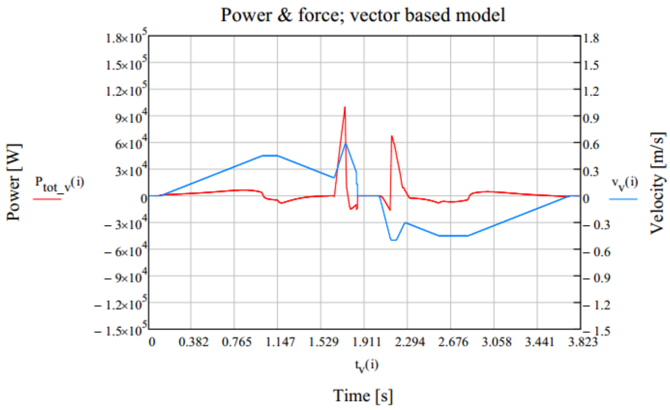

Acceleration speed: 1 m/s²

Evaluation sheet:

Total dry cycle time: $t_{dry} = 2.647\,s$

Max locking power: $P_{max\_lock} := 100kW$

	Acceleration	time	Energy in/out	Peak power
Acceleration to close	$a_{acc1} = 1\,\frac{m}{s^2}$	$t_{acc1} = 0.65\,s$	$E_{acc1} = 6.006 \cdot kJ$	$P_{acc1} = 16.613 \cdot kW$
Deceleration to close	$a_{dec1} = 1\,\frac{m}{s^2}$	$t_{dec1} = 0.45\,s$	$E_{dec1} = -4.279 \cdot kJ$	$P_{dec1} = -26.045 \cdot kW$
Acceleration to open	$a_{acc2} = 1\,\frac{m}{s^2}$	$t_{acc2} = 0.35\,s$	$E_{acc2} = -5.372 \cdot kJ$	$P_{acc2} = 29.898 \cdot kW$
Deceleration to open	$a_{dec2} = 1\,\frac{m}{s^2}$	$t_{dec2} = 0.65\,s$	$E_{dec2} = 4.463 \cdot kJ$	$P_{dec2} = -14.279 \cdot kW$

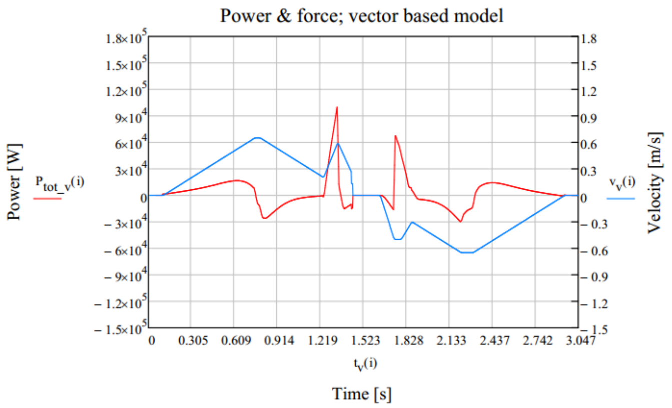

Acceleration speed: 1.5 m/s^2

Evaluation sheet:

Total dry cycle time: $t_{dry} = 2.295\,s$

Max locking power: $P_{max\_lock} := 100kW$

	Acceleration	time	Energy in/out	Peak power
Acceleration to close	$a_{acc1} = 1.5\,\frac{m}{s^2}$	$t_{acc1} = 0.5\,s$	$E_{acc1} = 7.182\cdot kJ$	$P_{acc1} = 29.59\cdot kW$
Deceleration to close	$a_{dec1} = 1.5\,\frac{m}{s^2}$	$t_{dec1} = 0.367\,s$	$E_{dec1} = -5.471\cdot kJ$	$P_{dec1} = -40.337\cdot kW$
Acceleration to open	$a_{acc2} = 1.5\,\frac{m}{s^2}$	$t_{acc2} = 0.3\,s$	$E_{acc2} = -7.737\cdot kJ$	$P_{acc2} = 45.35\cdot kW$
Deceleration to open	$a_{dec2} = 1.5\,\frac{m}{s^2}$	$t_{dec2} = 0.5\,s$	$E_{dec2} = 6.802\cdot kJ$	$P_{dec2} = -27.181\cdot kW$

Power & force; vector based model

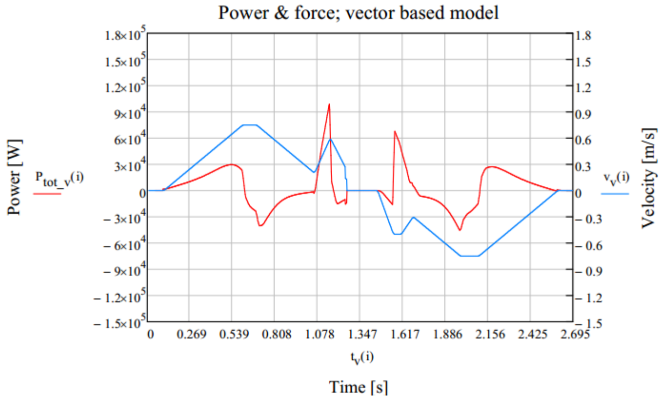

Acceleration speed: 2 m/s^2

Evaluation sheet:

Total dry cycle time: $t_{dry} = 2.07\,s$

Max locking power: $P_{max\_lock} := 100kW$

	Acceleration	time	Energy in/out	Peak power
Acceleration to close	$a_{acc1} = 2\,\frac{m}{s^2}$	$t_{acc1} = 0.435\,s$	$E_{acc1} = 9.594\cdot kJ$	$P_{acc1} = 44.839\cdot kW$
Deceleration to close	$a_{dec1} = 2\,\frac{m}{s^2}$	$t_{dec1} = 0.335\,s$	$E_{dec1} = -7.891\cdot kJ$	$P_{dec1} = -63.391\cdot kW$
Acceleration to open	$a_{acc2} = 2\,\frac{m}{s^2}$	$t_{acc2} = 0.285\,s$	$E_{acc2} = -10.321\cdot kJ$	$P_{acc2} = 71.837\cdot kW$
Deceleration to open	$a_{dec2} = 2\,\frac{m}{s^2}$	$t_{dec2} = 0.435\,s$	$E_{dec2} = 9.361\cdot kJ$	$P_{dec2} = -42.593\cdot kW$

Power & force; vector based model

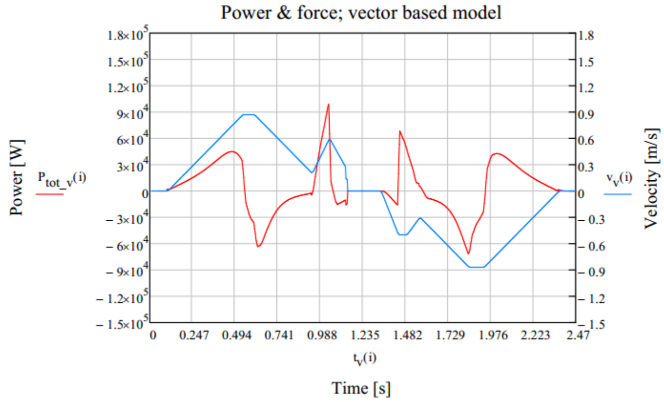

Acceleration speed: 2.5 m/s^2

Evaluation sheet:

Total dry cycle time: $t_{dry} = 1.913\,s$

Max locking power: $P_{max\_lock} := 100kW$

	Acceleration	time	Energy in/out	Peak power
Acceleration to close	$a_{acc1} = 2.5\,\frac{m}{s^2}$	$t_{acc1} = 0.388\,s$	$E_{acc1} = 11.852\cdot kJ$	$P_{acc1} = 62.047\cdot kW$
Deceleration to close	$a_{dec1} = 2.5\,\frac{m}{s^2}$	$t_{dec1} = 0.308\,s$	$E_{dec1} = -10.159\cdot kJ$	$P_{dec1} = -87.686\cdot kW$
Acceleration to open	$a_{acc2} = 2.5\,\frac{m}{s^2}$	$t_{acc2} = 0.268\,s$	$E_{acc2} = -12.801\cdot kJ$	$P_{acc2} = 99.052\cdot kW$
Deceleration to open	$a_{dec2} = 2.5\,\frac{m}{s^2}$	$t_{dec2} = 0.388\,s$	$E_{dec2} = 11.796\cdot kJ$	$P_{dec2} = -60.07\cdot kW$

Power & force; vector based model

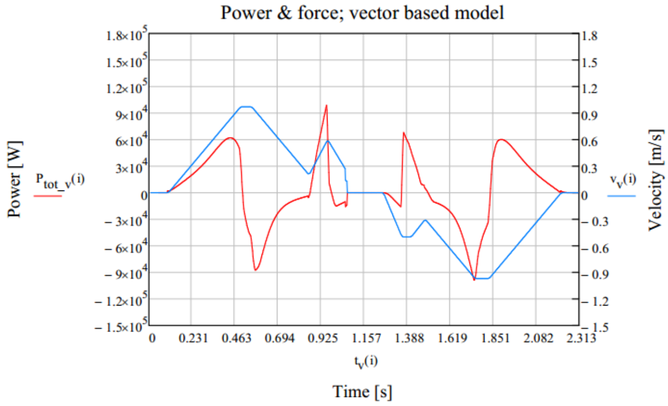

Acceleration speed: 3 m/s^2

Evaluation sheet:

Total dry cycle time: $t_{dry} = 1.806\,s$

Max locking power: $P_{max\_lock} := 100kW$

	Acceleration	time	Energy in/out	Peak power
Acceleration to close	$a_{acc1} = 3\,\frac{m}{s^2}$	$t_{acc1} = 0.333\,s$	$E_{acc1} = 11.408\cdot kJ$	$P_{acc1} = 80.979\cdot kW$
Deceleration to close	$a_{dec1} = 3\,\frac{m}{s^2}$	$t_{dec1} = 0.267\,s$	$E_{dec1} = -9.706\cdot kJ$	$P_{dec1} = -93.003\cdot kW$
Acceleration to open	$a_{acc2} = 3\,\frac{m}{s^2}$	$t_{acc2} = 0.233\,s$	$E_{acc2} = -14.211\cdot kJ$	$P_{acc2} = 104.385\cdot kW$
Deceleration to open	$a_{dec2} = 3\,\frac{m}{s^2}$	$t_{dec2} = 0.333\,s$	$E_{dec2} = 13.234\cdot kJ$	$P_{dec2} = -79.251\cdot kW$

Power & force; vector based model

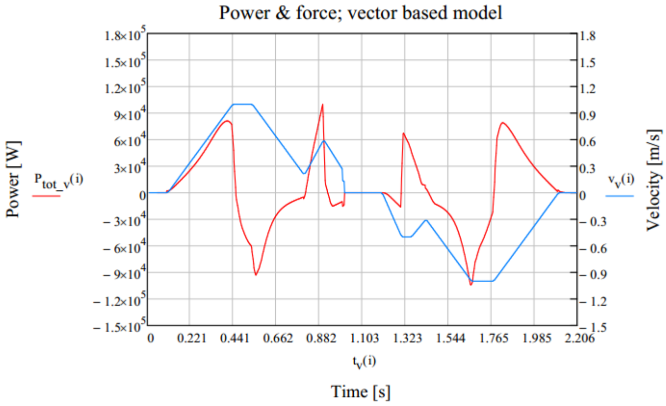

Acceleration speed: 3.5 m/s^2

Evaluation sheet:

Total dry cycle time: $t_{dry} = 1.731\,s$

Max locking power: $P_{max\_lock} := 100kW$

	Acceleration	time	Energy in/out	Peak power
Acceleration to close	$a_{acc1} = 3.5\frac{m}{s^2}$	$t_{acc1} = 0.286\,s$	$E_{acc1} = 9.961\cdot kJ$	$P_{acc1} = 101.438\cdot kW$
Deceleration to close	$a_{dec1} = 3.5\frac{m}{s^2}$	$t_{dec1} = 0.229\,s$	$E_{dec1} = -8.249\cdot kJ$	$P_{dec1} = -84.315\cdot kW$
Acceleration to open	$a_{acc2} = 3.5\frac{m}{s^2}$	$t_{acc2} = 0.2\,s$	$E_{acc2} = -14.579\cdot kJ$	$P_{acc2} = 96.415\cdot kW$
Deceleration to open	$a_{dec2} = 3.5\frac{m}{s^2}$	$t_{dec2} = 0.286\,s$	$E_{dec2} = 13.605\cdot kJ$	$P_{dec2} = -94.08\cdot kW$

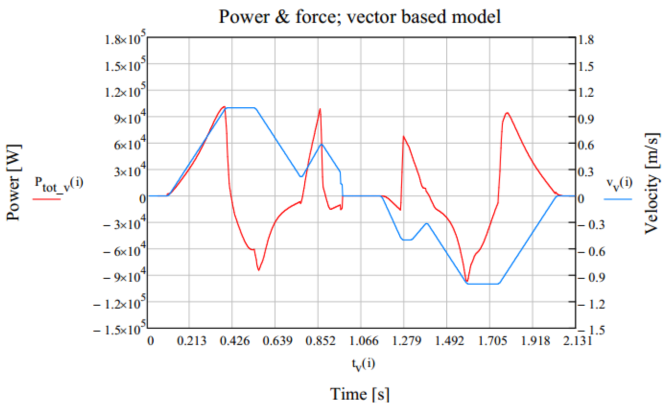

Acceleration speed: 4 m/s^2

Evaluation sheet:

Total dry cycle time: $t_{dry} = 1.675\,s$

Max locking power: $P_{max\_lock} := 100kW$

	Acceleration	time	Energy in/out	Peak power
Acceleration to close	$a_{acc1} = 4\frac{m}{s^2}$	$t_{acc1} = 0.25\,s$	$E_{acc1} = 8.919\cdot kJ$	$P_{acc1} = 119.496\cdot kW$
Deceleration to close	$a_{dec1} = 4\frac{m}{s^2}$	$t_{dec1} = 0.2\,s$	$E_{dec1} = -7.166\cdot kJ$	$P_{dec1} = -74.327\cdot kW$
Acceleration to open	$a_{acc2} = 4\frac{m}{s^2}$	$t_{acc2} = 0.175\,s$	$E_{acc2} = -14.636\cdot kJ$	$P_{acc2} = 89.865\cdot kW$
Deceleration to open	$a_{dec2} = 4\frac{m}{s^2}$	$t_{dec2} = 0.25\,s$	$E_{dec2} = 13.675\cdot kJ$	$P_{dec2} = -105.972\cdot kW$

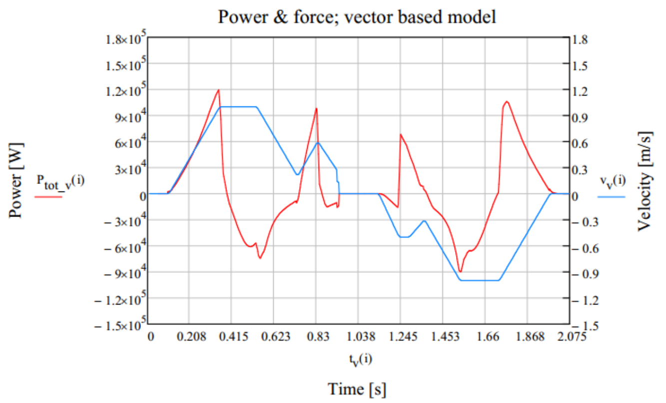

Acceleration speed: 4.5 m/s^2

Evaluation sheet:

Total dry cycle time: $t_{dry} = 1.632\,s$

Max locking power: $P_{max\_lock} := 100kW$

	Acceleration	time	Energy in/out	Peak power
Acceleration to close	$a_{acc1} = 4.5\frac{m}{s^2}$	$t_{acc1} = 0.222\,s$	$E_{acc1} = 8.183\cdot kJ$	$P_{acc1} = 132.935\cdot kW$
Deceleration to close	$a_{dec1} = 4.5\frac{m}{s^2}$	$t_{dec1} = 0.178\,s$	$E_{dec1} = -6.391\cdot kJ$	$P_{dec1} = -66.083\cdot kW$
Acceleration to open	$a_{acc2} = 4.5\frac{m}{s^2}$	$t_{acc2} = 0.156\,s$	$E_{acc2} = -14.572\cdot kJ$	$P_{acc2} = 84.544\cdot kW$
Deceleration to open	$a_{dec2} = 4.5\frac{m}{s^2}$	$t_{dec2} = 0.222\,s$	$E_{dec2} = 13.621\cdot kJ$	$P_{dec2} = -115.464\cdot kW$

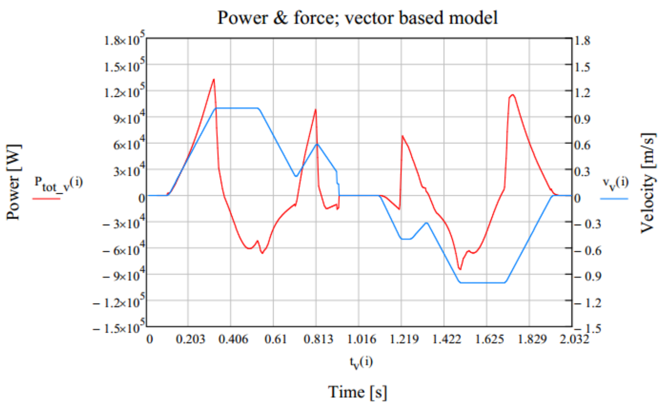

Acceleration speed: 5 m/s^2

Evaluation sheet:

Total dry cycle time: $t_{dry} = 1.597\,s$

Max locking power: $P_{max\_lock} := 100kW$

	Acceleration	time	Energy in/out	Peak power
Acceleration to close	$a_{acc1} = 5\frac{m}{s^2}$	$t_{acc1} = 0.2\,s$	$E_{acc1} = 7.778\cdot kJ$	$P_{acc1} = 146.018\cdot kW$
Deceleration to close	$a_{dec1} = 5\frac{m}{s^2}$	$t_{dec1} = 0.16\,s$	$E_{dec1} = -5.914\cdot kJ$	$P_{dec1} = -59.898\cdot kW$
Acceleration to open	$a_{acc2} = 5\frac{m}{s^2}$	$t_{acc2} = 0.14\,s$	$E_{acc2} = -14.456\cdot kJ$	$P_{acc2} = 80.748\cdot kW$
Deceleration to open	$a_{dec2} = 5\frac{m}{s^2}$	$t_{dec2} = 0.2\,s$	$E_{dec2} = 13.514\cdot kJ$	$P_{dec2} = -123.596\cdot kW$

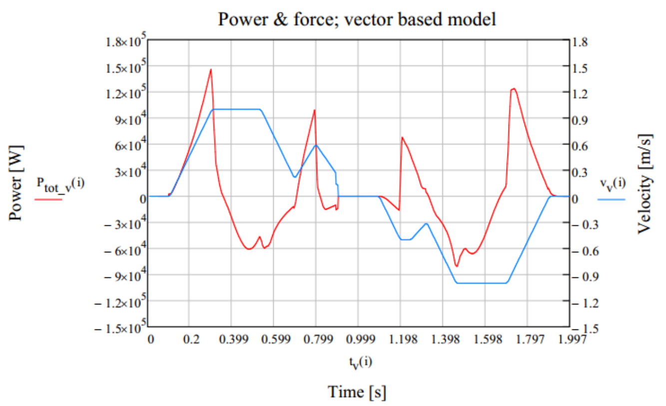

Acceleration speed: 5.5 m/s^2

Evaluation sheet:

Total dry cycle time: $t_{dry} = 1.569\,s$

Max locking power: $P_{max\_lock} := 100kW$

	Acceleration	time	Energy in/out	Peak power
Acceleration to close	$a_{acc1} = 5.5\frac{m}{s^2}$	$t_{acc1} = 0.182\,s$	$E_{acc1} = 7.39 \cdot kJ$	$P_{acc1} = 154.624 \cdot kW$
Deceleration to close	$a_{dec1} = 5.5\frac{m}{s^2}$	$t_{dec1} = 0.145\,s$	$E_{dec1} = -5.475 \cdot kJ$	$P_{dec1} = -55.346 \cdot kW$
Acceleration to open	$a_{acc2} = 5.5\frac{m}{s^2}$	$t_{acc2} = 0.127\,s$	$E_{acc2} = -14.338 \cdot kJ$	$P_{acc2} = 78.292 \cdot kW$
Deceleration to open	$a_{dec2} = 5.5\frac{m}{s^2}$	$t_{dec2} = 0.182\,s$	$E_{dec2} = 13.367 \cdot kJ$	$P_{dec2} = -131.114 \cdot kW$

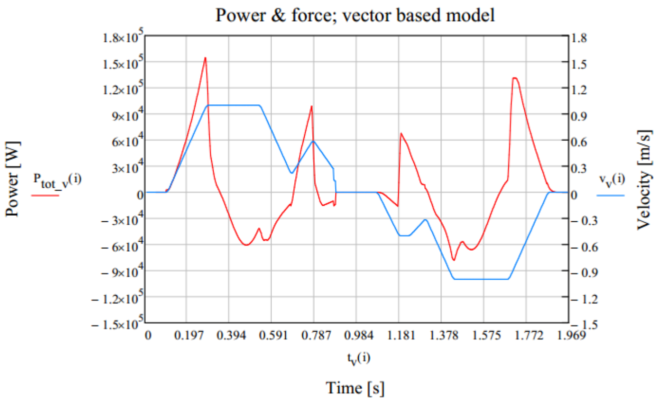

Acceleration speed: 6 m/s^2

Evaluation sheet:

Total dry cycle time: $t_{dry} = 1.545\,s$

Max locking power: $P_{max\_lock} := 100kW$

	Acceleration	time	Energy in/out	Peak power
Acceleration to close	$a_{acc1} = 6\frac{m}{s^2}$	$t_{acc1} = 0.167\,s$	$E_{acc1} = 7.102 \cdot kJ$	$P_{acc1} = 164.312 \cdot kW$
Deceleration to close	$a_{dec1} = 6\frac{m}{s^2}$	$t_{dec1} = 0.133\,s$	$E_{dec1} = -5.138 \cdot kJ$	$P_{dec1} = -54.635 \cdot kW$
Acceleration to open	$a_{acc2} = 6\frac{m}{s^2}$	$t_{acc2} = 0.117\,s$	$E_{acc2} = -14.263 \cdot kJ$	$P_{acc2} = 76.927 \cdot kW$
Deceleration to open	$a_{dec2} = 6\frac{m}{s^2}$	$t_{dec2} = 0.167\,s$	$E_{dec2} = 13.281 \cdot kJ$	$P_{dec2} = -139.085 \cdot kW$

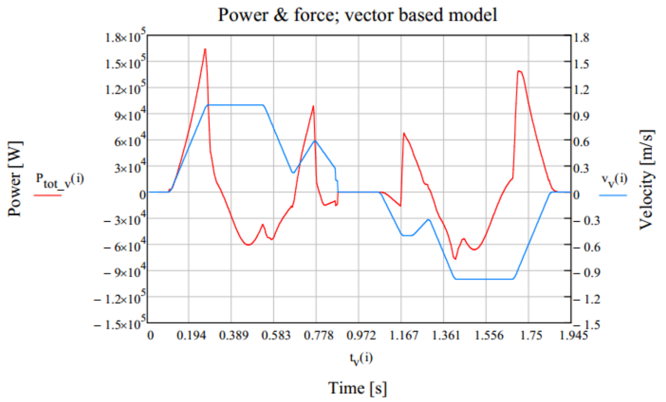

Acceleration speed: 6.5 m/s^2

Evaluation sheet:

Total dry cycle time: $t_{dry} = 1.525\,s$

Max locking power: $P_{max\_lock} := 100kW$

	Acceleration	time	Energy in/out	Peak power
Acceleration to close	$a_{acc1} = 6.5\frac{m}{s^2}$	$t_{acc1} = 0.154\,s$	$E_{acc1} = 6.885 \cdot kJ$	$P_{acc1} = 173.743 \cdot kW$
Deceleration to close	$a_{dec1} = 6.5\frac{m}{s^2}$	$t_{dec1} = 0.123\,s$	$E_{dec1} = -4.881 \cdot kJ$	$P_{dec1} = -54.847 \cdot kW$
Acceleration to open	$a_{acc2} = 6.5\frac{m}{s^2}$	$t_{acc2} = 0.108\,s$	$E_{acc2} = -14.176 \cdot kJ$	$P_{acc2} = 76.059 \cdot kW$
Deceleration to open	$a_{dec2} = 6.5\frac{m}{s^2}$	$t_{dec2} = 0.154\,s$	$E_{dec2} = 13.17 \cdot kJ$	$P_{dec2} = -146.767 \cdot kW$

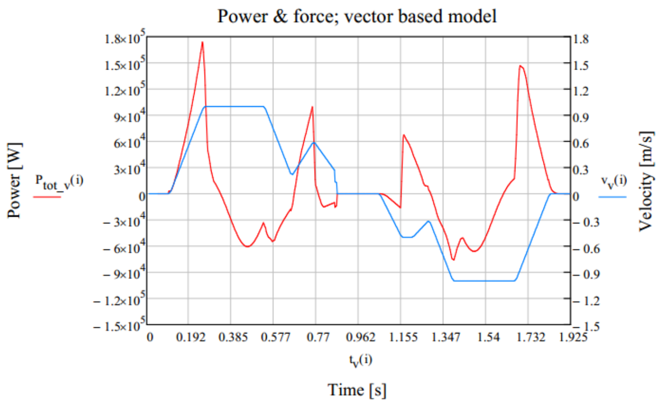

Acceleration speed: 7 m/s^2

Evaluation sheet:

Total dry cycle time: $t_{dry} = 1.508\,s$

Max locking power: $P_{max\_lock} := 100kW$

	Acceleration	time	Energy in/out	Peak power
Acceleration to close	$a_{acc1} = 7\frac{m}{s^2}$	$t_{acc1} = 0.143\,s$	$E_{acc1} = 6.718 \cdot kJ$	$P_{acc1} = 184.167 \cdot kW$
Deceleration to close	$a_{dec1} = 7\frac{m}{s^2}$	$t_{dec1} = 0.114\,s$	$E_{dec1} = -4.702 \cdot kJ$	$P_{dec1} = -55.553 \cdot kW$
Acceleration to open	$a_{acc2} = 7\frac{m}{s^2}$	$t_{acc2} = 0.1\,s$	$E_{acc2} = -14.07 \cdot kJ$	$P_{acc2} = 76.013 \cdot kW$
Deceleration to open	$a_{dec2} = 7\frac{m}{s^2}$	$t_{dec2} = 0.143\,s$	$E_{dec2} = 13.019 \cdot kJ$	$P_{dec2} = -154.349 \cdot kW$

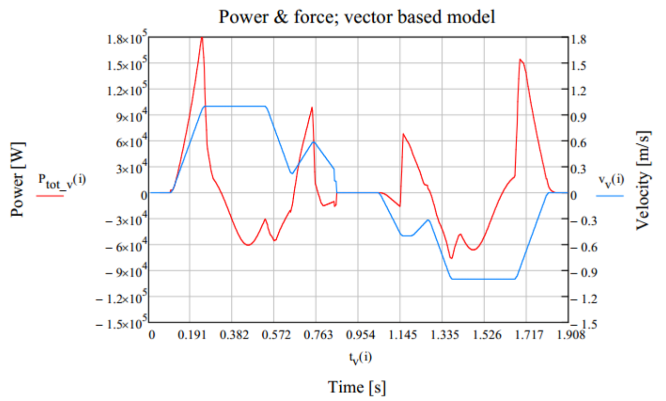

Appendix H. Model calculations

Three concepts are evaluated. The concepts are shown in the table below. The content of the electric mode, the hybrid mode and the determination of the motors are further explained in the report.

Concept name	Electrical motor power	Hydraulic volume displacement
	[kW]	*[cc/rot]*
Reference	70	-
2/3_concept	55	38,2
1/2_concept	35	103,6
1/3_concept	23	142,8

1/3_concept; electric mode

Total dry cycle time: $t_{dry} = 2.116\,s$

	Acceleration	time	Energy in/out	Peak power
Acceleration to close	$a_{acc1} = 2.25\,\frac{m}{s^2}$	$t_{acc1} = 0.333\,s$	$E_{acc1} = 4.553\cdot kJ$	$P_{acc1} = 40.904\cdot kW$
Deceleration to close	$a_{dec1} = 1.7\,\frac{m}{s^2}$	$t_{dec1} = 0.324\,s$	$E_{dec1} = -3.049\cdot kJ$	$P_{dec1} = -34.753\cdot kW$
Acceleration to open	$a_{acc2} = 1.3\,\frac{m}{s^2}$	$t_{acc2} = 0.346\,s$	$E_{acc2} = -6.893\cdot kJ$	$P_{acc2} = 39.679\cdot kW$
Deceleration to open	$a_{dec2} = 2.4\,\frac{m}{s^2}$	$t_{dec2} = 0.313\,s$	$E_{dec2} = 5.512\cdot kJ$	$P_{dec2} = -39.178\cdot kW$

Energy per destination:

	Energy in:	Theoretical regeneratable energy:
Rotational:	$E_{rot\_v\_in} = 1.067\cdot kJ$	$E_{rot\_v\_rec} = -1.067\cdot kJ$
Kinetic:	$E_{kin\_v\_in} = 11.517\cdot kJ$	$E_{kin\_v\_rec} = -11.517\cdot kJ$
Strain:	$E_{strain\_v\_in} = 4.423\cdot kJ$	$E_{strain\_v\_rec} = -4.423\cdot kJ$
Total:	$E_{tot\_v\_in} = 18.501\cdot kJ$	$E_{tot\_v\_rec} = -15.436\cdot kJ$

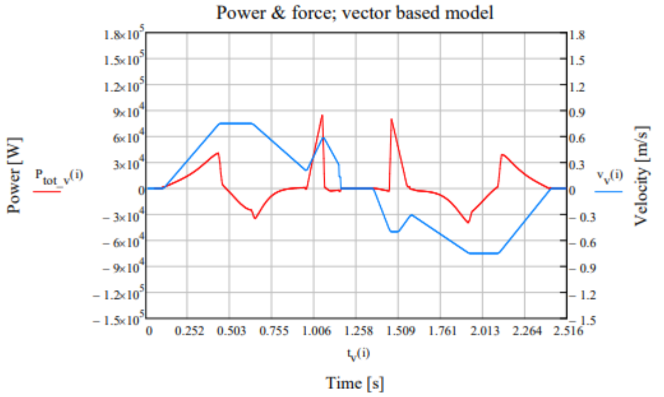

1/3_concept; hybrid mode

Total dry cycle time: $t_{dry} = 1.925\,s$

	Acceleration	time	Energy in/out	Peak power
Acceleration to close	$a_{acc1} = 4.2\,\frac{m}{s^2}$	$t_{acc1} = 0.202\,s$	$E_{acc1} = 8.264\cdot kJ$	$P_{acc1} = 80.335\cdot kW$
Deceleration to close	$a_{dec1} = 1.4\,\frac{m}{s^2}$	$t_{dec1} = 0.464\,s$	$E_{dec1} = -6.678\cdot kJ$	$P_{dec1} = -41.592\cdot kW$
Acceleration to open	$a_{acc2} = 7\,\frac{m}{s^2}$	$t_{acc2} = 0.1\,s$	$E_{acc2} = -9.856\cdot kJ$	$P_{acc2} = 65.358\cdot kW$
Deceleration to open	$a_{dec2} = 2.2\,\frac{m}{s^2}$	$t_{dec2} = 0.455\,s$	$E_{dec2} = 8.412\cdot kJ$	$P_{dec2} = -41.399\cdot kW$

Energy per destination:

	Energy in:	Theoretical regeneratable energy:
Rotational:	$E_{rot\_v\_in} = 1.473\cdot kJ$	$E_{rot\_v\_rec} = -1.473\cdot kJ$
Kinetic:	$E_{kin\_v\_in} = 16.509\cdot kJ$	$E_{kin\_v\_rec} = -16.509\cdot kJ$
Strain:	$E_{strain\_v\_in} = 4.423\cdot kJ$	$E_{strain\_v\_rec} = -4.423\cdot kJ$
Total:	$E_{tot\_v\_in} = 23.537\cdot kJ$	$E_{tot\_v\_rec} = -20.477\cdot kJ$

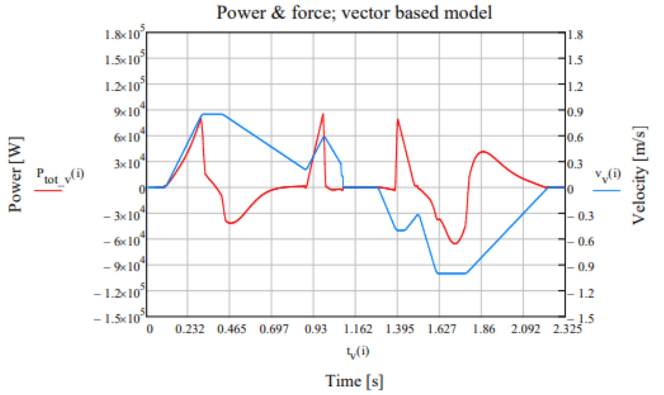

1/2_concept; electric mode

Total dry cycle time: $t_{dry} = 1.82\,s$

	Acceleration	time	Energy in/out	Peak power
Acceleration to close	$a_{acc1} = 2.75\,\frac{m}{s^2}$	$t_{acc1} = 0.364\,s$	$E_{acc1} = 5.092\cdot kJ$	$P_{acc1} = 62.693\cdot kW$
Deceleration to close	$a_{dec1} = 6\,\frac{m}{s^2}$	$t_{dec1} = 0.133\,s$	$E_{dec1} = -3.48\cdot kJ$	$P_{dec1} = -43.201\cdot kW$
Acceleration to open	$a_{acc2} = 1.6\,\frac{m}{s^2}$	$t_{acc2} = 0.344\,s$	$E_{acc2} = -9.651\cdot kJ$	$P_{acc2} = 60.362\cdot kW$
Deceleration to open	$a_{dec2} = 3.15\,\frac{m}{s^2}$	$t_{dec2} = 0.27\,s$	$E_{dec2} = 8.362\cdot kJ$	$P_{dec2} = -61.477\cdot kW$

<u>Energy per destination:</u>

	Energy in:	Theoretical regeneratable energy:
Rotational:	$E_{rot\_v\_in} = 4.733\cdot kJ$	$E_{rot\_v\_rec} = -4.733\cdot kJ$
Kinetic:	$E_{kin\_v\_in} = 16.993\cdot kJ$	$E_{kin\_v\_rec} = -16.993\cdot kJ$
Strain:	$E_{strain\_v\_in} = 4.423\cdot kJ$	$E_{strain\_v\_rec} = -4.423\cdot kJ$
Total:	$E_{tot\_v\_in} = 27.442\cdot kJ$	$E_{tot\_v\_rec} = -24.247\cdot kJ$

Power & force; vector based model

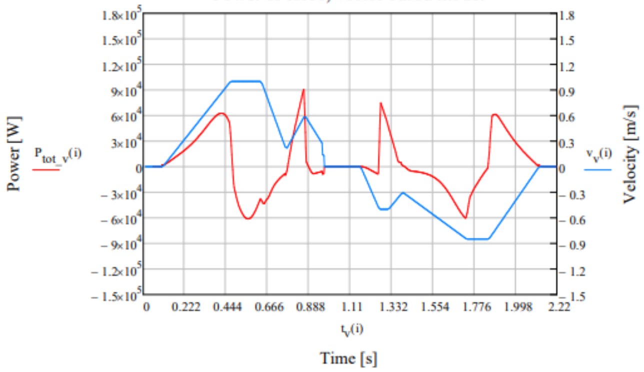

1/2_concept; hybrid mode

Total dry cycle time: $t_{dry} = 1.65\,s$

	Acceleration	time	Energy in/out	Peak power
Acceleration to close	$a_{acc1} = 4.2\,\frac{m}{s^2}$	$t_{acc1} = 0.238\,s$	$E_{acc1} = 5.181\cdot kJ$	$P_{acc1} = 110.781\cdot kW$
Deceleration to close	$a_{dec1} = 6\,\frac{m}{s^2}$	$t_{dec1} = 0.133\,s$	$E_{dec1} = -3.527\cdot kJ$	$P_{dec1} = -42.901\cdot kW$
Acceleration to open	$a_{acc2} = 7\,\frac{m}{s^2}$	$t_{acc2} = 0.1\,s$	$E_{acc2} = -12.688\cdot kJ$	$P_{acc2} = 65.804\cdot kW$
Deceleration to open	$a_{dec2} = 3.15\,\frac{m}{s^2}$	$t_{dec2} = 0.317\,s$	$E_{dec2} = 11.403\cdot kJ$	$P_{dec2} = -73.009\cdot kW$

<u>Energy per destination:</u>

	Energy in:	Theoretical regeneratable energy:
Rotational:	$E_{rot\_v\_in} = 5.322\cdot kJ$	$E_{rot\_v\_rec} = -5.322\cdot kJ$
Kinetic:	$E_{kin\_v\_in} = 20.276\cdot kJ$	$E_{kin\_v\_rec} = -20.276\cdot kJ$
Strain:	$E_{strain\_v\_in} = 4.423\cdot kJ$	$E_{strain\_v\_rec} = -4.423\cdot kJ$
Total:	$E_{tot\_v\_in} = 31.103\cdot kJ$	$E_{tot\_v\_rec} = -27.908\cdot kJ$

Power & force; vector based model

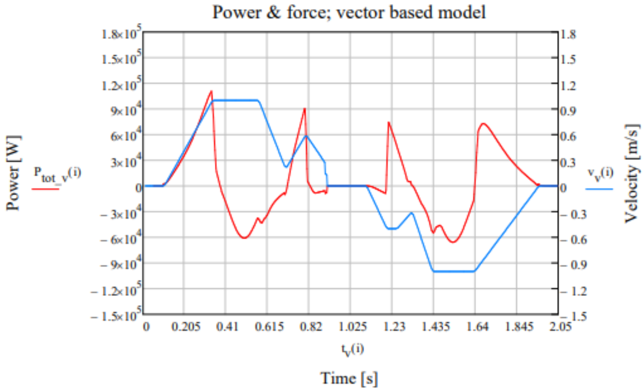

2/3_concept; electric mode

Total dry cycle time: $t_{dry} = 1.633\,s$

	Acceleration	time	Energy in/out	Peak power
Acceleration to close	$a_{acc1} = 3.65\,\frac{m}{s^2}$	$t_{acc1} = 0.274\,s$	$E_{acc1} = 5.81\cdot kJ$	$P_{acc1} = 98.823\cdot kW$
Deceleration to close	$a_{dec1} = 6\,\frac{m}{s^2}$	$t_{dec1} = 0.133\,s$	$E_{dec1} = -4.008\cdot kJ$	$P_{dec1} = -45.819\cdot kW$
Acceleration to open	$a_{acc2} = 7\,\frac{m}{s^2}$	$t_{acc2} = 0.1\,s$	$E_{acc2} = -13.485\cdot kJ$	$P_{acc2} = 65.836\cdot kW$
Deceleration to open	$a_{dec2} = 4.05\,\frac{m}{s^2}$	$t_{dec2} = 0.247\,s$	$E_{dec2} = 12.379\cdot kJ$	$P_{dec2} = -98.49\cdot kW$

<u>Energy per destination:</u>

	Energy in:	Theoretical regeneratable energy:
Rotational:	$E_{rot\_v\_in} = 6.86\cdot kJ$	$E_{rot\_v\_rec} = -6.86\cdot kJ$
Kinetic:	$E_{kin\_v\_in} = 20.416\cdot kJ$	$E_{kin\_v\_rec} = -20.416\cdot kJ$
Strain:	$E_{strain\_v\_in} = 4.423\cdot kJ$	$E_{strain\_v\_rec} = -4.423\cdot kJ$
Total:	$E_{tot\_v\_in} = 32.764\cdot kJ$	$E_{tot\_v\_rec} = -29.513\cdot kJ$

Power & force; vector based model

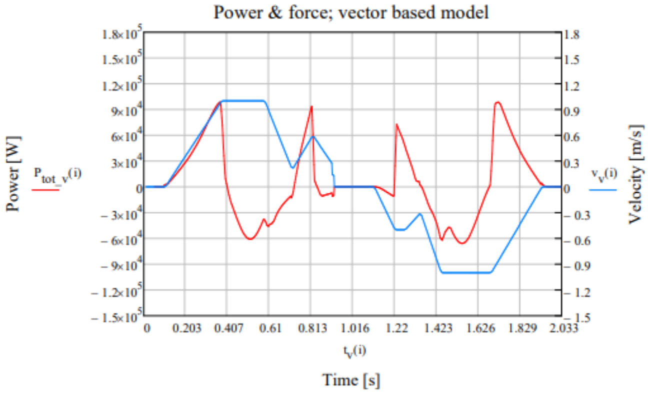

2/3_concept; hybrid mode

Total dry cycle time: $t_{dry} = 1.615\,s$

	Acceleration	time	Energy in/out	Peak power
Acceleration to close	$a_{acc1} = 4.2\,\frac{m}{s^2}$	$t_{acc1} = 0.238\,s$	$E_{acc1} = 5.86\cdot kJ$	$P_{acc1} = 115.689\cdot kW$
Deceleration to close	$a_{dec1} = 6\,\frac{m}{s^2}$	$t_{dec1} = 0.133\,s$	$E_{dec1} = -4.085\cdot kJ$	$P_{dec1} = -45.854\cdot kW$
Acceleration to open	$a_{acc2} = 7\,\frac{m}{s^2}$	$t_{acc2} = 0.1\,s$	$E_{acc2} = -13.499\cdot kJ$	$P_{acc2} = 65.877\cdot kW$
Deceleration to open	$a_{dec2} = 4.05\,\frac{m}{s^2}$	$t_{dec2} = 0.247\,s$	$E_{dec2} = 12.377\cdot kJ$	$P_{dec2} = -98.468\cdot kW$

<u>Energy per destination:</u>

	Energy in:	Theoretical regeneratable energy:
Rotational:	$E_{rot\_v\_in} = 6.859\cdot kJ$	$E_{rot\_v\_rec} = -6.859\cdot kJ$
Kinetic:	$E_{kin\_v\_in} = 20.427\cdot kJ$	$E_{kin\_v\_rec} = -20.427\cdot kJ$
Strain:	$E_{strain\_v\_in} = 4.423\cdot kJ$	$E_{strain\_v\_rec} = -4.423\cdot kJ$
Total:	$E_{tot\_v\_in} = 32.813\cdot kJ$	$E_{tot\_v\_rec} = -29.57\cdot kJ$

Power & force; vector based model

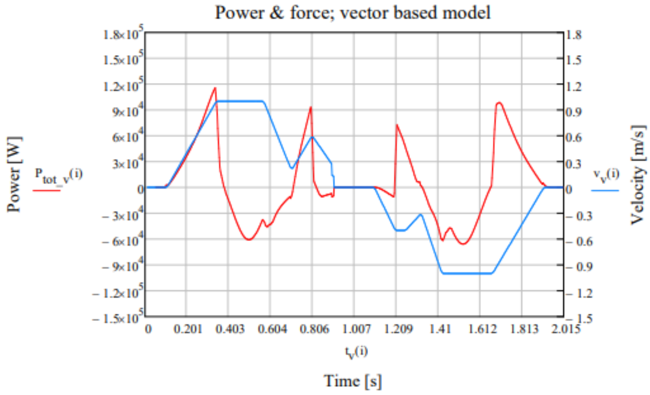

Appendix I. Evaluation sheet improvement current electric drive

Evaluation sheet:

Total dry cycle time: $t_{dry} = 1.656\,s$

	Acceleration	time	Energy in/out	Peak power
Acceleration to close	$a_{acc1} = 3.6\,\frac{m}{s^2}$	$t_{acc1} = 0.278\,s$	$E_{acc1} = 7.225\cdot kJ$	$P_{acc1} = 125.599\cdot kW$
Deceleration to close	$a_{dec1} = 7.5\,\frac{m}{s^2}$	$t_{dec1} = 0.107\,s$	$E_{dec1} = -5.532\cdot kJ$	$P_{dec1} = -63.297\cdot kW$
Acceleration to open	$a_{acc2} = 7.5\,\frac{m}{s^2}$	$t_{acc2} = 0.093\,s$	$E_{acc2} = -17.269\cdot kJ$	$P_{acc2} = 82.614\cdot kW$
Deceleration to open	$a_{dec2} = 3.9\,\frac{m}{s^2}$	$t_{dec2} = 0.256\,s$	$E_{dec2} = 16.328\cdot kJ$	$P_{dec2} = -124.686\cdot kW$

Energy per destination:

	Energy in:	Theoretical regeneratable energy:
Rotational:	$E_{rot\_v\_in} = 10.025\cdot kJ$	$E_{rot\_v\_rec} = -10.025\cdot kJ$
Kinetic:	$E_{kin\_v\_in} = 25.785\cdot kJ$	$E_{kin\_v\_rec} = -25.785\cdot kJ$
Strain:	$E_{strain\_v\_in} = 4.423\cdot kJ$	$E_{strain\_v\_rec} = -4.423\cdot kJ$
Total:	$E_{tot\_v\_in} = 41.205\cdot kJ$	$E_{tot\_v\_rec} = -37.763\cdot kJ$